A STUDY OF LOW-FREQUENCY BROADBAND NOISE CONTROL IN VENTILATION DUCTWORK SYSTEMS BASED ON HELMHOLTZ RESONATOR ARRAYS

CAI CHENZHI

PhD

The Hong Kong Polytechnic University

2018

The Hong Kong Polytechnic University

Department of Building Services Engineering

A study of low-frequency broadband noise control in ventilation ductwork systems based on Helmholtz resonator arrays

Cai Chenzhi

A thesis submitted in partial fulfillment of the requirements for the Degree of Doctor of Philosophy

June 2018

CERTIFICATE OF ORIGINALITY

I hereby declare that this thesis is my own work and that, to the best of my knowledge and belief, it reproduces no material previously published or written, nor material that has been accepted for the award of any other degree or diploma, except where due acknowledgement has been made in the text.

_____(Signed)

Cai Chenzhi (Name of student)

Dedication

To Dizi, my wife, for her enormous patience and love during this phase of our lives.

To Yiyi, my lovely daughter, for bringing happiness to the whole family.

To my parents, for their encouragement and continuous support.

Abstract

The ventilation ductwork system is an essential and significant part of the building to maintain good indoor environmental quality. However, it is common to encounter noise problem in a ventilation ductwork system. The accompanied duct noise from the ventilation system could propagate into the occupied zones through the waveguide and could deteriorate human being's working or living environment quality. The aims of this thesis are to achieve a low-frequency broadband noise control in the ventilation ductwork system based on Helmholtz resonator arrays.

Helmholtz resonator (HR hereafter) is one of the most basic acoustic models and has been widely used in engineering applications due to its simple, tunable and durable characteristics. In order to improve the noise attenuation performance of a HR, an extended neck or spiral neck taken the place of the traditional straight neck of a HR has been investigated. Based on the transmission loss index, the noise attenuation capacity index is first proposed in this thesis to evaluate the noise attenuation performance of a HR.

Since a single HR is qualified as a narrow band silencer, an array of HRs is one possible way to obtain a broader noise attenuation band. A theoretical study of the

acoustic performance of different HR configurations has been presented in this thesis. The proposed noise attenuation capacity is used to evaluate the acoustic performance of different HR array configurations. The predicted theoretical results fit well with the Finite Element Method simulation results.

The dispersion characteristics of sound wave propagation in a periodic ducted HR system has also been investigated. The Bloch wave theory and transfer matrix method are adopted to investigate the wave propagation in a periodic ducted HR system. Owing to the coupling of Bragg reflection and HR's resonance, it is found that a periodic ducted HR system can provide a much broader noise attenuation band. However, the broader the noise attenuation band, the lower the peak attenuation amplitude. It is therefore that a noise control zone compromising the attenuation bandwidth or peak amplitude is proposed for noise control optimization.

The transmission loss achieved by a periodic ducted HR system is depended on the structure and the number of HRs mounted on the duct. However, the number of HRs is restricted by the available space in longitudinal direction of the duct. Moreover, such system will occupy a large space and may have some spare space in the transverse direction of the duct. By adding HRs on the available space in the transverse direction, a modified ducted HR system is therefore proposed to improve the noise attenuation performance of the ducted HR system and fully utilizing the

available space. The results indicate that both the noise attenuation band and peak amplitude are increased by adding HRs on arbitrary side of the cross-section of the duct.

Aiming at broader noise attenuation bands for hybrid noise control at low frequencies, a periodic dual HR array is proposed and investigated. The dual HR which consists of two HRs connected in series (neck-cavity-neck-cavity) leads to two resonance frequencies. By analogy with a two degrees of freedom mechanical system, the resonance frequencies and transmission loss of a dual HR has been derived. The dual HR is also effective at its resonance pears with relative narrow bands. Owing to the coupling of Bragg reflection and dual HR's resonances, a periodic dual HR array can provide much broader noise attenuation bands at the designed resonance frequencies of the dual HR.

It is hoped that the present work can advance the investigation of noise control method for the ventilation ductwork systems or other research areas in respect of HR.

Publications Arising from the Thesis

Published papers

Chenzhi Cai and Cheuk Ming Mak. Generalized flow-generated noise method for multiple elements in air ducts. *Applied Acoustics* **135**, 136-141 (2018).

Chenzhi Cai and Cheuk Ming Mak. Hybrid noise control in a duct using a periodic dual Helmholtz resonator array. *Applied Acoustics* **134**, 119-124 (2018).

Chenzhi Cai and Cheuk Ming Mak. Noise attenuation performance of a Helmholtz resonator. *Advances in Engineering Software* **116**, 60-66 (2018).

Chenzhi Cai and Cheuk Ming Mak. Acoustic performance of different Helmholtz resonator array configurations. *Applied Acoustics* **130**, 204-209 (2018).

Chenzhi Cai, Cheuk Ming Mak and Xu Wang. Noise attenuation performance improvement by adding Helmholtz resonators on the periodic ducted Helmholtz resonator system. *Applied Acoustics* **122**, 8-15 (2017).

Chenzhi Cai, Cheuk Ming Mak and Xiaofeng Shi. An extended neck versus a spiral neck of the Helmholtz resonator. *Applied Acoustics* **115**, 74-80 (2017).

Chenzhi Cai and Cheuk Ming Mak. Noise control zone for a periodic ducted Helmholtz resonator system. *Journal of the Acoustical Society of America* **140(6)**, EL471-EL477 (2016).

Conference paper

Chenzhi Cai, Cheuk Ming Mak, Yijing Chu and Xu Wang. Noise attenuation performance of multiple Helmholtz resonator arrays system. *Proceeding of Inter-noise 2017*, Hong Kong, China, 2017.

Chenzhi Cai, Cheuk Ming Mak, Xiaofeng Shi and Xu Wang. The Helmholtz resonator with different types of necks. *24th International Congress on Sound and Vibration*, London, UK, 2017.

Acknowledgements

This thesis is the results of three-year hard work funded by a grant from the Research Grants Council of the Hong Kong Special Administrative Region, China (Project No. PolyU 152116/14E) and I feel deeply that my dissertation could not be completed without the help and support of many people. I sincerely thank and acknowledge my chief supervisor, Prof, Mak Cheuk Ming, for his invaluable guidance, constant encouragement and continued support throughout my study. No doubt his passion for research, profound knowledge and rigorous attitude have had a considerable effect not only upon my academic progress, but have also invigorated my beliefs and attitude for research in the future.

I wish to appreciate my co-supervisor, Prof. Wang Xu, from Tongji University, for his insightful view and continuous support in my study. His valuable suggestions regarding my research and papers improve this work.

Furthermore, I would like to express my thanks to all the members in the Indoor Environmental Quality Laboratory and my friends for their assistance and company during this memorable time. I would also like to thank all the staff and technicians for their kind support.

Finally, I wish to give special thanks to my wife, Dizi, for her love and extraordinary effort during this phase of our lives. I would also express my gratitude to my treasured little girl, Yiyi, for bringing the happiness to our family and turning my life into a brand new beginning. Last, but not least, I would like to express my deepest appreciation to my family for their unconditional support, love and understanding through my life, and for taking care of my daughter Yiyi

Table of Contents

List of Figures

List of Tables

Nomenclature

$A_{i,n}$	Modal amplitudes corresponding to components traveling in positive direction in different domains
$\mathbf{a}_{n+1}$	State vector of the complex wave amplitudes
$B_{i,n}$	Modal amplitudes corresponding to components traveling in negative direction in different domains
C_a	Sound capacitance
C_{TL}	Noise attenuation capacity
c_0	Sound speed of air
d	Periodic distance
F	Equivalent coefficient of the spiral neck
f_0	Resonance frequency of the Helmholtz resonator
I_n	Amplitude of the incident plane wave in the nth cell
J_0	Bessel function of the first kind and order 0
J_m	Bessel function of the first kind and order m
K_{11}	Stiffness of the first string to the front mass
K_{12}	Stiffness of the first string to the rear mass
K_2	Stiffness of the second spring
k	Wave number
k_0	Wave number of the zero mode
$k_{i,n}$	Wave number of different modal in different domains

l_n	Length of the neck of the Helmholtz resonator
l_n'	Effective length of the neck
l_c	Length of the cavity of the Helmholtz resonator
l_e	Length of extended neck into cavity
L_I	Length of straight duct I of the spiral neck
L_{II}	Length measured at the midline of the spiral duct
L_{III}	Length of straight duct III of the spiral neck
L_{III}'	Length of the equivalent straight tube
M_m	Mass of air in the neck
M_a	Sound mass
N	Turn number of the spiral neck
N_{total}	Sum of HRs mounted on the duct
p	Sound pressure
p_1	Sound pressure at point 1
p_2	Sound pressure at point 2
p_i	Sound pressure at different points
q	Bloch wave number
R_n	Amplitude of the reflected plane wave in the n^{th} cell
R_m	Damping coefficient
R_a	Sound resistance
R_0	Distance from the point of the curvature center

r_0	Radius of the cross sectional area of the spiral duct
r_n	Radius of the neck of the Helmholtz resonator
r_c	Radius of the cavity of the Helmholtz resonator
S_d	Cross-sectional area of the main duct
S_n	Cross-sectional area of the neck
S_n'	Cross-sectional area of the equivalent straight tube
$\mathbf{T}$	Transfer matrix
$\mathbf{T}_{duct}$	Transfer matrix of the straight duct
$\mathbf{T}_{duct}$	Transfer matrix between each two nearby cell
$\overline{TL}$	Average transmission loss
TL	Transmission loss
U	Volume velocity
u	Particle velocity
V_c	Cavity volume
$\mathbf{v}$	Eigenvector of the transfer matrix of the periodic system
W_{total}	Energy storage capacity
X_1	Magnitude of the first neck's displacement
X_2	Magnitude of the second neck's displacement
x_n	Local coordinates
Y_m	Bessel function of the second kind and order m
Z	Characteristic impedance of the plane mode

Z_d	Acoustic impedance of the duct
Z_r	Acoustic impedance of the Helmholtz resonator
δ	Length correction factor of the neck
ϕ	Curvature angle
$\alpha_{i,n}$	Root of the eigenfunction
ω	Angular frequency
ω_0	Angular resonance frequency
ω_m	Angular frequency of Bragg reflection
$\psi_{i,n}(r)$	Eigenfunction of Helmholtz equation
e^{-jqd}	Eigenvalue of the transfer matrix
λ	Eigenvalue of the transfer matrix
λ_0	Wavelength of resonance frequency
α	Reflection coefficient
μ	Propagation constant
ρ_0	Air density
Δ_{bw}	Bandwidth of the stopbands
Λ	Matrix of the whole ducted resonator system

Chapter 1

Introduction

1.1 Duct-borne noise control methods

A ventilation ductwork system is an essential system in buildings that provides conditioned or fresh air to indoor environments so as to ensure good indoor air quality. However, it is common to encounter a duct-borne noise problem in a ventilation ductwork system.[1,2] The components of the ductwork system, for instance, dampers, bends transition pieces, corners or even attenuators punctuate the original uniform ductwork, which are responsible for the generation of the undesired noise as the ductwork system begins to work.[3-7] These unavoidable discontinuities in a ventilation ductwork system result in the generation of localized turbulence. Some of the turbulence energy is converted into noise. Current design guides, the CIBSE Guide[8,9] and the ASHRAE Handbook[10], also provide a prediction method for the flow-generated noise produced in-duct element in a ventilation system. The accompanied duct noise from the ventilation system could propagate into the occupied zones through the waveguide and could deteriorate human being's working or living environment quality.[11-14] Given that people speed more and more time indoor and noise level is one of the key factors in the indoor environmental quality

assessment, alleviating such duct-borne noise is thus of great importance to obtain satisfaction with acoustics and overall environmental satisfaction.

Abatement of ductwork noise has always been a challenge, especially the low-frequency and broadband noise in a ventilation ductwork system due to its significant role in modern buildings to maintain good indoor environment. Therefore, it is not surprising that noise attenuation technologies for the ventilation ductwork system have received extensive attentions. Various noise control methods have been developed to reduce the noise propagation throughout the ductwork system. Generally, there are two types of noise control methods: active noise control and passive noise control. The principal of active noise control was first proposed by Lueg[15] in 1936, which a secondary source generating anti-noise was adopted to cancel noise from the primary source. In recent years, active noise control has become a rapidly developing area of duct-borne noise control.[16-21] An active noise control system can provide environmental-adaptive noise attenuation, especially at low frequencies. Nevertheless, there are still some problems related to its reliability and high cost. Further studies are needed to popularize the application of active noise control.

Most traditional passive noise control methods such as dissipative silencer and reactive silencer still suffer from some serious drawbacks despite these silencers are

widely used in ventilation ductwork system. The dissipative silencer in which the sound absorption materials in the silencers dissipate the sound energy into heat performances well at mid to high frequencies. However, the acoustical properties and the damping mechanism of the sound absorption materials determine that it is not effective for low-frequency noise control.[22-27] Meanwhile accumulation of dusts and bacterial breeding in porous sound absorption materials are noticeable concerns, especially in some public buildings like hospitals. Reactive silencers, the Helmholtz resonator and expansion chamber are typical examples, show stable noise attenuation performance and can be tuned conveniently. Nevertheless, the volume of the expansion chamber needs to be sufficiently large in order to deal with low-frequency noise.[28-30] The presence of HR offers a solution of low-frequency noise control, yet it qualifies as a narrow band noise attenuator that it is only effective at its resonance with a relative narrow frequency range.[31-34]

Over the years, a number of investigators have tried to devise a method to control the duct-borne noise in the low-frequency and with wide working frequency range. However, most of them achieved low-frequency and broad-band sound attenuation by combing several different Helmholtz resonators, which means using serial or parallel arrangement of Helmholtz resonators with different resonant frequencies to obtain a wide band of noise control in ducts.[35-40] Because Helmholtz resonators are only useful against noise centralized in a very narrow frequency band, to achieve a

wide noise reduction band, many resonators should be used. Such kind of noise reduction structure will occupy a large space and is impractical to be used in an actual ventilation ductwork system. An array of identical HRs mounted periodically is one possible way to realize the low-frequency and broadband noise attenuation band in the duct. Bradly[41,42] analyzed the propagation of time harmonic acoustic wave in periodic waveguides theoretically and experimentally. Sugimoto and Horioka[43,44] investigated the peculiar dispersion characteristics of sound waves propagation in a tunnel with an array of identical HRs mounted periodically, marked as stopbands and passbands. The Bloch wave cannot transmit at some frequencies is called stopbands, otherwise it is called the passbands. Owing to the coupling of Bragg reflection and HR's resonance, it is found that a periodic ducted HR system can provide a much broader noise attenuation band.[45-50]

1.2 Helmholtz resonator

Helmholtz resonator (or HR hereafter) is one of the most basic acoustic models and has been widely used in engineering applications due to its simple, tunable and durable characteristics. The Helmholtz resonator, which consist of a cavity communicating with an external duct through an orifice, is a well-known device to reduce noise centralized in a narrow band at its resonance frequency. Owing to the resonance frequency of a HR is only determined by its geometries, it is therefore

straightforward to obtain a HR with a desired resonance frequency. Therefore, the HR has been utilized in numerous duct-structure systems, such as ventilation and air conditioning system in buildings, automotive duct systems and aero-engines, for the attenuation of noise produced by unavoidable in-ducted elements.[51,52] The HR could also be an effective method to suppress the propagation of sound waves and pressure generated by a high-speed train entering and moving in a tunnel. The tunnel aerodynamics and acoustics become a significant issue with the developing high-speed trains projects with a lot of tunnel structures. The HR has been investigated theoretically and experimentally to countercheck noise generated by tunnel portals and eliminate the shock wave in the tunnel.[53-55]

Since the widespread applications of the HR, it has received a great deal of attentions worldwide. Many studies have tried to obtain an accurate prediction of the resonance frequency. Mainly through the labours of Helmholtz, Rayleight, Ingard, Sondhauss and Wertheim, the classical lumped approach for a HR is supposed to be analogous to the mechanical mass-spring system with end-correction factors for the sake of the accuracy.[32] The mass of air in the neck is driven by an external force and the air inside the cavity acts as a spring. The end-correction factor for the neck length is introduced to regard the sound energy radiation from the neck as an additional mass. However, the large discrepancies between the measured and predicted resonance frequencies lead to the developing method for a more accuracy prediction. Therefore, a

considerable number of researchers have developed the wave propagation in both the duct and the HR in theoretical analysis from an initial one-dimensional wave propagation approach to a multidimensional approach in order to account for nonplanar effects.[56-59] The multidimensional approach has been proven by experiment to be a better theoretical analysis method.

The HR is qualified as narrow band silencer and it is only effective at its resonance peak. Various modification forms of HRs have been examined in order to improve the acoustic performance of a HR. Chanaud[60] investigated the effects of different orifice shapes and cavity geometries on the resonance frequency of a HR. Tang and Sirignano[61] showed that resonance frequency of a HR was reduced by increasing the neck length. In order to lengthen the neck, an extended neck and a spiral neck were proposed by Selamet and Lee[62] and Shi and Mak[63] respectively. Tang[64] examined the HR with tapered necks of increasing cross-sectional area towards cavity both experimentally and theoretically. Griffin et al.[65] demonstrated the mechanically coupled HRs through a thin membrane to obtain three resonance frequencies instead of two. Xu et al.[66] derived expressions of two resonance frequencies and the transmission loss of a dual HR formed by a pair of neck and cavity connected in series. Selamet et al.[67] presented another approach by lining the HR with fibrous material to improve the attenuation performance without changing the geometries of the HR.

1.3 Objective and Scope of Research

This thesis aims at investigating low-frequency broadband noise control in ventilation ductwork systems based on Helmholtz resonator arrays. The Helmholtz resonator is widely used as an effective silencer for low-frequency duct-borne noise control due to its characteristics of being tunable, durable, and affordable. A good design for a Helmholtz resonator is important for noise attenuation in ventilation ductwork systems. Therefore, the first objective of this thesis is to improve the noise attenuation performance of the HR at low frequencies with a limited space. An extended neck or a spiral neck takes the place of the traditional straight neck of the HR. The acoustic performances of the HR with these two types of necks are analyzed theoretically and numerically.

The second objective of this thesis is to evaluate the acoustic performance of a HR based on the proposed noise attenuation capacity index. The transmission loss index is mainly used to evaluate the acoustic transmission performance. However, almost all researches concentrate on the shapes of the transmission loss curve while ignoring the area under the transmission loss curve. The noise attenuation capacity index defined as the integral of transmission loss in the frequency domain is therefore proposed to be one of the key parameters to evaluate HR’s noise attenuation

performance.

The third objective of this thesis is to investigate the dispersion characteristics of sound wave propagation in a periodic ducted HR and evaluate the coupling effects of Bragg reflection and HR's resonance. Periodic ducted HR systems struggle to obtain the necessary broad attenuation bandwidth and high-peak attenuation amplitude at the same time. However, the broader the noise attenuation band, the lower the peak attenuation amplitude. It is therefore that this thesis looks into the limitations of the attenuation bandwidth and peak amplitude for a periodic ducted HR system.

The last objective of this thesis is to improve the noise attenuation performance of a ducted HR system. The noise attenuation performance of the ducted HR system is fairly depended on the number of HRs. By adding HRs on the available space in the transverse direction, a modified ducted HR system is proposed to increase both the peak amplitude and noise attenuation bandwidth at the same time and fully utilize the available space. In practical ventilation ductwork system, hybrid noise often occurs due to interaction effects of different localized turbulence and discontinuities. In order to deal with hybrid noise, a periodic dual HR system is introduced to obtain several broadband noise attenuation bands in low-frequency range.

1.4 Outline

The thesis is arranged in the following six chapters. The current Chapter covers the background of the present study including the literature review of related works and the objectives of this study.

Chapter 2 is devoted to improve the noise attenuation the noise attenuation performance of the Helmholtz resonator (HR) at low frequencies with a limited space. An extended neck or a spiral neck takes the place of the traditional straight neck of the HR. The acoustic performance of the HR with these two types of necks is analyzed theoretically and numerically. The transmission loss index is mainly used to evaluate the acoustic transmission performance. Based on the transmission loss index, the noise attenuation capacity index is proposed to be one of the key parameters to evaluate the noise attenuation performance of a HR. The theoretical formula of a HR's noise attenuation capacity is derived theoretically.

Chapter 3 presents a theoretical and numerical study of the acoustic performance of different HR array configurations. A dual HR consisting of two HRs connected in

series (neck-cavity-neck-cavity) could be considered as a serial HR array. Two HRs mounted on the same cross-section of the duct constitute a parallel HR array. A lined HR array is composed of two HRs installed on the longitudinal direction of the duct. The noise attenuation capacity of these HR array configurations are compared, which use a distinct parameter to evaluate the noise attenuation performance and ability of different array configurations.

Chapter 4 includes a theoretical study of the dispersion characteristics of sound wave propagation in a periodic ducted HR system. An array of HR mounted on the duct periodically could provide a much broader noise attenuation band. The bandwidths and positions of noise attenuation bands have been investigated. The transfer matrix method and Bloch wave theory are developed to conduct the investigation. The limitations of the noise attenuation for a ducted HR system are illustrated in this chapter. The broader the noise attenuation band the lower the peak attenuation amplitude. A noise control zone compromising the attenuation bandwidth or peak amplitude is proposed for noise control optimization.

Chapter 5 focuses on improving the noise attenuation performance of a ducted HR system and fully utilizing available spaces. By adding HRs on the available space in the transverse direction, a modified ducted HR system is therefore proposed and investigated. In order to deal with hybrid noise in ventilation ductwork system, a

periodic dual HR array is introduced. The dual HR which consists of two HRs connected in series leads to two resonance frequencies. The mechanism of Bragg reflection and dual HR's resonances motivate us to achieve several broadband noise attenuation bands in low-frequency range.

The final chapter, Chapter 6 summarizes all the investigations and findings in this thesis and forecasts further investigations based on the present work.

Chapter 2

Acoustic characteristics of a Helmholtz resonator

2.1 Helmholtz resonator with different types of necks

The HR is known to be an effective silencer at low frequencies, sometimes its application may be limited by space. It is important to shift the resonance frequency when there is a space constraint. In order to improve the noise attenuation performance at low frequencies when there is limited space. A spiral neck or an extended neck may by a feasible way to shift the resonance frequency in such situations. The extended neck will lower the resonance frequency without an extra cavity volume requirement, and the spiral neck can make the neck as long as possible under a space constraint to reduce the resonance frequency. The acoustic performance of HRs with these two types of necks is analyzed both theoretically and numerically. A modified one-dimensional analytical approach with a length correction factor is used in this paper to accurately predict the acoustic performance of an HR with an extended neck. The length correction factor is introduced due to the apparent multidimensional sound field inside the cavity of an HR with an extended neck. The length correction factor is obtained using a two-dimensional analytical

approach. The wave propagation of an HR with a spiral neck is also analyzed. The curvature of the spiral neck changes the impedance, and the spiral neck can then be considered equivalent to a straight neck with a corrected neck length and cross-section area. The spiral neck is then translated to a traditional straight neck, and the acoustic performance is predicted using a one-dimensional analytical approach.

2.1.1 Analytical approach of the HR with an extended neck

The sound fields inside an HR with an extended neck are clearly multidimensional.[52,68] A modified one-dimensional analytical model, which includes a length correction to account for the non-planar effects at the neck-cavity interface, is proposed here to improve the accuracy of the acoustic performance prediction. The length correction is derived using a two-dimensional analytical approach. Figure. 2.1 shows the geometries of the circular concentric HR with an extended neck. The two-dimensional sound wave propagations in both the extended neck and the cavity are governed by the Helmholtz equation in cylindrical coordinates as:

$$\nabla^2 P(r,x) + k^2 P(r,x) = 0 \tag{2.1}$$

The sound pressure and particle velocity can be solved by Eq. (2.1) as[52]:

$$P_i(r,x_i) = \sum_{n=0}^{+\infty} (A_{i,n} e^{-jk_{i,n}x_i} + B_{i,n} e^{jk_{i,n}x_i}) \psi_{i,n}(r) \tag{2.2}$$

$$u_i(r,x_i)=\frac{1}{\rho_0\omega}\sum_{n=0}^{+\infty}k_{i,n}(A_{i,n}e^{-jk_{i,n}x_i}-B_{i,n}e^{jk_{i,n}x_i})\psi_{i,n}(r) \tag{2.3}$$

$$k_{i,n}=\begin{cases}\sqrt{k_0{}^2-(\alpha_{1,n}/a_i)^2}, k_0>\alpha_{1,n}/a_i\\ -\sqrt{k_0{}^2-(\alpha_{1,n}/a_i)^2}, k_0<\alpha_{1,n}/a_i\end{cases} \tag{2.4}$$

where $i=1,2,3$ represents different coordinate axis x domains, $A_{i,n}$ and $B_{i,n}$ represent the modal amplitudes corresponding to components traveling in positive and negative directions in different domains, respectively, ρ_0 represents the air density, $k_{i,n}$ represents the wave number, k_0 represents the wave number of the zero mode, and $\psi_{i,n}(r)$ represents the eigenfunction. The eigenfunction $\psi_{i,n}(r)$ is given as:

$$\psi_{i,n}(r)=\begin{cases}J_0(\alpha_{i,n}\frac{r}{a_i}), & i=1,3\\ J_0(\alpha_{2,n}\frac{r}{a_2})-\frac{J_1(\alpha_{2,n})}{Y_1(\alpha_{2,n})}Y_0(\alpha_{2,n}\frac{r}{a_2}), & i=2\end{cases} \tag{2.5}$$

where J_m is the Bessel function of the first kind and order m, Y_m is the Bessel function of the second kind and order m, and $\alpha_{i,n}$ is the root matching the rigid wall condition of $\psi_{i,n}(r)=0$.

The walls of the neck and the cavity are set to be rigid. At $x_2=0$ or $x_3=l_r$, the rigid wall condition gives $v_2=0, v_3=0$. At $x_1=l_e+l_n$ or $x_3=0$, the pressure continuity condition at neck-cavity interface gives $P_1=P_3$. Similarly, at $x_2=l_e$ or $x_3=0$, it gives $P_2=P_3$. The volume velocity continuity condition at $x_1=l_e+l_n$ or $x_3=0$ gives $u_1S_n+u_2(S_c-S_n)=u_3S_c$. Set the relation of initial oscillation sound pressure

P_0 and particle velocity u_p at $x_1 = 0$ as $P_0 = \rho_0 c_0 u_p = 1$ (c_0 represents the sound speed). Then all unknown $A_{i,n}$ and $B_{i,n}$ can be obtained by combining all the boundary conditions above.

The frequency range considered here is well below the cut-off frequency of the resonator neck and the cavity. This means that the non-planar wave excited at the abrupt cross-section change (the neck-cavity interface) will decay exponentially. Therefore, it is assumed that only planar waves exist in the HR. The multidimensional effects associated with evanescent high modes at a sudden area change are considered as the "length correction factor." As a consequence, Eq. (2.2) and Eq. (2.3) can be simplified as:

$$P_i(r, x_i) = A_{i,0} e^{-jk_0 x_i} + B_{i,0} e^{jk_0 x_i} \tag{2.6}$$

$$u_i(r, x_i) = \frac{1}{\rho_0 c_0} (A_{i,0} e^{-jk_0 x_i} + B_{i,0} e^{jk_0 x_i}) \tag{2.7}$$

Then, at the neck-cavity interface ($x_1 = l_e + l_n$ or $x_3 = 0$), the discontinuity effects will be equivalent to the equation[69]:

$$P_1 = P_3 + \delta Z S_n u_1 \tag{2.8}$$

where S_n is neck area, Z is the characteristic impedance of the plane mode given as $Z = j\rho_0 c_0 / S_n$, and δ represents the length correction factor. Combining Eq. (2.6) and Eq. (2.7) with Eq. (2.8) gives:

$$\delta = \left| \frac{P_1 - P_3}{j\rho_0 c_0 V_1} \right| = \left| \frac{(A_{1,0} + B_{1,0}) - (A_{3,0} + B_{3,0})}{jk(A_{1,0} - B_{1,0})} \right| \tag{2.9}$$

Based on the two-dimensional analytical results, an approximate formula for the length correction factor could be given as:

$$\delta = 0.6165 r_n - 0.7046 r_n^{\,2} / r_c + 0.2051 e^{-1.7226 l_e / r_c} r_n - 0.3749 e^{-1.3012 l_e / r_c} r_n^{\,2} / r_c \qquad (2.10)$$

The approximate δ formula agrees well with the simulation and experimental results for $r_n / r_c < 0.5$.[62,70] Combining only one-dimensional propagation in the axial x direction in the neck and cavity with regard to the effects of the non-planar wave as length correction factor δ, the transmission loss of a side branch HR with an extended neck mounted on the duct with cross-sectional area S_d can be expressed as:

$$TL = 10 \log_{10} \left[1 + \left(\frac{S_n}{2 S_d} \frac{\tan k(l_n + l_e + \delta) + \left(S_c / S_n \right) \tan k(l_c - \delta)}{1 - \left(S_c / S_n \right) \tan k(l_c - \delta) \tan k(l_n + l_e + \delta)} \right)^2 \right] \qquad (2.11)$$

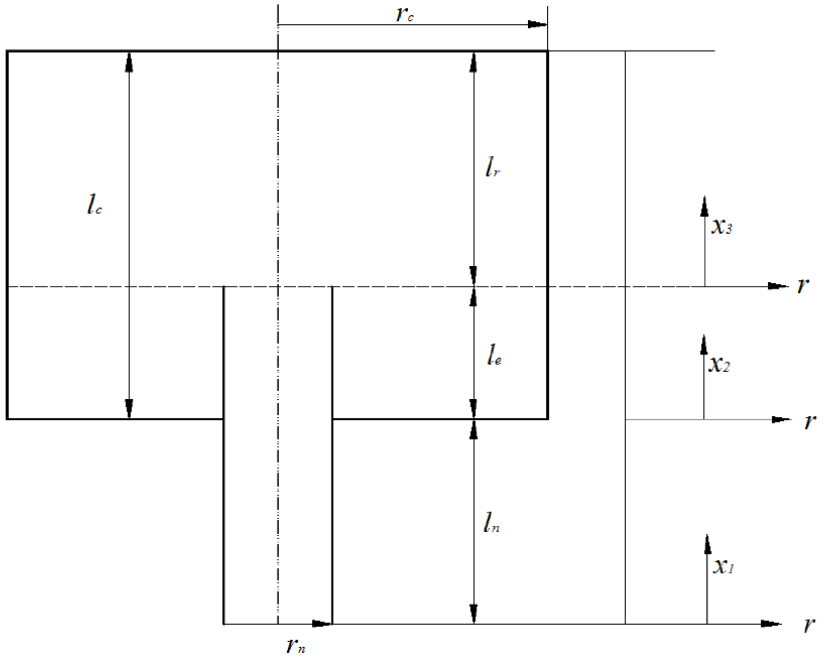

Figure 2.1 Helmholtz resonator with extended neck.

2.1.2 Analytical approach of the HR with a spiral neck

The traditional short neck is replaced by a spiral neck to make the neck as long as possible when there is a space constraint. Meanwhile, the curvature of the spiral neck changes the impedance[71], and it can then be considered equivalent to the traditional straight neck. For these reasons, this kind of HR can improve noise reduction performance at low frequencies within a limited space.

Figure. 2.2(a) illustrates a HR with a spiral neck. The spiral neck can be divided into three parts: two straight tubes of lengths L_I and L_{II} respectively, and the spiral tube, which takes N turns of total length $L_{III} = N*2\pi*R_0$, as shown in Figure. 2.2(b). The cross-section area of these three parts is the constant S_n. The particle velocity along the toroidal axis in the spiral tube is determined by the radial dependence of the sound pressure and the curvature dependence of the sound pressure. However, the radial dependence of the sound pressure is quite small due to the low frequency range considered in this paper. This means that the sound pressure remains the same over the cross-section area.[72] Therefore, the particle velocity is simplified as:

$$v(R_0,\phi) = \frac{-1}{j\omega\rho_0}\frac{1}{R_0}\frac{\partial P}{\partial \phi} \tag{2.12}$$

where P is the sound pressure, ω is the angular frequency, ρ_0 is the air density, ϕ

is the curvature angle, and R_0 is the distance from the point of the curvature center. The curvature changes the impedance of the spiral tube, and it can then be considered equivalent to a straight tube. For the spiral tube with cross-section area S_n and length L_{III} shown in Figure. 2.2(b), the equivalent straight tube with cross-section area S_n' and L_{III}' is expressed as:

$$S_n' = S_n / \sqrt{F}\ , L_{III}' = L_{III}\sqrt{F} \tag{2.13}$$

where $F = 0.5(r_0 / R_0)^2 \Big/ (1-\sqrt{1-(r_0 / R_0)^2})$ is the equivalent coefficient as a result of the curvature in the tube and r_0 / R_0 indicates the abruptness of the bend and its effects on the equivalent coefficient.

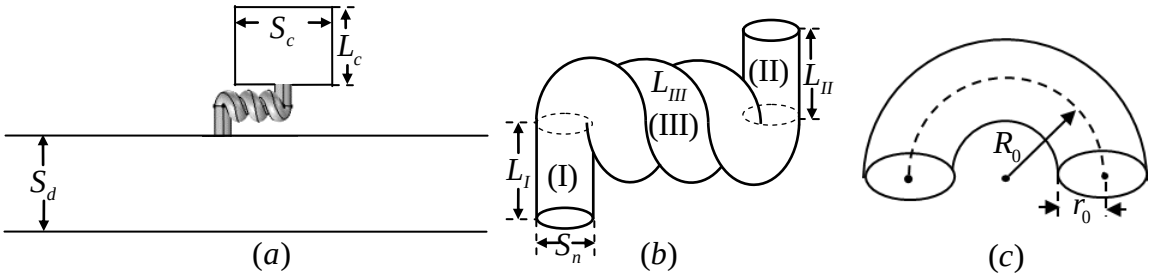

Figure 2.2 (a) a Helmholtz resonator with a spiral neck; (b) the spiral neck with three turns; (c) a section of the curved tube.

The equivalent coefficient F is practically less than unity, which means that the equivalent straight tube has a larger area ($S_n' > S_n$) and a shorter length ($L_{III}' < L_{III}$). The spiral neck could therefore be considered a combination of three connected straight tubes in a theoretical analysis. The equivalent theoretical model of a HR with

a spiral neck is shown in Figure. 2.3.

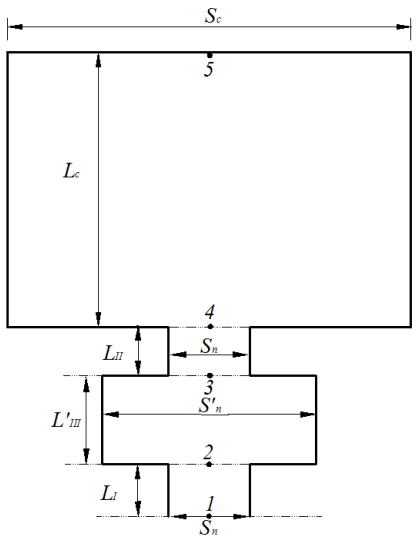

Figure 2.3 The equivalent Helmholtz resonator.

The frequency range considered here is well below the cut-off frequency, so only planar waves propagate in the neck and cavity. The relation of point 1 to point 5 could be obtained through the transfer matrix method[73,74] as:

$$\begin{bmatrix} P_1 \\ \rho_0 S_n u_1 \end{bmatrix} = \begin{pmatrix} \cos(k_0 L_I) & j(\frac{c_0}{S_n})\sin(k_0 L_I) \\ j(\frac{S_n}{c_0})\sin(k_0 L_I) & \cos(k_0 L_I) \end{pmatrix} \begin{pmatrix} \cos(k_0 L'_{III}) & j(\frac{c_0}{S'_n})\sin(k_0 L'_{III}) \\ j(\frac{S'_n}{c_0})\sin(k_0 L'_{III}) & \cos(k_0 L'_{III}) \end{pmatrix}$$
$$\begin{pmatrix} \cos(k_0 L_{II}) & j(\frac{c_0}{S_n})\sin(k_0 L_{II}) \\ j(\frac{S_n}{c_0})\sin(k_0 L_{II}) & \cos(k_0 L_{II}) \end{pmatrix} \begin{pmatrix} \cos(k_0 L_c) & j(\frac{c_0}{S_c})\sin(k_0 L_c) \\ j(\frac{S_c}{c_0})\sin(k_0 L_c) & \cos(k_0 L_c) \end{pmatrix} \begin{bmatrix} P_5 \\ \rho_0 S_c u_5 \end{bmatrix} \tag{2.14}$$

Eq. (2.14) could be simplified as:

$$\begin{bmatrix} P_1 \\ \rho_0 S_n u_1 \end{bmatrix} = \begin{pmatrix} T_{11} & T_{12} \\ T_{21} & T_{22} \end{pmatrix} \begin{bmatrix} P_5 \\ \rho_0 S_c u_5 \end{bmatrix} \tag{2.15}$$

where P_1 , u_1 and P_5 , u_5 are the sound pressures and particle velocities at point 1 and point 5, respectively. Assuming the walls of the cavity are rigid, the particle velocity at point 5 equals zero ($V_5 = 0$). The impedance of HR with a spiral neck could be derived from Eq. (2.15) as:

$$Z_r = \frac{P_1}{u_1 S_n} = \rho_0 \frac{T_{11}}{T_{21}} \tag{2.16}$$

Once the resonator impedance has been obtained, the transmission loss of a side-branch HR with a spiral neck can be described as:

$$TL = 20\log_{10}\left(\frac{1}{2}\left|2 + \frac{\rho_0 c_0}{S_d}\frac{1}{Z_r}\right|\right) \tag{2.17}$$

2.1.3 Comparison of HRs with different types of necks

For a HR with fixed cavity, the effects of the two neck types on transmission loss are each analyzed. The theoretical predictions are compared to the Finite Element Method (FEM) simulation results using commercial software (COMSOL Multiphysics)[75,76]. The HR with an extended neck is shown in Figure. 2.1. The geometries of the HR used here are: cavity length $l_c = 21\,\text{cm}$, cavity radius $r_c = 6.6$ cm, neck radius $r_n = 1\,\text{cm}$, and base neck length $l_n = 8\,\text{cm}$. The cross-section area of the main duct is $S_d = 36\,\text{cm}^2$. The effects of extension length l_e on the transmission loss of the HR are investigated at first.

The transmission loss of a HR with different extension lengths that is analyzed by the modified one-dimensional approach is shown in Figure. 2.4. It can be seen that with the increase in neck extension length, the resonance frequency decreases with a narrower attenuation band. Figure. 2.5 compares the predicted results to the FEM simulation results. It is shown that the modified one-dimensional analytical approach predictions fit well with the FEM simulation results. Note that a 15.08cm change in extension length results in a 22 Hz shift in the resonance frequency, while the resonance frequency of a HR without an extended neck is only 59Hz, as shown in Figure. 2.4. The alteration in resonance frequency is apparent and significant at low frequency range. Furthermore, no change in cavity volume is required for the reduction in resonance frequency.

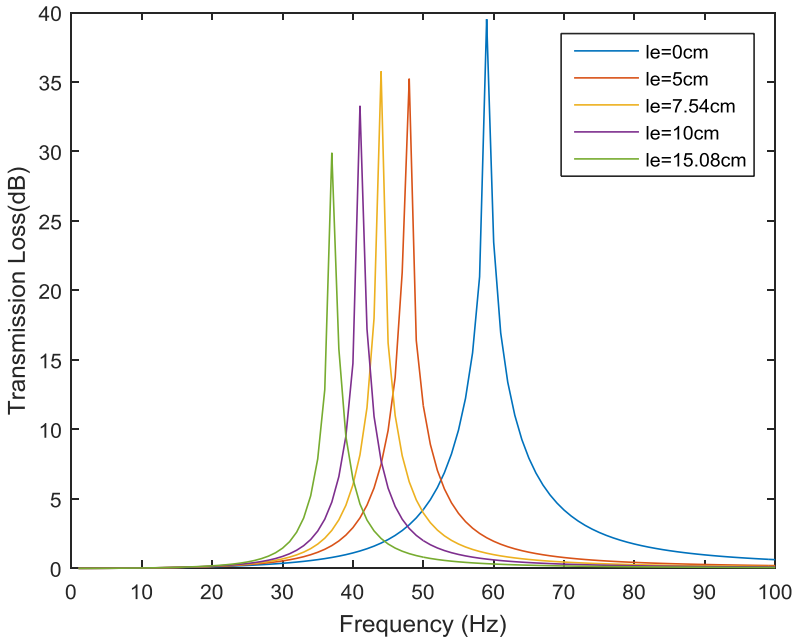

Figure 2.4 Transmission loss of the HR with different extension neck lengths.

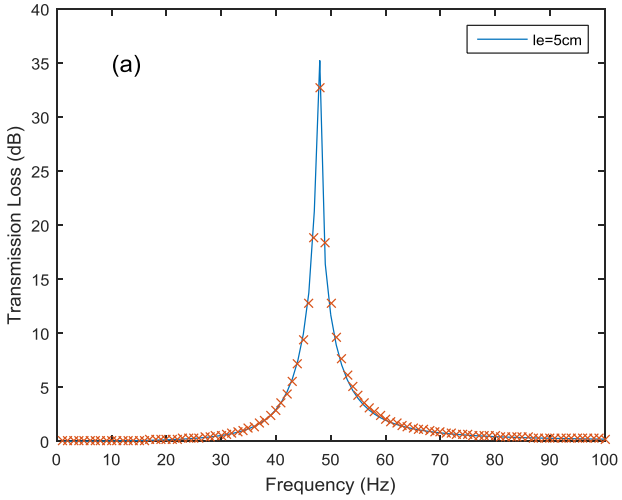
(a)
le=5cm
Transmission Loss (dB)
Frequency (Hz)
0
5
10
15
20
25
30
35
40
0
10
20
30
40
50
60
70
80
90
100

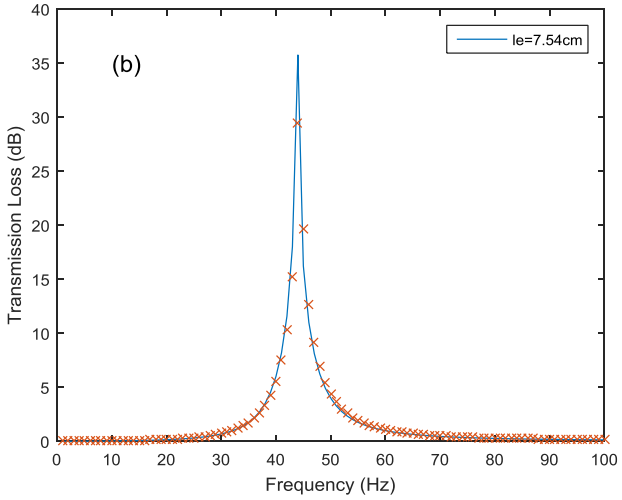
(b)
le=7.54cm
Transmission Loss (dB)
Frequency (Hz)
0
5
10
15
20
25
30
35
40
0
10
20
30
40
50
60
70
80
90
100

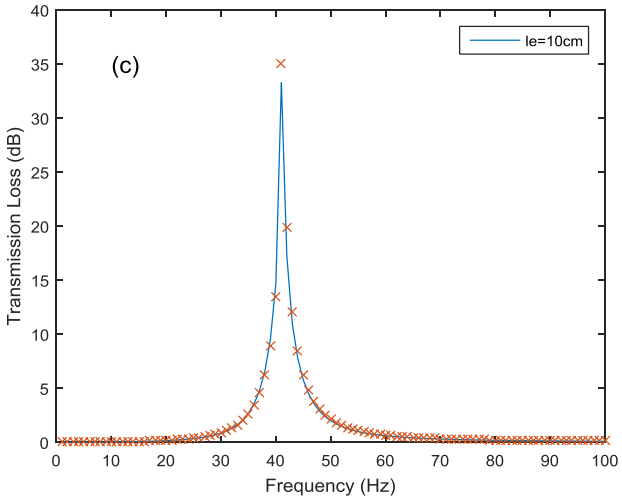
(c)
le=10cm
Transmission Loss (dB)
Frequency (Hz)
0
5
10
15
20
25
30
35
40
0
10
20
30
40
50
60
70
80
90
100

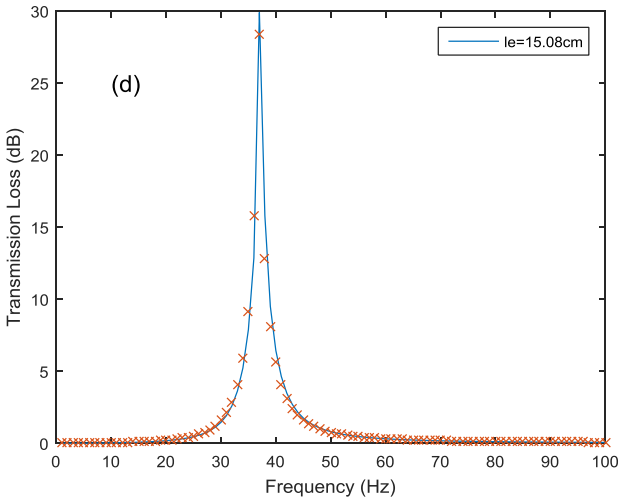

Figure 2.5 Comparison of the analytical approach predictions and the FEM simulation for different extension neck lengths (solid lines represent the theoretical prediction, and dotted crosses represent the FEM simulation results).

Selamet and Lee[62] experimented on the Helmholtz resonator with different extension lengths. The geometries of their experimental HR are: $l_v = 20.32\,\text{cm}$, $r_v = 7.62\,\text{cm}$, $r_n = 2\,\text{cm}$, $l_n = 8.5\,\text{cm}$, and $S_d = 18.49\,\text{cm}^2$, which are different from the geometries used in this paper. Figure. 2.6 illustrates a good agreement between the predictions of the modified one-dimensional analytical approach and the results of Selamet and Lee's experiment. Their experimental results are directly extracted from their publication to verify the accuracy of the modified one-dimensional method. Similarly, a 15cm extension length into the cavity results in a 33 Hz shift in resonance frequency without a change in the cavity volume, which is distinct when compared to the resonance frequency of 98 Hz for a HR without the extended neck.

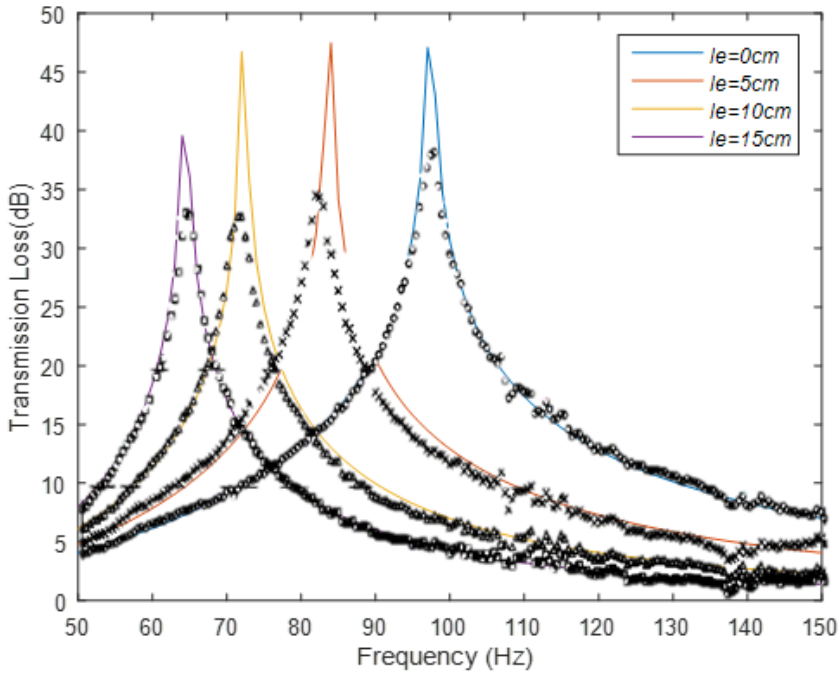

Figure 2.6 Comparison of the modified one-dimensional analytical approach predictions and the experiment for a Helmholtz resonator with different extension lengths (the dotted symbols represent the experiment's results).

The HR with a spiral neck is shown in Figure. 2.2. The geometries of the HR are: cavity length $l_c = 21\,\text{cm}$, cavity radius $r_c = 6.6\,\text{cm}$, fixed neck radius $r_n = 1\,\text{cm}$, straight tube length $L_I = L_{II} = 4\,\text{cm}$, $R_0 = 1.2\,\text{cm}$, and length of spiral tube $L_{III} = N * 2\pi R_0 = N * 7.54\,\text{cm}$ (length of each turn is $7.54\,\text{cm}$). The cross-section area of the main duct is $S_d = 36\,\text{cm}^2$. The N is an integer here, and it indicates the turns of the spiral tube. When N equals zero, this means that the spiral tube is non-existent and the neck only contains two straight tubes, which actually make it a traditional straight neck. Besides, the spiral tube could be treated as equivalent to a

straight tube in a theoretical model, as shown in Figure. 2.3, when $N \neq 0$.

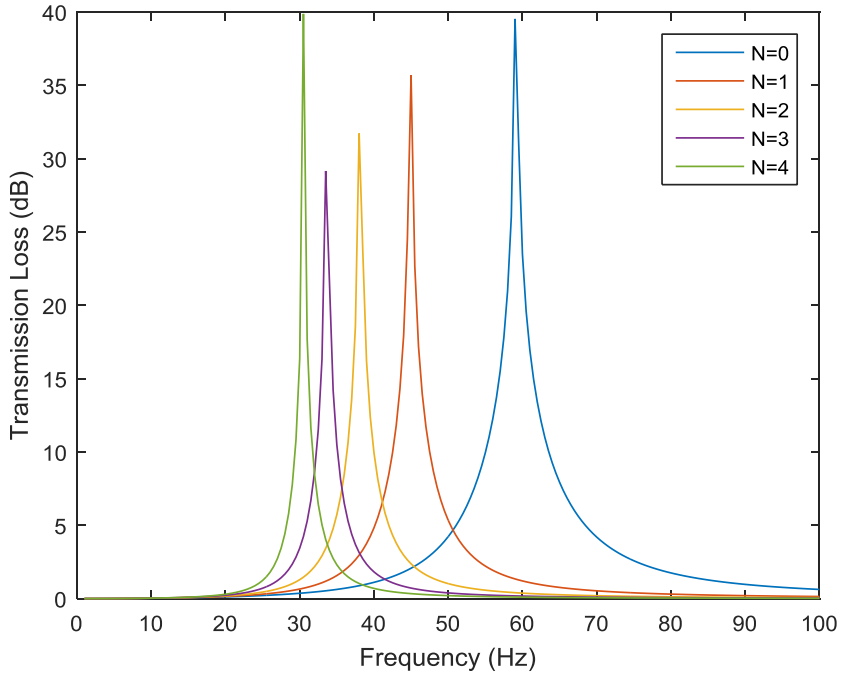

Figure 2.7 Transmission loss of a Helmholtz resonator with a spiral neck.

The predicted transmission loss of a HR with different turn number ($N = 0,1,2,3,4$) is exhibited in Figure. 2.7. Added spiral turns will decrease the resonance frequency and narrow the attenuation band, as well. Figure. 2.8 compares the prediction results with the FEM simulation results, and the prediction results are in good agreement with the FEM simulation results. The resonance frequency of the HR without a spiral neck ($N = 0$) is 59Hz. However, the resonance frequency decreases to 45Hz, 38Hz, 34Hz, and 30 Hz for $N = 1,2,3,4$, respectively. This also means that a spiral tube with 30.16cm ($N = 4$) change results in a 29Hz decrease in the resonance frequency

without changing the cavity volume. The effects of a spiral tube on the resonance frequency are obvious, especially at a low frequency range. No change of cavity volume is required for the reduction in the resonance frequency. Moreover, more turns will result in a much lower resonance frequency. When the total neck length is comparable to the wavelength of oscillation, for instance $N = 4$ in this paper, the peak amplitude will increase due to the long neck length.

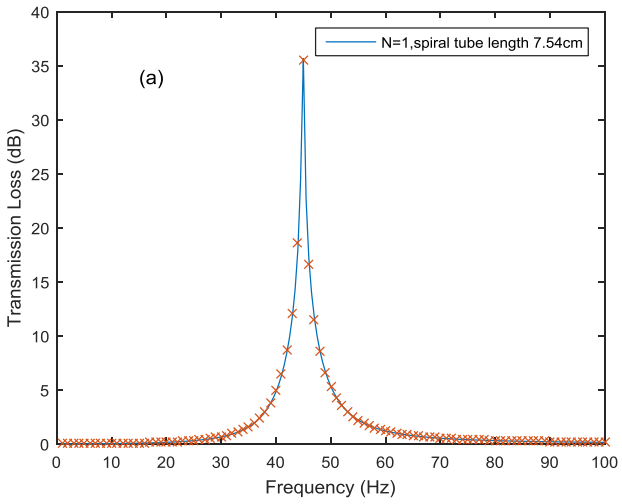

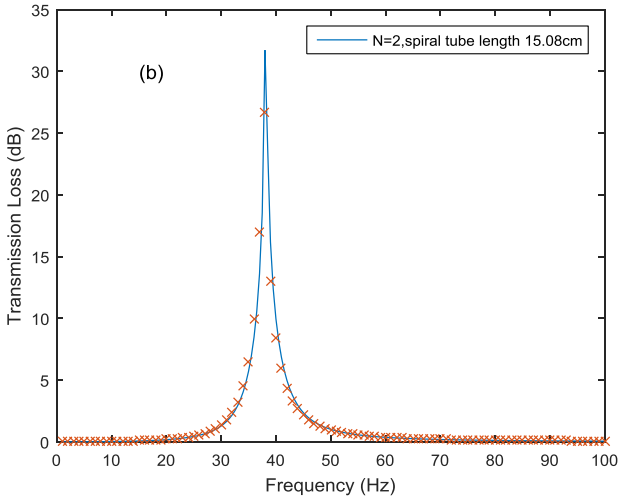

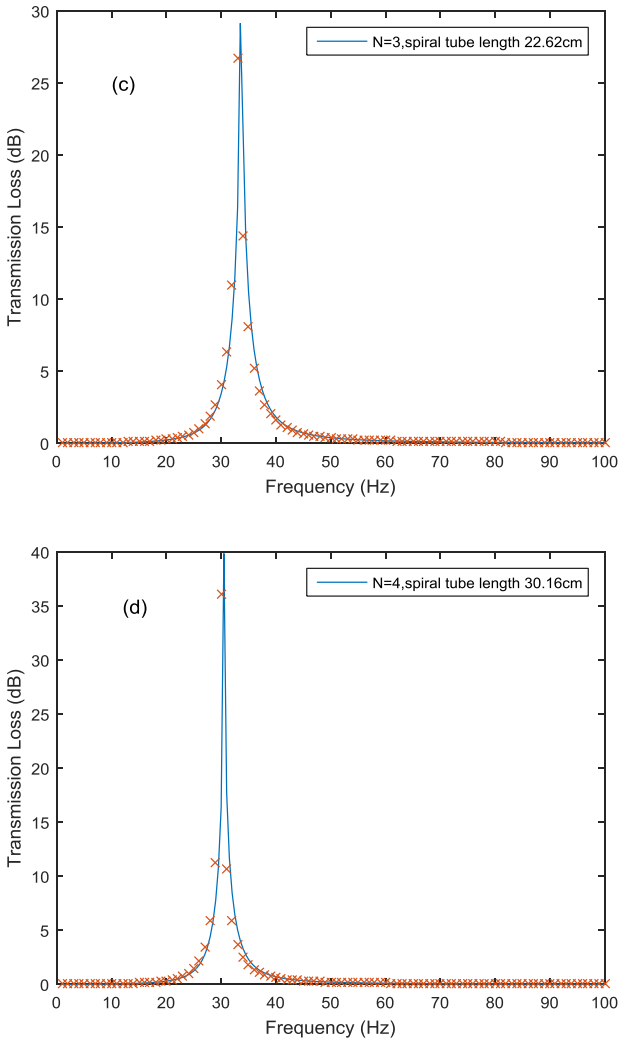

Figure 2.8 Comparison of predictions with FEM simulation for different spiral tube lengths (solid lines represent the theoretical prediction, and dotted crosses represent the FEM simulation results).

As described above, the cavity geometries of HRs with different neck types are the same, as are as the neck radiuses. The relation of the base neck length in Figure. 2.1 to the length of the two straight tubes in Figure. 2.2 can be expressed as: $l_n = L_I + L_{II}$. This means that the resonance frequency of the HR without the extended neck or the

spiral neck is 59Hz. Figure. 2.9 compares the amount of transmission loss between the HRs with different neck types. The results show that a 7.54cm and a 15.08cm extension length change or spiral tube length change result in a 14Hz and a 21Hz decrease in the resonance frequency, respectively. The effect of the extension neck length on resonance frequency is nearly the same as the effect of the spiral tube length on resonance frequency.

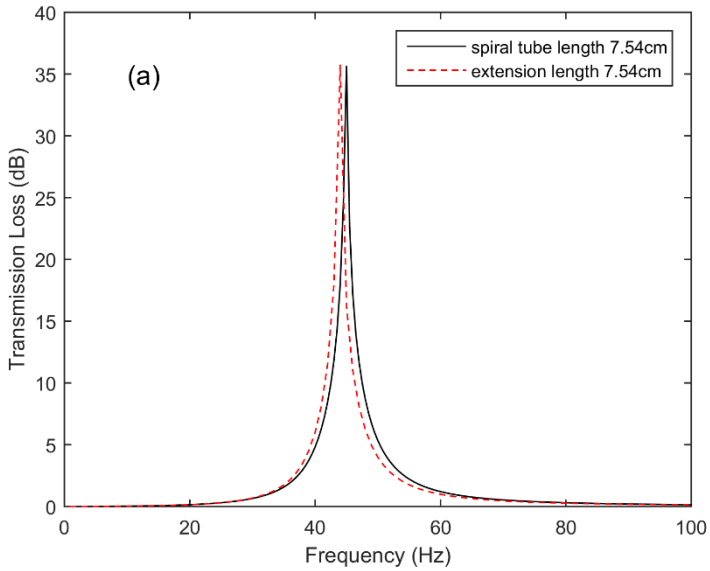

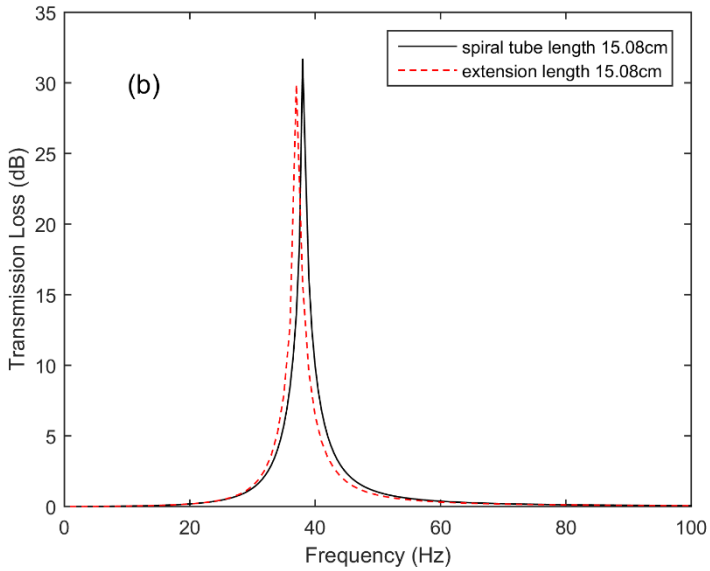

Figure 2.9 Comparison of the HR with an extended neck and the HR with a spiral neck (dashed lines represent the HR with an extended neck, and solid lines represent the HR with a spiral neck).

The extension length could be changed flexibly to satisfy the required resonance frequency, but it is limited to the cavity length. For the spiral tube, there is no limit to the number of possible turns. The HR with a spiral neck can shift the resonance frequency to a much lower extent by having more turns added. For instance, the spiral tube with $N = 4$ means that the length of the tube comes to 30.16cm, which is much longer than the extension length limitation. However, the length of each turn is invariable at $2\pi R_0$. For a certain designed resonance frequency of HR, the utilization of the extended neck or the spiral neck can reduce the cavity volume. The acoustic characteristics of HRs with these two different neck types have a potential application in noise control, especially at low frequencies within a constrained space.

2.2 Noise attenuation capacity of a Helmholtz resonator

The transmission loss index is indeed a major index and has been widely used to assess the acoustic transmission performance in the frequency domain. However, almost all researches concentrate on the shapes of the transmission loss curve while ignoring the area under the transmission loss curve. The noise attenuation capacity index defined as the integral of transmission loss in the frequency domain is therefore proposed to be one of the key parameters to evaluate HR's noise attenuation performance. The theoretical formula of a HR's noise attenuation capacity is first derived in this thesis.

2.2.1 The classical lumped approach of a Helmholtz resonator

The classical equivalent spring-mass system is adopted here to reveal the noise attenuation capacity of the HR. For the sake of completeness, a brief review of the classical lumped approach of a HR is appropriate here. A mechanical analogy of a single HR is illustrated in Figure. 2.10. The mass of air in the neck $M_m = \rho_0 S_n l_n'$ is driven by an external time-harmonic sound pressure force $F_e = S_n p_0 e^{j\omega t}$ and the cavity is regarded as a massless spring with stiffness $K_m = \rho_0 c_0^2 S_n^{\ 2} / V_c$ (where p_0 is the oscillation sound pressure, ρ_0 is air density, c_0 is the speed of sound in the air , l_n' and S_n are the neck's effective length and area respectively, ω is the angular frequency, and V_c is the cavity volume). The damping coefficient R_m of a HR is

mainly caused by viscous dissipation through the neck, which is determined by acoustic screen across the area of the neck. By applying the Newton's second law of motion to the one degree of freedom HR, the oscillatory differential equation can be expressed as[52]:

$$M_m \frac{d^2x}{dt^2} + R_m \frac{dx}{dt} + K_m x = S_n p_0 e^{j\omega t} \tag{2.18}$$

where x is the displacement of the mass, $v = dx/dt$ represents the velocity of the mass.

Owing to the different concerns between an acoustic system and a mechanical system, Eq. (2.18) should be rewritten in the form of volume velocity $U = vS_n$ as:

$$M_a \frac{dU}{dt} + R_a U + C_a \int U dt = p_0 e^{j\omega t} \tag{2.19}$$

where $M_a = M_m / S_n^{\,2}$, $R_a = R_m / S_n^{\,2}$ and $C_a = S_n^{\,2} / K_m$ represent the sound mass, sound resistance and sound capacitance respectively in analogy of a circuit. The impedance of the HR can be derived from the solution of Eq. (2.19) as:

$$Z_r = \frac{p}{U} = R_a + j(\omega M_a - \frac{1}{\omega C_a}) \tag{2.20}$$

It is therefore that the resonance frequency of the HR can be derived from Eq. (2.20) and be expressed as $f_0 = \sqrt{1/M_a C_a}\,/2\pi = c_0\sqrt{S_n / l_n' V_c}\,/2\pi$. Once the impedance is obtained, the transmission loss of a side-branch HR mounted on a duct with cross-sectional area S_d can be expressed as:

$$TL = 20\log_{10}(\frac{1}{2}\left|2 + \frac{\rho_0 c_0}{S_d}\frac{1}{Z_r}\right|) \tag{2.21}$$

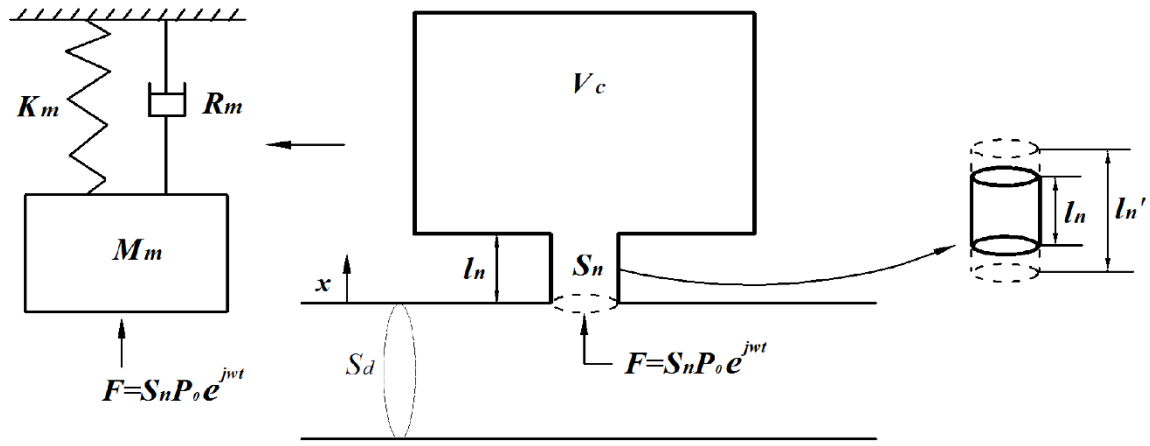

Figure 2.10 Mechanical analogy of a Helmholtz resonator.

2.2.2 Theoretical derivation

The transmission loss index is mainly used to evaluate the acoustic transmission performance in the frequency domain. However, it cannot provide a quantitative characteristic of the noise attenuation band. It is therefore that this paper proposes the noise attenuation capacity index as one of the key parameters to evaluate the HR's noise attenuation performance quantitatively and distinctly. The noise attenuation capacity C_{TL} which is defined as the integral of transmission loss in the frequency domain, could be expressed as:

$$C_{TL} = \int TL df = \frac{1}{2\pi}\int TL d\omega = \frac{1}{2\pi}\int 20\log_{10}\left(\frac{1}{2}\left|2+\frac{\rho_0 c_0}{S_d}\frac{1}{Z_r}\right|\right)d\omega \qquad (2.22)$$

The effect of viscous dissipation through the neck is ignored for simplicity. It is therefore that R_a in Eq. (2.20) equals zero. Then, substituting Eq. (2.20) into Eq. (2.22) gives:

$$\int TL d\omega = \int 10\log_{10}\left((B\omega^2 - C)^2 + A^2\omega^2\right)d\omega - \int 10\log_{10}(B\omega^2 - C)^2 d\omega$$

(2.23)

where $A = \rho_0 c_0 / 2S_d$, $B = \rho_0 l_n' / S_n$ and $C = \rho_0 {c_0}^2 / V_c$ are constants related to geometries of the HR and the duct. The antiderivative of the first term on the right-hand side of Eq. (2.23) can be solved as:

$$\begin{aligned}&\int 10\log_{10}\left((B\omega^2 - C)^2 + A^2\omega^2\right)d\omega = \int 10\log_{10}\left(B^2(\omega^2 + a)(\omega^2 + b)\right)d\omega \\ &= \int 10\log_{10}B^2 d\omega + \int 10\log_{10}(\omega^2 + a)d\omega + \int 10\log_{10}(\omega^2 + b)d\omega\end{aligned} \tag{2.24}$$

and

$$\begin{cases} \int 10\log_{10}B^2 d\omega = 20\omega\log_{10}B \\ \int 10\log_{10}\left((\omega^2 + a)\right)d\omega = 10\left[\dfrac{\omega\ln(\omega^2 + a)}{\ln 10} - \dfrac{2[\omega - \sqrt{a}\arctan(\omega/\sqrt{a})]}{\ln 10}\right] \\ \int 10\log_{10}\left((\omega^2 + b)\right)d\omega = 10\left[\dfrac{\omega\ln(\omega^2 + b)}{\ln 10} - \dfrac{2[\omega - \sqrt{b}\arctan(\omega/\sqrt{b})]}{\ln 10}\right] \end{cases} \tag{2.25}$$

where a and b should satisfy the requirements of $a + b = (A^2 - 2BC)/B^2$ and $ab = C^2/B^2$ simultaneously.

The antiderivative of the second term on the right-hand side of Eq. (2.23) can be derived as:

$$\begin{aligned}&\int 10\log_{10}\left((B\omega^2 - C)^2\right)d\omega = \int 10\log_{10}B^2 d\omega + \int 10\log_{10}(\omega^2 - c)^2 d\omega \\ &= 20\omega\log_{10}B + 10\left[\frac{\omega\ln(\omega^2 - c)^2}{\ln 10} - \frac{4\omega - \sqrt{c}\left(\ln\left(\dfrac{\omega + \sqrt{c}}{\sqrt{c}}\right)^2 - \ln\left(\dfrac{\omega - \sqrt{c}}{\sqrt{c}}\right)^2\right)}{\ln 10}\right]\end{aligned} \tag{2.26}$$

Combining Eq. (2.24), Eq. (2.25) and Eq. (2.26), Eq. (2.24) can be rearranged as:

$$\int TLd\omega = \frac{10}{\ln 10}\left[\omega \ln\frac{(\omega^2+a)(\omega^2+b)}{(\omega^2-c)^2} + 2\sqrt{a}\arctan(\omega/\sqrt{a}) + 2\sqrt{b}\arctan(\omega/\sqrt{b}) - \sqrt{c}\ln\frac{(\omega+\sqrt{c})^2}{(\omega-\sqrt{c})^2}\right] \tag{2.27}$$

According to Eq. (2.27), the integral of transmission loss in the circular frequency domain can be calculated as:

$$\int_0^\infty TLd\omega = \frac{10\pi}{\ln 10}(\sqrt{a}+\sqrt{b}) = \frac{10\pi}{\ln 10}\frac{A}{B} = \frac{5\pi}{\ln 10}\frac{c_0 S_n}{S_d l_n'} \tag{2.28}$$

It should be noted that the quantities of a and b do not need to be solved to obtain the $\sqrt{a}+\sqrt{b}$. The quantity of $\sqrt{a}+\sqrt{b}$ can be obtained according to the relation of $(\sqrt{a}+\sqrt{b})^2 = (a+b)+2\sqrt{ab} = (A/B)^2$ (where a and b should satisfy the requirements of $a+b=(A^2-2BC)/B^2$ and $ab=C^2/B^2$ simultaneously).

It is therefore that the noise attenuation capacity C_{TL} is derived as:

$$C_{TL} = \int_0^\infty TLdf = \frac{1}{2\pi}\int_0^\infty TLd\omega = \frac{5}{2\ln 10}\frac{c_0 S_n}{S_d l_n'} \tag{2.29}$$

It can be seen from Eq. (2.29) that the noise attenuation capacity C_{TL} in the frequency domain is only related to the geometries of the neck and the cross-sectional area of the duct. The cavity volume has no effects on the HR's noise attenuation capacity. Similar to the resonance frequency, Eq. (2.29) provides a distinct parameter to evaluate the HR's noise attenuation band quantitatively. Moreover, Eq. (2.29) indicates that the noise attenuation bandwidth and peak attenuation amplitude are complimentary to each other. There is no trick to noise control. It points out distinctly the impossibility for some struggles to obtain a broader noise attenuation band with

higher peak amplitude for a determined side-branch HR system. The C_{TL} can therefore be considered as one of the main acoustic characteristics of a HR and be taken into consideration in noise control optimization and HR design.

2.2.3 Numerical simulation results

The three-dimensional FEM simulation using commercial software (COMSOL Multiphysics)[75,76] is used to validate the correctness of the proposed theoretical formula of noise attenuation capacity. As low frequencies are the main concerns here, the frequency range considered here is well below the duct's cutoff frequency. Hence, only planar wave is assumed to propagate through the duct in all the FEM simulations. An oscillation sound pressure at a magnitude of $P_0 = 1$ Pa is applied at the beginning of the duct. An anechoic termination is applied at the end of the duct to avoid reflected waves.

Three different HRs with fixed neck geometries $l_n = 4\,\text{cm}$, $S_n = \pi\,\text{cm}^2$ and three different cavity volumes $V_1 = 392.04\pi\,\text{cm}^3, V_2 = 479.16\pi\,\text{cm}^3$ and $V_3 = 653.4\pi\,\text{cm}^3$ are used here, annotated as HR1, HR2 and HR3 respectively. The cross-sectional area of the main duct is set as $S_d = 36\,\text{cm}^2$. The acoustic FEM models of these three side-branch HRs are built separately, as illustrated in Figure. 2.11. To ensure the accuracy, a fine mesh spacing of no more than 2.2 cm is maintained for these models.

The mesh divides these three models more than 8000 triangular elements. The maximum element is observed in the duct with a side length of around 2.2 cm; the minimum element can be observed in both the neck-duct interface and the neck-cavity interface with a side length of around 0.16 cm.

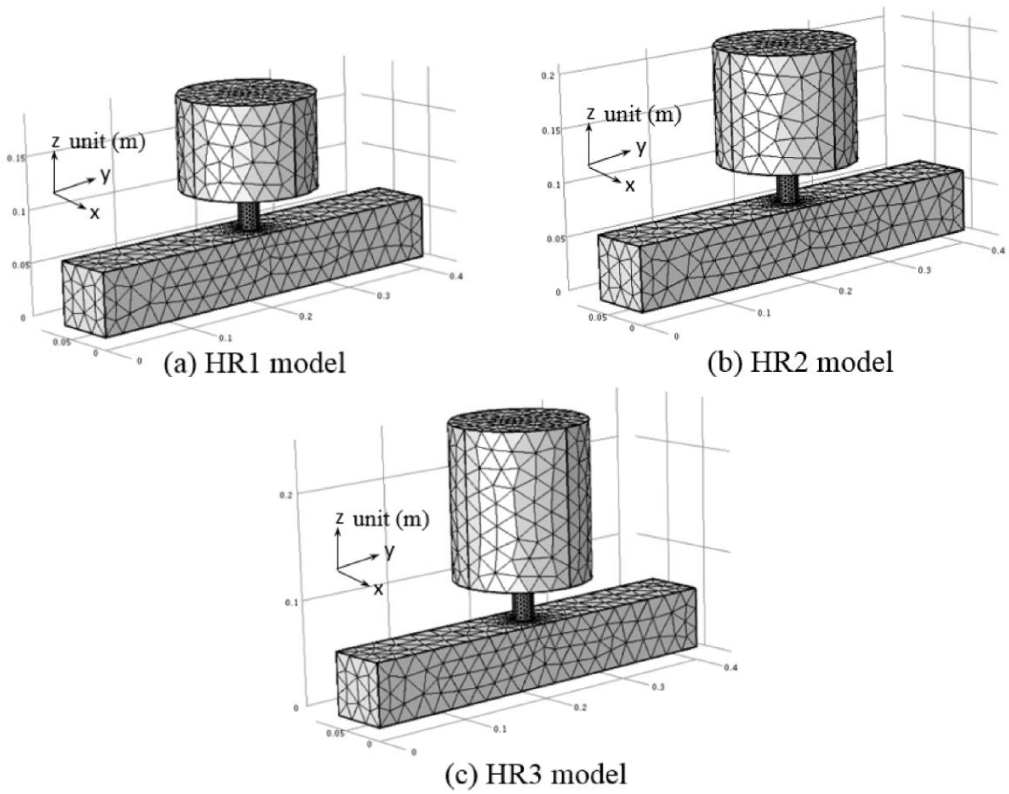

Figure 2.11 The acoustic FEM models of side-branch HRs with respect to different HRs: (a) HR1 model, (b) HR2 model, (c) HR3 model.

The comparison of theoretical predicted transmission loss and the FEM simulation results with respect to different HRs are illustrated in Figure. 2.12, and the predicted results are in good agreement with the FEM simulation results. The solid lines represent the theoretical predictions, and dashed crosses represent the FEM

simulation results. It can also be observed that the resonance frequency of the HR decreased with the increasing cavity volume, as a well-known principle. However, the normalized predicted transmission losses of these three models are almost the same by normalizing to their corresponding resonance frequency, as demonstrated in Figure. 2.13. It indicates that the cavity volume has no effects on C_{TL}.

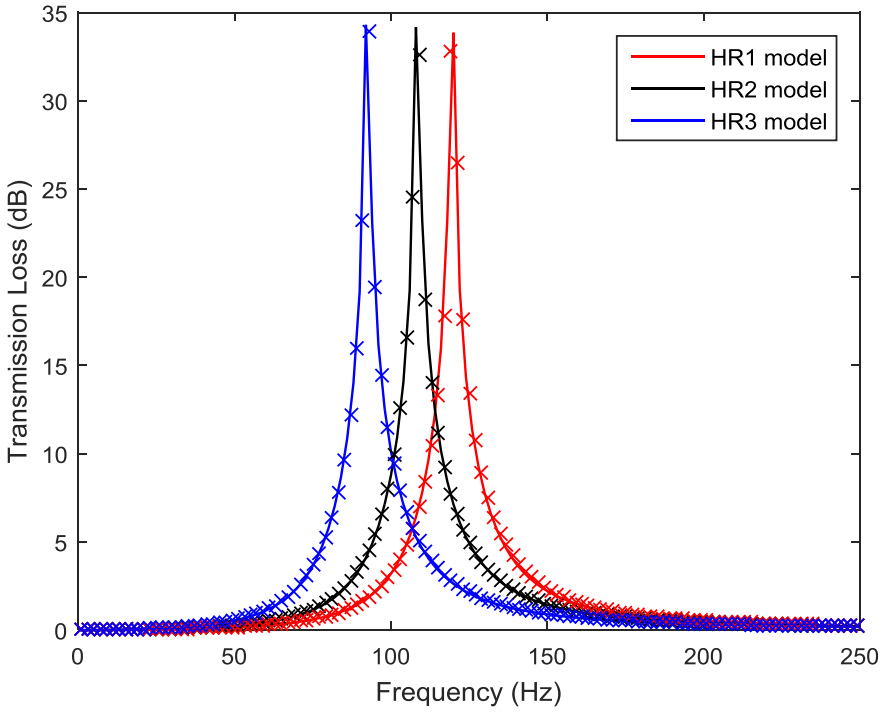

Figure 2.12 Comparison of theoretical predictions and the FEM simulation results with respect to different HRs.

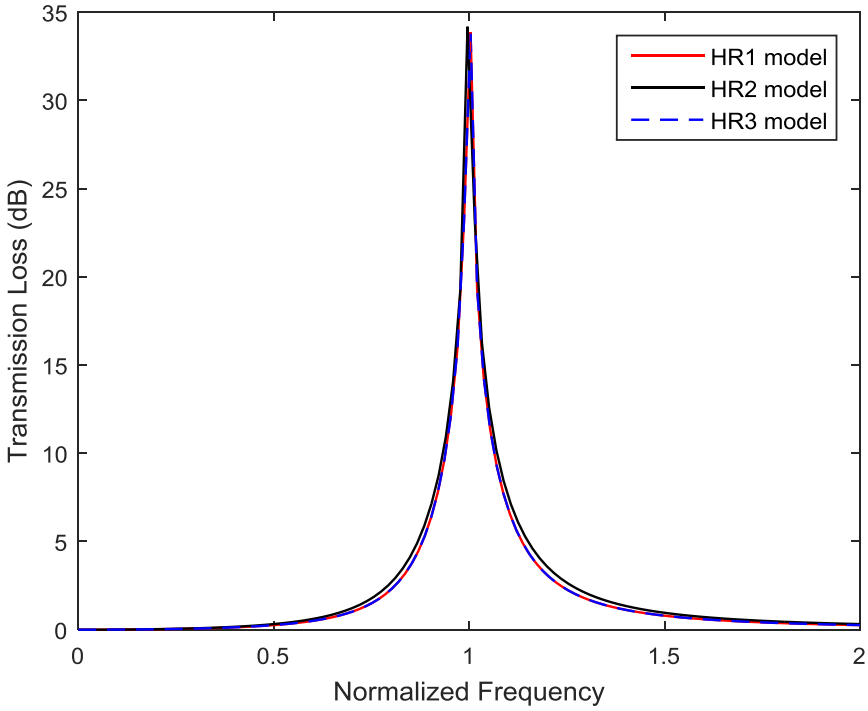

Figure 2.13 Normalized transmission loss of different HRs.

The acoustic FEM models of the identical HR mounted on ducts in respect of different cross-sectional areas are demonstrated in Figure. 2.14, annotated as Sd1 model, Sd2 model and Sd3 model corresponding to different duct's cross-sectional areas $S_{d1} = 25$ cm^2, $S_{d2} = 36$ cm^2 and $S_{d3} = 64$ cm^2 respectively. Similar to aforementioned acoustic FEM models, a fine mesh system is conducted and it is not described in details here for simplicity. Figure. 2.15 compares the transmission loss of these models between the theoretical predictions and FEM simulation results. The solid lines represent the theoretical predictions, and dashed crosses represent the FEM simulation results. The theoretical predicted results agree well with the FEM simulation results. It can be observed that the resonance frequencies of these

three models remain unchanged due to the same HR used here. However, a much broader band with higher peak can be obtained through the decrease of the duct's cross-sectional area.

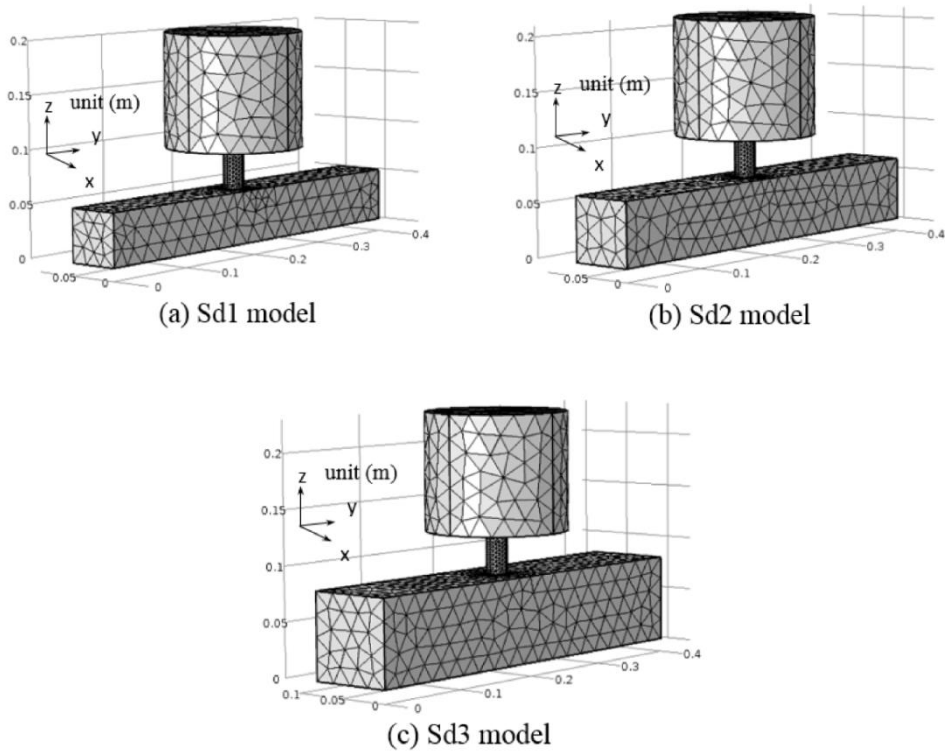

Figure 2.14 The acoustic FEM models of the identical HR mounted on different ducts with respect to different cross-sectional areas: (a) Sd1 model, (b) Sd2 model, (c) Sd3 model.

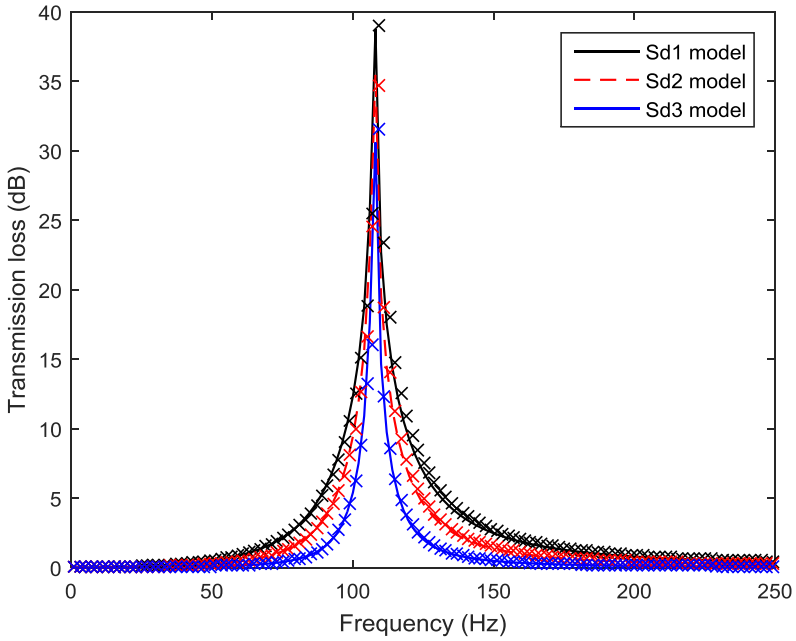

Figure 2.15 The transmission loss of the identical HR mounted on ducts with different cross-sectional areas.

Six different HRs with fixed cavity volume $V = 479.16\pi$ cm^3 and different neck geometries are installed on the duct of cross-sectional area $S_d = 36\,\text{cm}^3$ separately. The acoustic FEM models are exhibited in Figure. 2.16. The models annotated as ln1 model, ln2 model and ln3 model are corresponding to different necks with fixed cross-sectional area $S_n = \pi$ cm^2 and different neck lengths $l_{n1} = 2$ cm, $l_{n2} = 4$ cm and $l_{n3} = 8$ cm respectively. The models annotated as Sn1 model, Sn2 model and Sn3 model are corresponding to necks with fixed length $l_n = 4$ cm and different cross-sectional areas $S_{n1} = 0.36\pi$ cm^2, $S_{n2} = \pi$ cm^2 and $S_{n3} = 2.25\pi$ cm^2 respectively. It should be noted that an identical model is named after two different names as ln2 model and Sn2 model in order for the convenience of investigations

here.

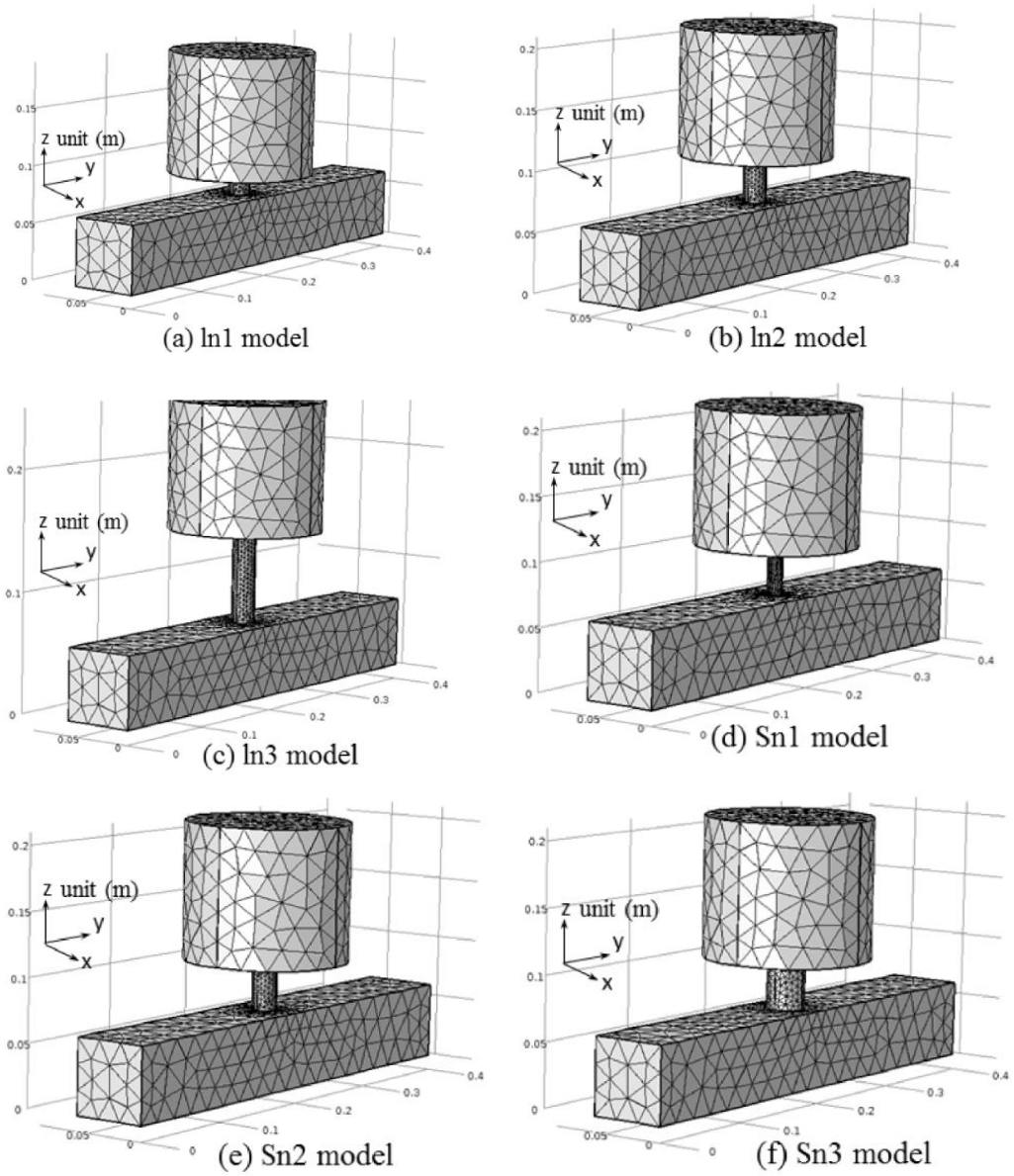

Figure 2.16 The acoustic FEM models of side-branch HRs in respect of different neck geometries: (a) ln1 model, (b) ln2 model, (c) ln3 model, (d) Sn1 model, (e) Sn2 model, (f) Sn3 model.

Figure. 2.17(a) compares the transmission loss between theoretical predictions and

FEM simulation results with respect to different neck lengths. The comparison of theoretical predicted results and the FEM simulation results in respect of different cross-sectional areas of necks are demonstrated in Figure. 2.17(b). The predicted results fit well with FEM simulation results in both Figure. 2.17(a) and Figure. 2.17(b). It can be observed in Figure. 2.17(a) that the increased neck length will decrease HR's resonance frequency as well as the bandwidth. Whereas, a broader bandwidth compromised with a higher resonance frequency can be obtained by increasing the cross-sectional area of the neck, as illustrated in Figure. 2.17(b). The changes in the resonance frequency of a HR is also a well-known principle. It is therefore that the concerns here focus on the noise attenuation bandwidth. The normalized predicted transmission losses of these models are demonstrated in Figure. 2.18(a) and Figure. 2.18(b) corresponding to variations in neck length and neck's cross-sectional area respectively. A more obvious change of noise attenuation bandwidth due to the geometries of neck can be observed in Figure. 2.18.

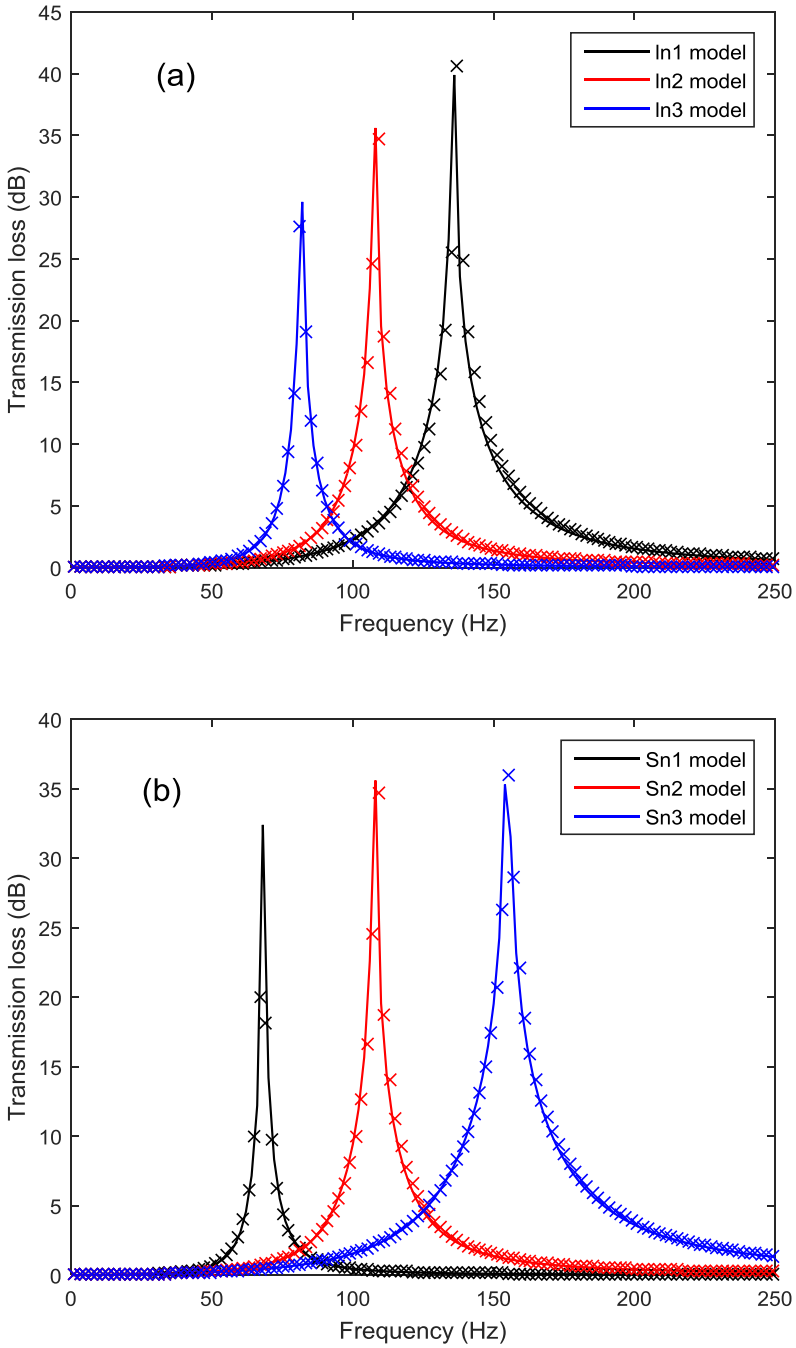

Figure 2.17 Comparison of theoretical predictions and the FEM simulation results with respect to different HRs (solid lines represent the theoretical predictions, and dashed crosses represent the FEM simulation results).

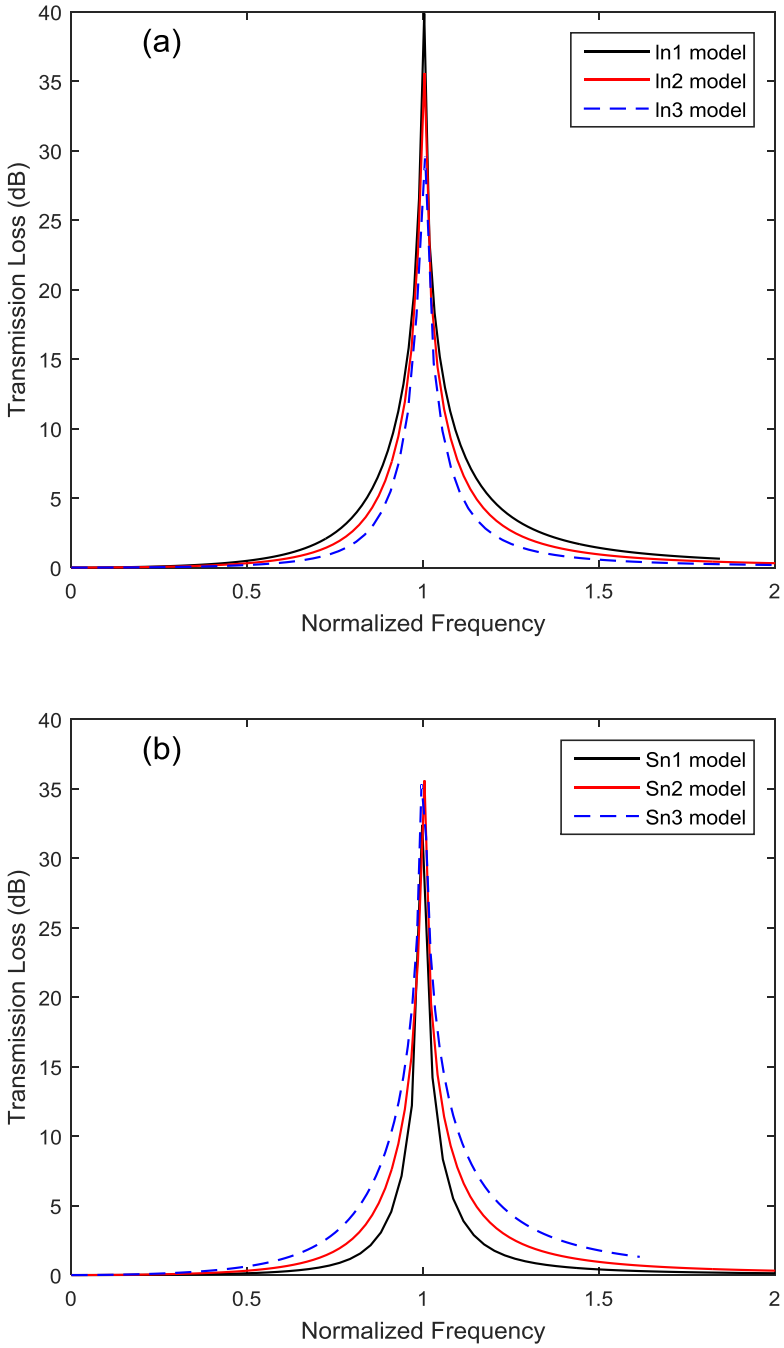

Figure 2.18 Normalized transmission loss of different HRs.

The aforementioned models imply the correctness of proposed Eq. (2.29). Furthermore, the noise attenuation capacity C_{TL} of those models above is exhibited

in Table 2.1. It can be observed from Table 2.1 that the relative errors between the FEM simulation results and calculated values of Eq. (2.29) are less than 6%, 6.1% and 2.5% in the frequency ranges of 0~250 Hz, 0~350 Hz and 0~1000 Hz respectively. The transmission loss of ln1 model and Sn3 model do not approach zero at 250 Hz as demonstrated in Figure. 2.17. It is therefore that the chosen frequency range is 0~350 Hz rather than 0~250 Hz for the last six models. The results indicate that correctness of the C_{TL} calculated by Eq. (2.29) .The C_{TL} is only related to the geometries of the neck and the duct's cross-sectional area. The cavity volume of the HR has no effects on the C_{TL}. Similar to the significance of HR's resonance frequency, the proposed Eq. (2.29) for C_{TL} should therefore be considered as one of the main acoustic characteristics of a HR. It provides a distinct parameter to evaluate the HR's noise attenuation band quantitatively and illuminates the limitations in HR's noise control applications. Furthermore, it can be extended to other research areas related to HR, for instance notch filters[77] and metamaterials[79-81].

Table 2.1 Relative error between the FEM simulation result and value of Eq.(2.29)

		Models					
		HR1 model	HR2 model	HR3 model	Sd1 model	Sd2 model	Sd3 model
C_{TL}	FEM (0~250 Hz)	568.47	568.25	569.24	817.96	568.47	325.64
	Eq.(2.29)		603.58		869.15	603.58	339.51
	Relative error	5.8%	5.9 %	5.7%	5.9%	5.8%	4%
	FEM (0~1000 Hz)	589.76	590.2	589.69	848.17	590.2	331.52
	Eq.(2.29)		603.58		869.15	603.58	339.51
	Relative error	2.3%	2.2%	2.3%	2.4%	2.2%	2.4%
		Models					
		ln1 model	ln2 model	ln3 model	Sn1 model	Sn2 model	Sn3 model
C_{TL}	FEM (0~350 Hz)	902.17	575.1	334.83	244.51	575.1	1130.4
	Eq.(2.29)	958.63	603.58	346.74	242.43	603.58	1202.2
	Relative error	5.9%	4.7%	3.4%	0.9%	4.7%	6%
	FEM (0~1000 Hz)	935.89	590.2	340.32	248.36	590.2	1185.3
	Eq.(2.29)	958.63	603.58	346.74	242.43	603.58	1202.2
	Relative error	2.4%	2.2%	1.9%	2.4%	2.2%	1.4%

2.3 Summary

In order to improve the noise attenuation performance of the HR at low frequencies with a constrained space. This chapter presents theoretical and numerical studies of a HR with an extended neck and a HR with a spiral neck. With the increasing of the extension length or the spiral neck length, resonance frequency decreases significantly. An identical change in the extension neck length or the spiral neck length will produce the same decrease in resonance frequency. It is clear that a 22Hz decrease in resonance frequency is obtained without changing the cavity volume, a significant difference from the resonance frequency of 59Hz that exists for HRs without these two types of necks. For a certain designed resonance frequency of HR, the utilization of the extended neck or the spiral neck can reduce the cavity volume. The acoustic characteristics of HRs with these two different neck types have a potential application in noise control at low frequencies within a constrained space.

The noise attenuation capacity of the HR is proposed and the theoretical formula of it has been derived theoretically. The noise attenuation capacity is defined as the integral of transmission loss in the frequency domain. The effects of the neck length, cross-sectional area of the neck, cavity volume and cross-sectional area of the duct on C_{TL} are analyzed theoretically and numerically. The C_{TL} is only related to the geometries of the neck and the cross-sectional area of the duct. The cavity volume has no effects on the C_{TL}. Similar to the significance of the HR's resonance frequency,

the proposed theoretical formula of C_{TL} should therefore be considered as one of the main acoustic characteristics of the HR. It provides a distinct parameter to evaluate the HR's noise attenuation band quantitatively and illuminates the limitations in HR's noise control applications. It is an important supplement to the theoretical studies and engineering applications of HRs.

Chapter 3

Different Helmholtz resonator array configurations

A dual HR consisting of two HRs connected in series (neck-cavity-neck-cavity) could be considered as a serial HR array. Two HRs mounted on the same cross-section of the duct constitute a parallel HR array. A lined HR array is composed of two HRs installed on the longitudinal direction of the duct. Since HR is reactive silencer without energy consumption, the noise attenuation capacity of different HR array configurations is evaluated based on the concept of the noise attenuation capacity. On the basis of low frequency range of interest here, the dimensions of HRs considered here are significant small compared to the wavelengths. It is therefore that the evanescent high-order modes can be considered by introducing an end correction factor to improve the accuracy of the classical lumped approach. The effect of viscous dissipation through the necks will be ignored for simplicity.

3.1 The serial HR array

A dual HR formed by two HRs connected in series (neck-cavity-neck-cavity), which

could be considered as a serial HR array, leads to two resonance frequencies. A dual HR could be analogous to a two degrees of freedom mechanical system[82], as illustrated in Figure. 3.1. According to Hooke's law, it should be noted that the first string has different stiffness (K_{11} and K_{12}) to the front and rear masses connected on it. By applying the Newton's second law of motion to the first mass M_1 and the second M_2 respectively yield:

$$\begin{cases} M_1 \dfrac{d^2 x_1}{dt^2} + R_1 \dfrac{dx_1}{dt} + K_{11} x_1 = S_1 p_0 e^{j\omega t} \\ M_2 \dfrac{d^2 x_2}{dt^2} + R_2 \dfrac{dx_2}{dt} + K_{22} x_2 = K_{12} x_2 \end{cases} \tag{3.1}$$

where $M_1 = \rho_0 S_1 l_{n1}'$ and $M_2 = \rho_0 S_2 l_{n2}'$ are the corresponding mass of air in the necks including the end-correction factor, R_1 and R_2 are damping coefficients of necks, K_{11} and K_{12} represent the stiffness of the first spring to the first mass and second mass respectively, $K_{22} = \rho_0 c_0^2 {S_2}^2 / V_2$ is the stiffness of the second spring, $e^{j\omega t}$ is the time-harmonic disturbance. Appling the Hooke's law to the mechanical analogy of a dual HR, the stiffness K_{11} and K_{12} could be obtained as:

$$\begin{cases} K_{11} = \dfrac{\rho_0 c_0^2 S_1}{V_1 x_1} (S_1 x_1 - S_2 x_2) \\ K_{12} = \dfrac{\rho_0 c_0^2 S_2}{V_1 x_2} (S_1 x_1 - S_2 x_2) \end{cases} \tag{3.2}$$

With the introduction of Eq. (3.2), Eq. (3.1) could be rewritten as:

$$\begin{cases} M_1 \dfrac{d^2 x_1}{dt^2} + R_1 \dfrac{dx_1}{dt} + \dfrac{\rho_0 c_0^2 S_1}{V_1} (S_1 x_1 - S_2 x_2) = S_1 p_0 e^{j\omega t} \\ M_2 \dfrac{d^2 x_2}{dt^2} + R_2 \dfrac{dx_2}{dt} + \dfrac{\rho_0 c_0^2 S_2^2}{V_2} x_2 - \dfrac{\rho_0 c_0^2 S_2}{V_1} (S_1 x_1 - S_2 x_2) = 0 \end{cases} \tag{3.3}$$

Substituting $x_1 = X_1 e^{j\omega t}$ and $x_2 = X_2 e^{j\omega t}$ into Eq. (3.3) and rearranging in the matrix form as:

$$\begin{bmatrix} -\omega^2 M_1 + j\omega R_1 + \dfrac{\rho_0 c_0^2 S_1^2}{V_1} & -\dfrac{\rho_0 c_0^2 S_1 S_2}{V_1} \\ -\dfrac{\rho_0 c_0^2 S_1 S_2}{V_1} & -\omega^2 M_2 + j\omega R_2 + \rho_0 c_0^2 S_2^2 \dfrac{(V_1 + V_2)}{V_1 V_2} \end{bmatrix} \begin{Bmatrix} X_1 e^{j\omega t} \\ X_2 e^{j\omega t} \end{Bmatrix} = \begin{Bmatrix} S_1 p_0 e^{j\omega t} \\ 0 \end{Bmatrix} \tag{3.4}$$

where X_1 and X_2 are the magnitude of the first and the second neck's displacement respectively. Eq. (3.4) could be simplified as:

$$\begin{bmatrix} a_{11} & a_{12} \\ a_{21} & a_{22} \end{bmatrix} \begin{Bmatrix} X_1 \\ X_2 \end{Bmatrix} = \begin{Bmatrix} p_0 S_1 \\ 0 \end{Bmatrix} \tag{3.5}$$

where $\begin{bmatrix} -\omega^2 M_1 + j\omega R_1 + \dfrac{\rho_0 c_0^2 S_1^2}{V_1} & -\dfrac{\rho_0 c_0^2 S_1 S_2}{V_1} \\ -\dfrac{\rho_0 c_0^2 S_1 S_2}{V_1} & -\omega^2 M_2 + j\omega R_2 + \rho_0 c_0^2 S_2^2 \dfrac{(V_1 + V_2)}{V_1 V_2} \end{bmatrix} = \begin{bmatrix} a_{11} & a_{12} \\ a_{21} & a_{22} \end{bmatrix}$.

According to Eq. (3.5), the relation of X_1 and $p_0 S_1$ could be described as $X_1 = p_0 S_1 a_{22} / (a_{11} a_{22} - a_{12} a_{21})$. It is therefore that the acoustic impedance of the dual HR could be obtained as:

$$Z_r = \frac{p_0}{j\omega X_1 S_1} = \frac{1}{j\omega S_1^{\,2}} \frac{a_{11} a_{22} - a_{12} a_{21}}{a_{22}} \tag{3.6}$$

By ignoring the effect of viscous dissipation through the necks for simplicity ($R_1 = R_2 = 0$), Eq.(3.6) could be rewritten as:

$$Z_r = \frac{1}{j\omega S_1^{\,2}} \frac{M_1 M_2 \omega^4 - \rho_0 c_0^2 [M_1 S_2^2 (\frac{1}{V_1} + \frac{1}{V_2}) + M_2 S_1^2 \frac{1}{V_1}] \omega^2 + \frac{\rho_0^{\,2} c_0^4 S_1^{\,2} S_2^{\,2}}{V_1 V_2}}{\rho_0 c_0^2 S_2^2 (\frac{1}{V_1} + \frac{1}{V_2}) - M_2 \omega^2} \tag{3.7}$$

Once the acoustic impedance of the dual HR has been obtained according to Eq. (3.7), the transmission loss of the dual HR could be calculated through Eq. (2.17) in Chapter 2.

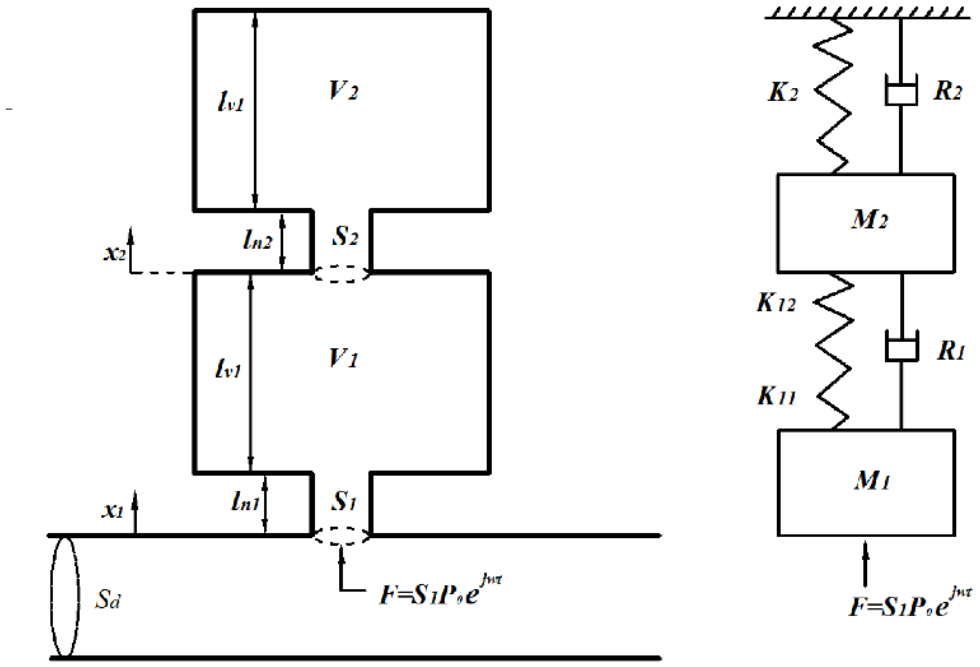

Figure 3.1 Mechanical analogy of a dual Helmholtz resonator.

3.2 The parallel Helmholtz resonator array

Two Helmholtz resonators mounted on the same cross-section of the duct is illustrated in Figure. 3.2. The classical lumped approach is adopted here and the acoustic impedance of these two HRs can be calculated by Eq. (2.20), expressed as Z_{r1} and Z_{r2} respectively. By ignoring the reflected waves from downstream of the duct, the continuity conditions of sound pressure and volume velocity at the

duct-neck interface give:

$$p_1 = p_2 = p_{f1} = p_{f2},\ S_d u_1 = S_d u_2 + \frac{p_{f1}}{Z_{r1}} + \frac{p_{f2}}{Z_{r2}} \tag{3.8}$$

where p with subscript represents sound pressure, u_1 and u_2 are the particle velocity at point 1 and point 2 respectively.

The relation between point 1 and point 2 could be obtained by combining the continuity conditions as:

$$\begin{bmatrix} p_1 \\ \rho_0 c_0 u_1 \end{bmatrix} = \begin{pmatrix} 1 & 0 \\ \frac{\rho_0 c_0}{S_d} \frac{Z_{r1} + Z_{r2}}{Z_{r1} Z_{r2}} & 1 \end{pmatrix} \begin{bmatrix} p_2 \\ \rho_0 c_0 u_2 \end{bmatrix} \tag{3.9}$$

Then the transmission loss of the parallel HR array can be determined by the four-pole parameters method as:

$$TL = 20 \log_{10}\left(\frac{1}{2}\left|2 + \frac{\rho_0 c_0}{S_d} \frac{Z_{r1} + Z_{r2}}{Z_{r1} Z_{r2}}\right|\right) \tag{3.10}$$

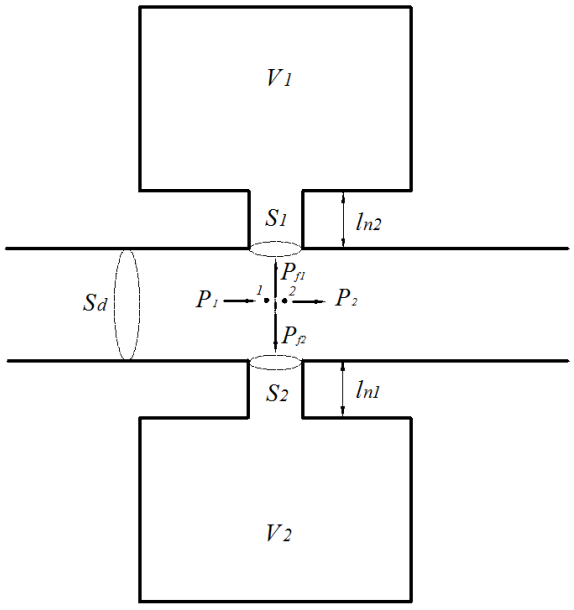

Figure 3.2 A parallel Helmholtz resonator array

3.3 The lined Helmholtz resonator array

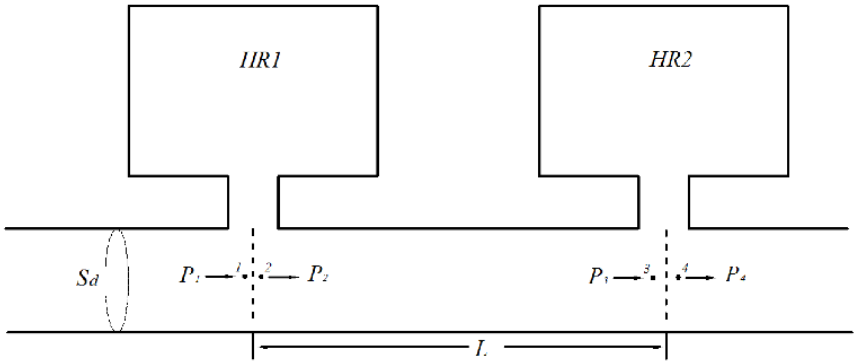

Figure 3.3 Schematic diagram of a lined Helmholtz resonator array.

A single HR has a high transmission loss peak with narrow band at its resonance frequency. Combining several HRs in line is a possible way to obtain a broader noise attenuation band. Figure. 3.3 demonstrates an array of two lined HRs mounted on the duct. Similar to Eq. (3.9), by combining the continuity conditions of the sound pressure and volume velocity at neck-neck interfaces, the relation between point 1 and point 2 and that between point 3 to point 4 could be obtained respectively as:

$$\begin{bmatrix} p_1 \\ \rho_0 c_0 u_1 \end{bmatrix} = \begin{pmatrix} 1 & 0 \\ \dfrac{\rho_0 c_0}{S_d}\dfrac{1}{Z_{r1}} & 1 \end{pmatrix} \begin{bmatrix} p_2 \\ \rho_0 c_0 u_2 \end{bmatrix} = \mathbf{T}_{r1} \begin{bmatrix} p_2 \\ \rho_0 c_0 u_2 \end{bmatrix} \tag{3.11}$$

$$\begin{bmatrix} p_3 \\ \rho_0 c_0 u_3 \end{bmatrix} = \begin{pmatrix} 1 & 0 \\ \dfrac{\rho_0 c_0}{S_d}\dfrac{1}{Z_{r2}} & 1 \end{pmatrix} \begin{bmatrix} p_4 \\ \rho_0 c_0 u_4 \end{bmatrix} = \mathbf{T}_{r2} \begin{bmatrix} p_4 \\ \rho_0 c_0 u_4 \end{bmatrix} \tag{3.12}$$

Only the planar wave is assumed to propagate through the duct due to the interest of low-frequency range here. It means that there is only a phase delay of the wave propagation in the straight duct from point 2 to point 3. Thus, the relation of point 2 and point 3 could be described as:

$$\begin{bmatrix} p_2 \\ \rho_0 c_0 u_2 \end{bmatrix} = \begin{pmatrix} \cos(kL) & j\sin(kL) \\ j\sin(kL) & \cos(kL) \end{pmatrix} \begin{bmatrix} p_3 \\ \rho_0 c_0 u_3 \end{bmatrix} = \mathbf{T}_{duct} \begin{bmatrix} p_3 \\ \rho_0 c_0 u_3 \end{bmatrix} \tag{3.13}$$

where L represents the distance between two HRs, $\mathbf{T}_{duct}$ is the transfer matrix of the straight duct, k is the number of wave. Then, the relation of point 1 and point 4 could be described in the matrix form as:

$$\begin{bmatrix} p_1 \\ \rho_0 c_0 u_1 \end{bmatrix} = \mathbf{T}_{r1}\mathbf{T}_{duct}\mathbf{T}_{r2} \begin{bmatrix} p_4 \\ \rho_0 c_0 u_4 \end{bmatrix} = \begin{bmatrix} t_{11} & t_{12} \\ t_{21} & t_{22} \end{bmatrix} \begin{bmatrix} p_4 \\ \rho_0 c_0 u_4 \end{bmatrix} \tag{3.14}$$

Once the transfer matrix $\mathbf{T}_{r1}\mathbf{T}_{duct}\mathbf{T}_{r2}$ has been obtained, the transmission loss of the lined HR array can be calculated from the expression as:

$$TL = 20\log_{10}\left(\frac{1}{2}\left|t_{11} + t_{12} + t_{21} + t_{22}\right|\right) \tag{3.15}$$

3.4 Comparison of different configurations

The transmission loss index is used to evaluate acoustic transmission performance in the frequency domain. However, it cannot be used to analyze the attenuation characteristics quantitatively. The concept of noise attenuation performance, which is based on the transmission loss index and discussed above, could give us a distinct parameter to evaluate the noise attenuation performance and ability of different array

configurations. Based on the aforementioned definition of the noise attenuation capacity, the noise attenuation capacity C_{TL} of a HR array is defined as the integration of transmission loss TL in the frequency domain and is expressed as:

$$C_{TL} = \int TL df = \sum_{i=0}^{f} TL_i (f_{i+1} - f_i) \tag{3.16}$$

The dual HR could be considered as two HRs connected in series (neck-cavity-neck-cavity), as illustrated in Figure. 3.1. There are two kinds of HRs with same neck dimensions and different cavity volumes are adopted here, annotated as HR1 and HR2 respectively. The geometries of HRs used in here are: same neck area $S_n = 2.25\pi$ cm^2 and neck length $l_n = 2.5$ cm, cavity volume $V_{R1} = 653.4\pi$ cm^3 and $V_{R1} = 261.36\pi$ cm^3 corresponding to HR1 and HR2 respectively. The cross-sectional area of the main duct is $S_d = 25$ cm^2. The resonance frequency of a HR is only determined by its geometries. It is therefore that the resonance frequencies of HR1 and HR2 are 152 Hz and 244 Hz respectively according to the discussion above. Figure. 3.4 illustrates the configuration of two dual HR cases: HR1-HR2 model and HR2-HR1 model respectively.

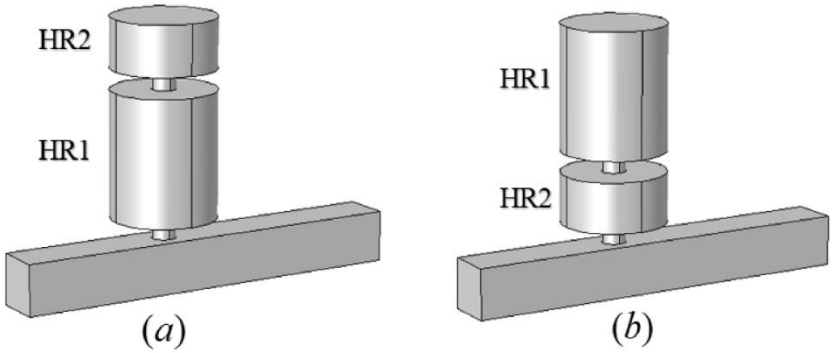

Figure 3.4 Configuration of two dual HR cases: (a) HR1-HR2 model, (b) HR2-HR1 model.

The predicted transmission loss of these two cases are compared with two individual HRs, as shown in Figure. 3.5. It can be observed that the dual HR cases have two resonance frequencies. The first resonance frequency of HR1-HR2 model and HR2-HR1 model are 121 Hz and 103 Hz respectively, which are both lower than 152 Hz (HR1's resonance frequency). The second resonance frequency of HR1-HR2 model and HR2-HR1 model are 301 Hz and 361 Hz, which are both higher than 244 Hz (HR2's resonance frequency). The HR2-HR1 model could provide a lower first resonance frequency than the HR1-HR2 model, however, the decreased first resonance frequency compromises an increasing second resonance frequency. The comparison of the analytical predicted results and the FEM simulation results are illustrated in Figure. 3.6, and the prediction results are in good agreement with the FEM simulation results. The solid lines represent the theoretical predictions, and dashed lines represent the FEM simulation results.

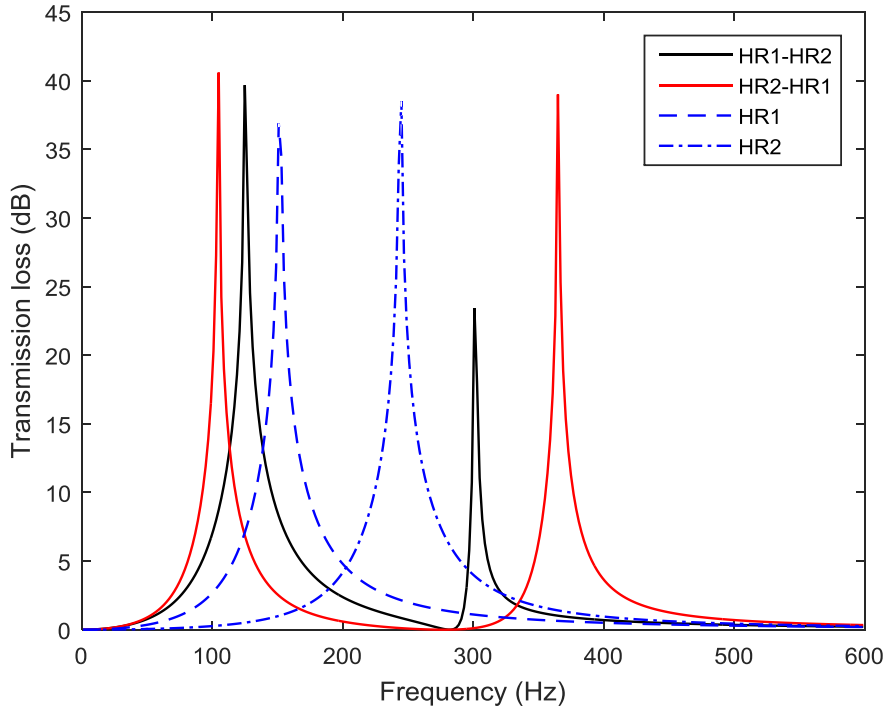

Figure 3.5 Configuration of two dual HR cases: (a) HR1-HR2 model, (b) HR2-HR1 model.

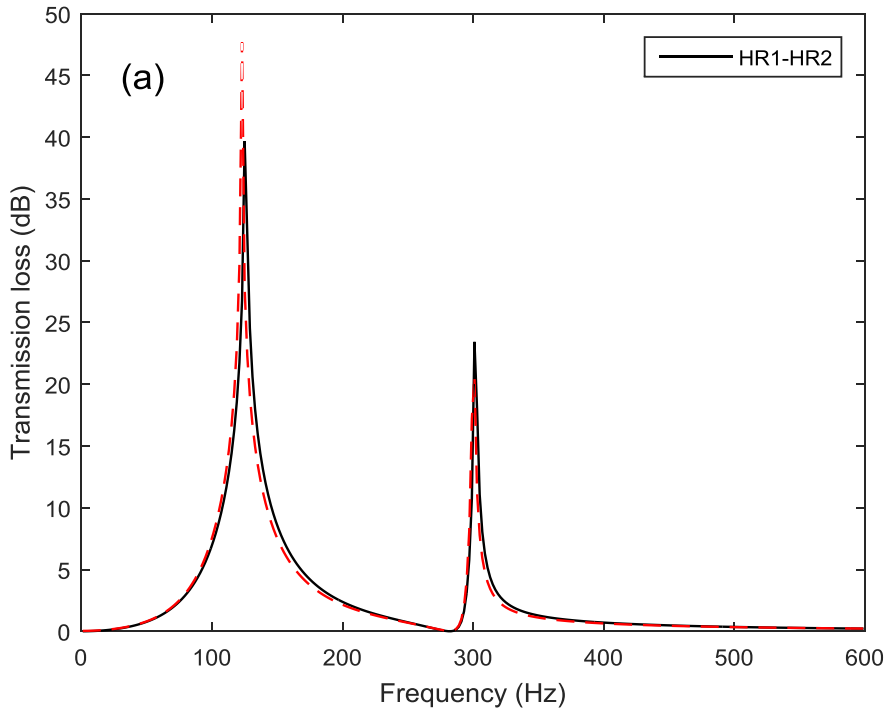

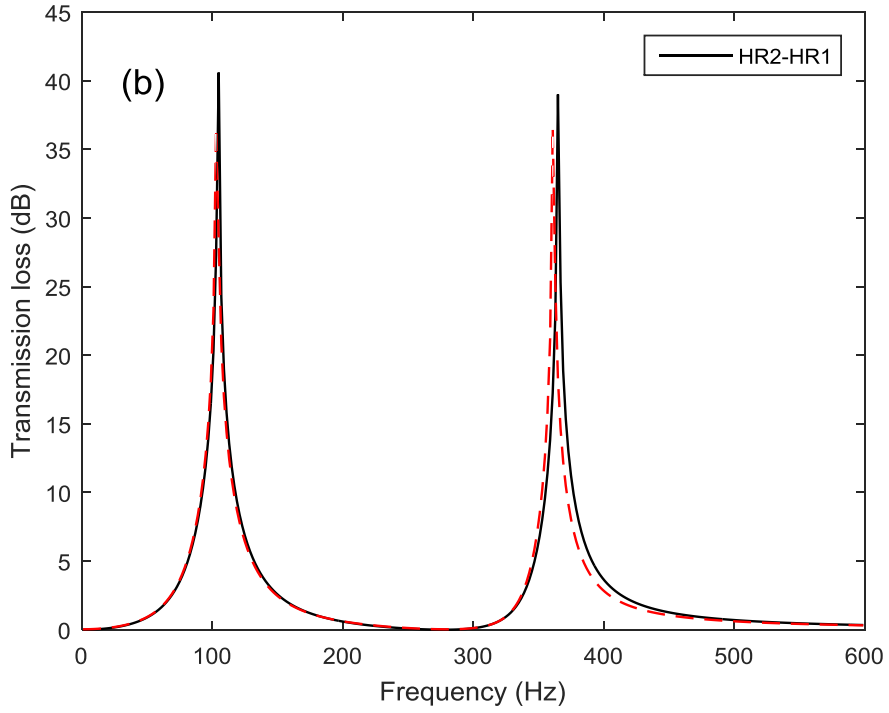

Figure 3.6 Comparison of the analytical predictions and the FEM simulation in respect of different dual HR models.

The parallel HR array consisting of two HRs mounted on the same cross-section of the duct is shown in Figure. 3.2. The two kinds of HRs used here are the same as HR1 and HR2 above, as is as the cross-section area of main duct. On the basis of low-frequency range considered in this paper, only planar wave is assumed to propagate in the duct. It is therefore that these two HRs can be mounted on arbitrary side of the cross-section of the duct. Figure. 3.7 compares the transmission loss between the parallel HR array and each HR. The parallel HR array has two resonance frequencies with nearly the same peak amplitudes corresponding to each HR's resonance frequency and peak amplitude. There is also a frequency at the intersection

of two individual HRs' *TL* curve, suggesting as an anti-resonance behavior. A good agreement between the theoretical predicted *TL* results and the FEM simulation results can also be seen in Figure. 3.8. The solid line represents the theoretical predictions, and dashed line represents the FEM simulation results. The parallel HR array could be approximated as the superposition of two individual HRs' *TL* curve.

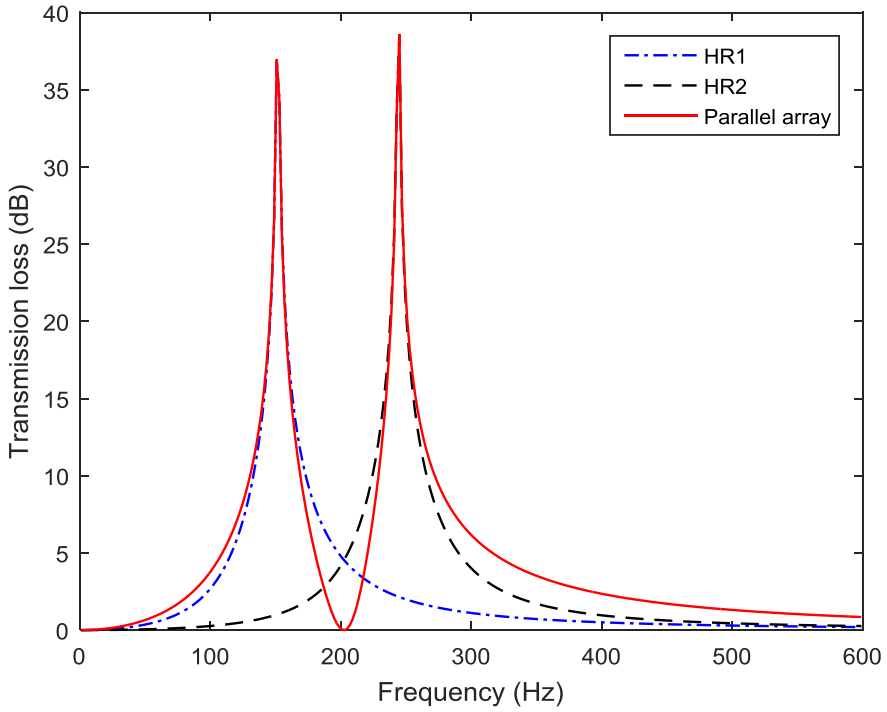

Figure 3.7 Transmission loss of the parallel HR array and individual HRs.

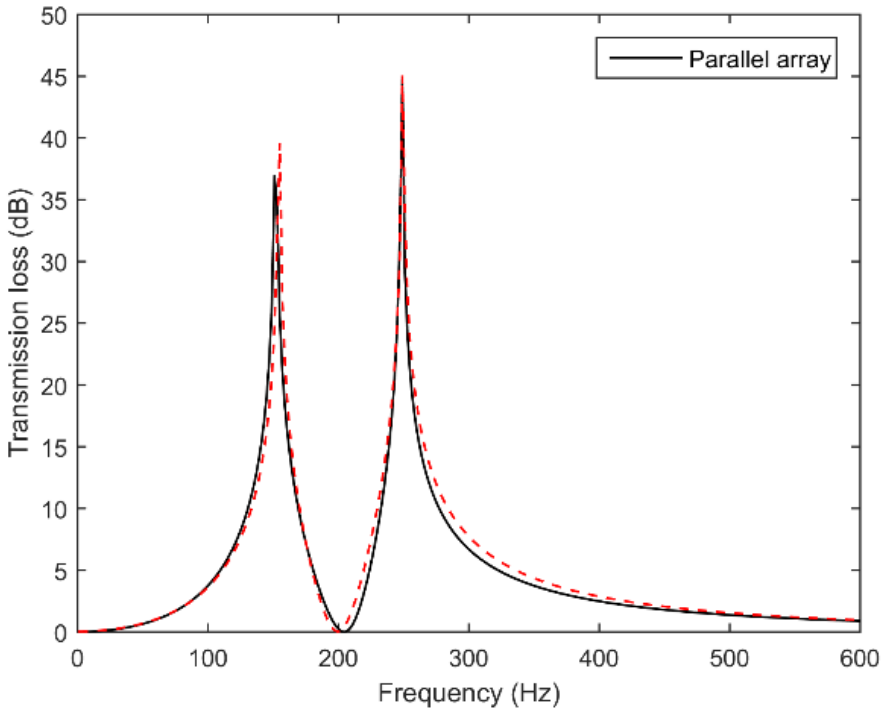

Figure 3.8 Comparison of the analytical predictions and the FEM simulation in respect of the parallel HR array.

The schematic diagram of a lined Helmholtz resonator array, which is composed of two HRs, is exhibited in Figure. 3.3. The used HRs (HR1 and HR2) and the main duct are the same as mentioned above. The optimal distance is corresponding to the quarter-wavelength of HRs' mean frequency defined as $f_m=2f_{HR1}* f_{HR2}/(f_{HR1}+ f_{HR2})$[83]. As a consequence, the distance L between two HRs used in this paper is $L=0.46m$. The comparison of theoretical predicted transmission loss between the lined HR array and each HR is shown in Figure. 3.9. Two peak amplitudes corresponding to each HR's resonance frequency could be observed from the lined HR array. Moreover, the lined HR array provides a much broader noise attenuation band between the

resonance frequencies of these two HRs. Figure. 3.10 shows that the theoretical predicted results fit well with the FEM simulation results.

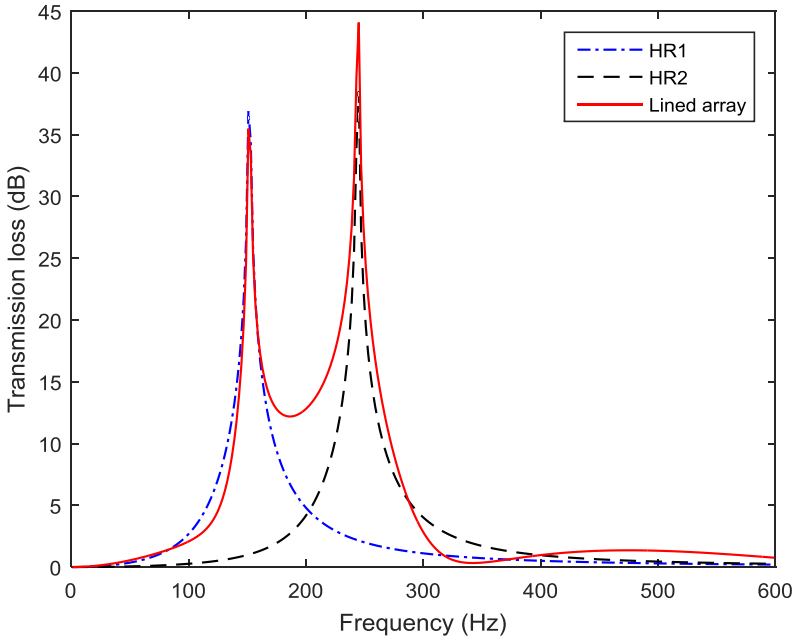

Figure 3.9 Transmission loss of the lined HR array and individual HRs

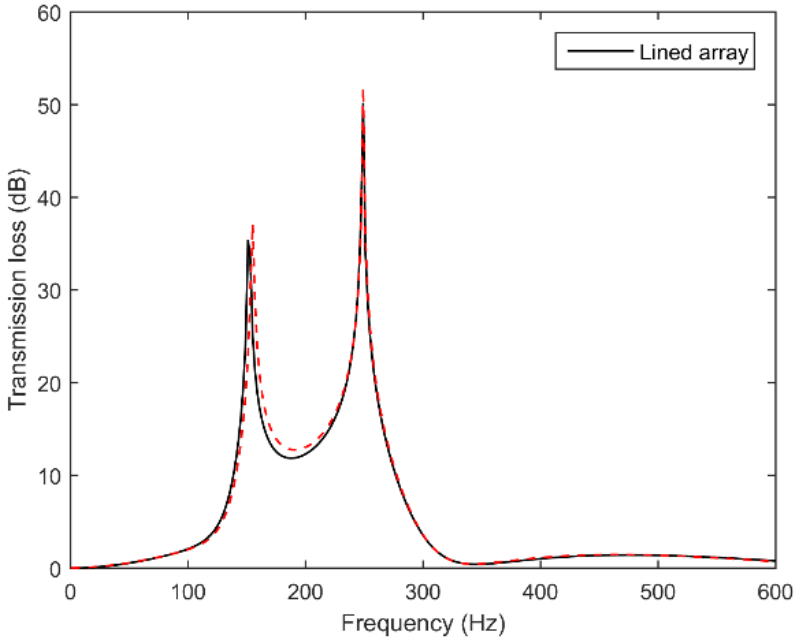

Figure 3.10 Comparison of the analytical predictions and the FEM simulation in respect of the

lined HR array (solid line represents the theoretical predictions, and dashed line represents the FEM simulation results).

The noise attenuation capacity C_{TL} of those cases as described above is exhibited in Table 3.1. The maximum relative errors of C_{TL} between the theoretical analysis and FEM simulation are less than 5% in frequency range of 0~600 Hz (parallel case) and less than 1% in frequency range of 0~1000 Hz respectively. It should be noted that the C_{TL} of HR1 equals to the C_{TL} of HR2. It means that the change of the cavity volume has no effect on the C_{TL}. The theoretical formula of a HR has derived in Chapter 2, which shows that the C_{TL} is only related to the geometries of the neck and the cross-sectional area of the duct. It should also be noted that although the dual HR contains two HRs, the C_{TL} of the dual HR equals to the C_{TL} of each single component HR mounted on the ducted. The added HR in series leads to two resonance frequencies, however, these two noise attenuation bands compromises with a narrower noise attenuation band. The added HR in series could be considered as the added volume of the cavity. Therefore, the C_{TL} of the dual HR equals to the C_{TL} of each single component HR. Besides, being bulky is another disadvantage for a dual HR when compared with its component HRs.

Table 3.1 C_{TL} with different frequency range

	C_{TL} with different frequency range			
	0~600 Hz		0~1000 Hz	
Cases	Theory	FEM	Theory	FEM
HR1	1.622×10^3	1.625×10^3	1.647×10^3	1.644×10^3
HR2	1.627×10^3	1.633×10^3	1.659×10^3	1.66×10^3
HR1-HR2	1.631×10^3	1.626×10^3	1.669×10^3	1.671×10^3
HR2-HR1	1.641×10^3	1.644×10^3	1.664×10^3	1.674×10^3
Parallel array	3.012×10^3	3.129×10^3	3.216×10^3	3.286×10^3
Lined array	3.164×10^3	3.239×10^3	3.249×10^3	3.279×10^3

Although the transmission loss performance of the lined HR array is different from the parallel array, as depicted in Figure. 3.11. The parallel array could be approximated as the combination of the transmission loss performance of HR1 and HR2, as illustrated as Figure. 3.8. The lined HR array could provide a much broader noise attenuation band between two resonance frequencies. However, the C_{TL} of the parallel HR array equals to the C_{TL} of the lined HR array, which is twice the C_{TL} of the dual HR cases. The lined HR array and the parallel HR array demand the same space as the dual HR, but in different ways.

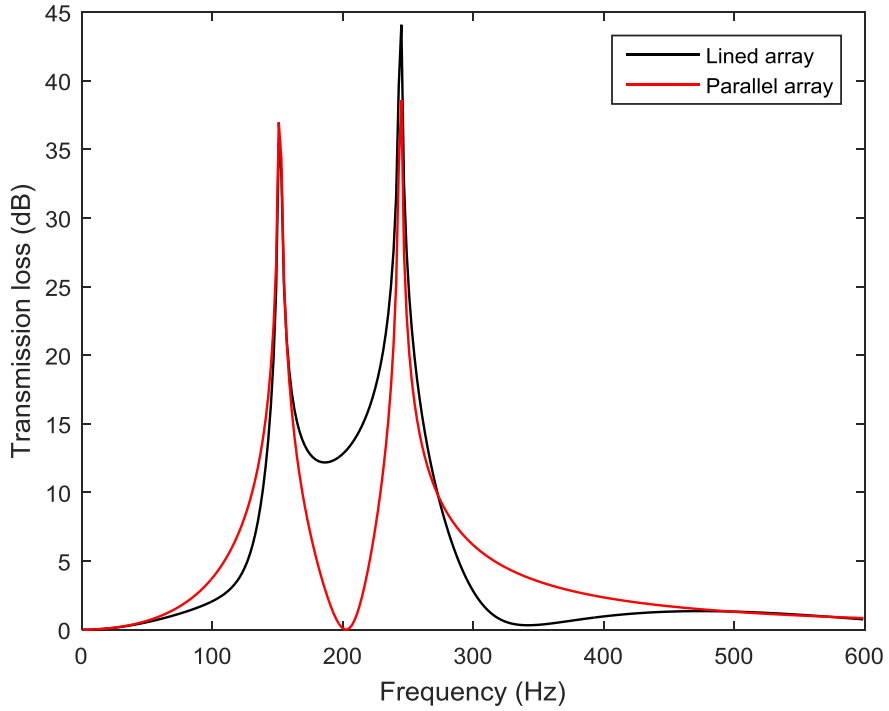

Figure 3.11 Transmission loss of the lined HR array and the parallel HR array.

3.5 Summary

The acoustic performance of three kinds of HR arrays are investigated theoretically and numerically. The dual HR consist of two HRs connected in series is considered as a serial HR array. Two HRs mounted on the same cross-section of the duct constitute a parallel HR array. The lined HR array is composed of two HRs installed on the longitudinal direction of the duct. Different installation methods have significant effects on the curve of the transmission loss in the frequency domain. The dual HR could provide two resonance frequencies, which the first and second resonance frequency are lower and higher than the resonance frequency of any component HRs

respectively. By altering the connected sequence of two HRs in the dual HR, the reduced first resonance frequency compromises an increasing second resonance frequency could be observed. The parallel HR array has two resonance frequencies with nearly the same peak amplitudes corresponding to each HR's resonance frequency and peak amplitude. It could be approximated as the superposition of two individual HRs' *TL* curve. The lined HR array provides a much broader noise attenuation band between the resonance frequencies of these two HRs. The two resonance frequencies corresponding to each HR's resonance frequency could also be observed.

In consideration of noise attenuation capacity, it should be noted that the C_{TL} of the dual HR equals to the C_{TL} of each single component HR mounted on the ducted. It is because that the added HR in series could be considered as the added volume of the cavity. The change of the cavity volume has no effect on the C_{TL}. It indicates that the dual HR could only provide two narrow noise attenuation bands. The C_{TL} of the parallel HR array equals the C_{TL} of the lined HR array, which is twice the C_{TL} of the dual HR or each component HR. In addition, a dual HR is bulky when compared with its component HRs. The lined HR array and the parallel HR array demand the same space as the dual HR, but in different ways. The quantitative parameter C_{TL} should therefore be considered as one of the main acoustic characteristics to evaluate the acoustic performance and be taken into consideration in noise control

optimization and HR design.

Chapter 4

Dispersion relation of sound wave in a periodic ductwork system

4.1 Periodic Helmholtz resonator array

4.1.1 A duct with an array of Helmholtz resonator

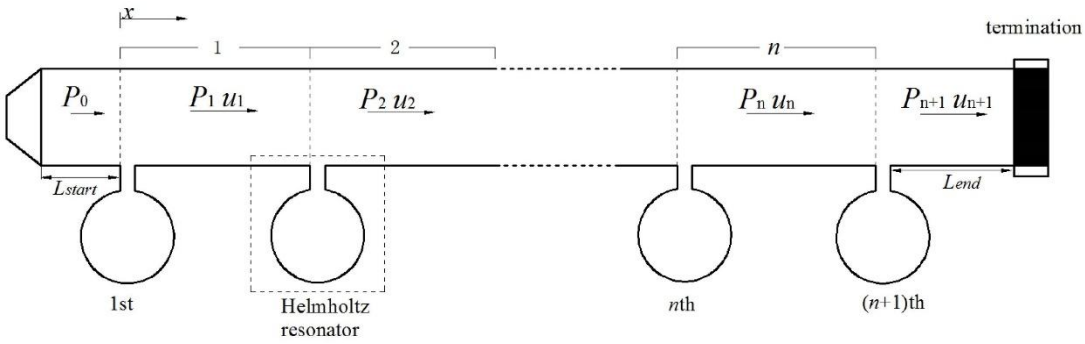

Figure 4.1 Schematic diagram of a periodic ducted HR system with finite resonators.

Since a single resonator has a narrow noise attenuation band, an array of resonators is one way to obtain a broader noise attenuation band. An array of Helmholtz resonators mounted on the duct periodically is illustrated in Figure. 4.1. A duct segment with a resonator constitutes a typical periodic cell. The duct segment's length is regarded as a periodic distance based on the assumption that the diameter of the resonator's neck

is negligible in a periodic cell. The sound pressure and particle velocity in the duct segment of the nth cell, as shown in Figure. 4.1, can be described as $p_n(x)$ and $u_n(x)$ with a suffix of n. The sound pressure is a combination of two wave propagations in opposite directions of axial x. Assuming a time-harmonic disturbance in the form of $e^{j\omega t}$, the sound pressure can be expressed as[84,85]:

$$p_n(x) = I_n e^{-jk(x-x_n-\omega t)} + R_n e^{jk(x-x_n+\omega t)} \tag{4.1}$$

where k is the number of waves, $x_n = (n-1)d$ represents the local coordinates, d is the periodic distance, I_n and R_n represent respective complex wave amplitudes. Combining the continuity of sound pressure and volume velocity at $x = nd$ yields:

$$\begin{bmatrix} I_{n+1} \\ R_{n+1} \end{bmatrix} = \begin{bmatrix} (1-\frac{Z_d}{2Z_r})\exp(-jkd) & -\frac{Z_d}{2Z_r}\exp(jkd) \\ \frac{Z_d}{2Z_r}\exp(-jkd) & (1+\frac{Z_d}{2Z_r})\exp(jkd) \end{bmatrix} \begin{bmatrix} I_n \\ R_n \end{bmatrix} = \mathbf{T} \begin{bmatrix} I_n \\ R_n \end{bmatrix} \tag{4.2}$$

where Z_d is the acoustic impedance of the duct, $\mathbf{T}$ is the transfer matrix. Once the initial sound pressure is given, the sound pressure and particle velocity in an arbitrary cell can be determined successively by Eq. (4.2). According to Bloch wave theory, the transfer matrix can be set as $\mathbf{T} = \lambda$ (λ is set to be $\exp(-jqd)$, and q is the Bloch wave number and is allowed to be a complex value).

The analysis of the periodic structure translates to an eigenvalue and its corresponding eigenvector problem. From the definition of λ, q must satisfy the following dispersion relation:

$$\cos(qd) = \cos(kd) + j\frac{Z_d}{2Z_r}\sin(kd) = \cos(kd) + \frac{\psi kd\sin(kd)}{2[(\omega/\omega_0)^2 - 1]} \tag{4.3}$$

where $\psi = V_c / S_d d$ (V_c represents the HR's volume, S_d the cross-sectional area of the duct). The Bloch wave number q is a complex value comprising a real part, q_r, and imaginary part, q_i; the solutions of $\lambda = \exp(-jqd)$ describe the propagation properties of Bloch waves. Assuming that $q_r > 0$ and $q_i > 0$, the two solutions $q = q_r - jq_i$ and $q = -(q_r - jq_i)$ represent the propagation properties of positive-x and negative-x Bloch waves respectively, corresponding to the eigenvalues λ_1 and λ_2. The eigenvectors corresponding to eigenvalues λ_1 and λ_2 can be expressed as $[v_{I1}, v_{R1}]^{\mathrm{T}}$ and $[v_{I2}, v_{R2}]^{\mathrm{T}}$ respectively.

4.1.2 Dispersion relation

The solution of q is a function of the wave frequency, periodic distance, and geometric dimensions of a duct resonator system. The dispersion relation of sound waves in a duct can be described by solutions of q. When q contains an imaginary part, this implies that a sound wave decays as it travels; the frequency ranges of such a sound wave are called stopbands. Passbands are sound waves that have only a phase delay during travel when q only contains a real part. Stopbands are brought about physically by two mechanisms. One is when sound wave frequency coincides with the resonator's resonance frequency, which is also the mechanism of a single-resonator case. The other is Bragg reflection. Based on these two mechanisms,

a theoretical prediction of stopband position and its bandwidth is studied.

When the asymptotic wave frequency $\omega \to \omega_0$ is considered, setting $\omega / \omega_0 = 1 + \Delta$ ($|\Delta|$ is assumed to be well below unity). When Eq. (4.3) is set to be unity, the approximate stopbands at $\Delta = \Delta_+$ and $\Delta = \Delta_-$ are expressed in the form of Taylor series:

$$\Delta_+ = \frac{V_c k_0}{4S_d}[\cot(\frac{k_0 d}{2}) + \frac{\cot'(k_0 d/2)}{1!}\frac{k_0 d}{2}\Delta_+ + \cdots + \frac{\cot^{(n)}(k_0 d/2)}{n!}\frac{k_0 d}{2}\Delta_+] \qquad (4.4)$$

$$\Delta_- = -\frac{V_c k_0}{4S_d}[\tan(\frac{k_0 d}{2}) + \frac{\tan'(k_0 d/2)}{1!}\frac{k_0 d}{2}\Delta_- + \cdots + \frac{\tan^{(n)}(k_0 d/2)}{n!}\frac{k_0 d}{2}\Delta_-] \qquad (4.5)$$

where $k_0 = \omega_0 / c_0$ is the wave number of resonance frequency and c_0 is the sound velocity. The stopband of resonance can be expressed as $[(1+\Delta_-)\omega_0, (1+\Delta_+)\omega_0]$. For the sake of simplicity, when only zero-order correction is considered, the bandwidth is given as $\Delta_{bw} = V_c k_0 \omega_0 |\cot(k_0 d/2) + \tan(k_0 d/2)| / 4S_d$.

The stopband is also due to Bragg reflection; it occurs near $\omega_m = m\pi c_0 / d$ (m is an integer). Then $kd = m\pi$ (m is an integer) can be obtained, indicating the approximate positions of stopbands. When the asymptotic wave frequency $\omega \to \omega_m$ is considered, setting $\omega / \omega_m = 1 + \Delta$. Then, Eq. (4.3) is rewritten as:

$$\cos(qd) = \cos(m\pi(1+\Delta)) + \frac{\psi m\pi(1+\Delta)\sin(m\pi(1+\Delta))}{2[(\omega_m(1+\Delta)/\omega_0)^2 - 1]} = (-1)^m[1 - \frac{(m\pi)^2}{2}(\Delta^2 - \Delta\Delta_m)] \qquad (4.6)$$

Thus stopbands of Bragg reflection appear at $[(1-\Delta_m/2)\omega_m, (1+\Delta_m/2)\omega_m]$, where

$\Delta_{bw} = \omega_m \Delta_m = \psi\omega_m \Big/ \left|(\omega_m / \omega_0)^2 - 1\right|$ represents the bandwidth. As the integer number m increases, the width of the stopband becomes narrower as $1/m^2$ and the maximum value of the imaginary part becomes smaller as $1/m$.

In practice, the special case where the designed resonance frequency ω_0 coincides with the Bragg reflection frequency ω_m is applied to achieve a broader noise stopband at resonance frequency. The stopband is thus a combination of resonance and Bragg reflection. Then Eq. (4.6) is converted to $\cos(qd) = (-1)^m[1-(m\pi)^2(\Delta^2 - \psi/2)/2]$. Thus the stopband of the special case can be obtained at $[(1-\sqrt{\psi/2})\omega_0, (1+\sqrt{\psi/2})\omega_0]$, with bandwidth $\Delta_{bm} = 2\omega_0\sqrt{\psi/2}$. The bandwidth decreases with increasing d ($d = m\lambda_0/2$), where $\lambda_0 = 2\pi c_0 / \omega_0$ is the wavelength of resonance frequency. For the sake of a broader stopband at resonance frequency, $d = \lambda_0/2$ is often chosen as a periodic distance.

4.2 Transmission loss of periodic ducted HR systems

4.2.1 Transmission loss of periodic ducted HR systems

According to the definition of the eigenvalue, Eq. (4.2) can be expressed in eigenvector form as:

$$\begin{bmatrix} I_{n+1} \\ R_{n+1} \end{bmatrix} = \mathbf{T}\begin{bmatrix} I_n \\ R_n \end{bmatrix} = \mathbf{T}^2\begin{bmatrix} I_{n-1} \\ R_{n-1} \end{bmatrix} = \ldots = \mathbf{T}^n\begin{bmatrix} I_1 \\ R_1 \end{bmatrix} = A_0\lambda_1^n\begin{bmatrix} v_{I1} \\ v_{R1} \end{bmatrix} + B_0\lambda_2^n\begin{bmatrix} v_{I2} \\ v_{R2} \end{bmatrix} \qquad (4.7)$$

where A_0 and B_0 are complex constants determined by boundary conditions. The end boundary conditions with reflection coefficient α give:

$$\frac{R_n e^{jk(x-x_n+\omega t)}}{I_n e^{-jk(x-x_n-\omega t)}} = \frac{A_0 \lambda_1^{n-1} v_{R1} e^{jkL_{end}} + B_0 \lambda_1^{n-1} v_{R2} e^{jkL_{end}}}{A_0 \lambda_1^{n-1} v_{I1} e^{-jkL_{end}} + B_0 \lambda_1^{n-1} v_{I2} e^{-jkL_{end}}} = \alpha \tag{4.8}$$

Similarly, the initial condition gives:

$$\begin{aligned} p_0 &= I_0 e^{-jk(x+d)} + R_0 e^{jk(x+d)}\Big|_{x=-L_{start}} \\ &= (A_0 \lambda_1^{-1} v_{I1} + B_0 \lambda_2^{-1} v_{I2}) e^{-jk(d-L_{start})} + (A_0 \lambda_1^{-1} v_{R1} + B_0 \lambda_2^{-1} v_{R2}) e^{jk(d-L_{start})} \end{aligned} \tag{4.9}$$

Thus the average transmission loss can be expressed as:

$$\overline{TL} = \frac{20}{n+1} \log_{10} \left| \frac{I_0}{I_{n+1}} \right| = \frac{20}{n+1} \log_{10} \left| \frac{A_0 \lambda_1^{-1} v_{I1} + B_0 \lambda_2^{-1} v_{I2}}{A_0 \lambda_1^{n-1} v_{I1} + B_0 \lambda_2^{n-1} v_{I2}} \right| \tag{4.10}$$

When the duct ends with an anechoic termination, the reflection α equals zero, and λ_1 describes positive-direction propagation, it means that $|\lambda_1| < 1, |\lambda_2| > 1$. $B_0 = 0$ is required in this situation. The average transmission loss of a duct with an anechoic termination loaded with infinity resonators can be expressed as: $\overline{TL} = -20 \log_{10} |\lambda_1|$.

4.2.2 Noise attenuation capacity of periodic ducted HR systems

The transmission loss index is mainly used to evaluate the acoustic transmission performance. Base on the transmission loss index, the noise attenuation capacity index as one of the key parameters to evaluate the noise attenuation performance of a HR has been proposed and derived. The concept of noise attenuation capacity can also be adopted to evaluate the acoustic performance of periodic ducted HR systems

as well. Since HR is reactive silence without energy consumption, therefore, the sound power is introduced to evaluate the noise attenuation performance. According to the definition of the transmission loss as:

$$TL = Lw_i - Lw_t = 10\lg\left(w_i / w_t\right) \tag{4.11}$$

where $w_i = S_i \left|p_i\right|^2 \big/ \rho c$ and $w_t = S_t \left|p_t\right|^2 \big/ \rho c$ are the incident sound power and transmission sound power respectively. Since HRs are reactive silencers without energy consumption, their energy storage capacity in a frequency domain is expressed as:

$$W_{total} = \int (w_i - w_t) = \int (w_i - w_i / 10^{\frac{TL}{10}}) = \sum_{1}^{fr} (w_i - w_i / 10^{\frac{TL_{fr}}{10}}) \tag{4.12}$$

When the dimensions of a duct resonator system and the incident sound power are determined, the noise attenuation capacity of a HR and the HRs' energy storage capacity remains unchanged. The periodic distance only affects stopbands' position, bandwidth, and amplitude; however, it has no effect on HRs' energy storage capacity. Owing to multiple relationships between the integration of $\overline{TL}$ curve or W_{total} in a frequency domain, the integration of $\overline{TL}$ curves can be used to evaluate HRs' energy storage capacity and noise control optimization design.

4.3 Results and discussion

A duct resonator system with the geometries $S_d = 36$ cm^2, $l_n = 2.5$ cm, $S_n = 4\pi$ cm^2, and $V = 101.25\pi$ cm^3 was used in this study. The three-dimensional finite

method was used to validate theoretical prediction. An oscillating sound pressure at a magnitude of $P_0 = 1$ was applied at the beginning of the duct. An anechoic termination was set at the end to avoid reflected waves.

Figure. 4.2 shows $\omega_0 \neq \omega_m$ cases ($n = 1, 3, 10$) with two types of stopband separately. The $\overline{TL}$ of two different special cases ($\omega_0 = \omega_1 = \pi d$ and $\omega_0 = \omega_m = 2\pi d$) was compared with a single-branch HR in Figure. 4.3, in which the stopband near the resonance frequency is a combination of Bragg reflection and resonance effect. The relationship between integer number m and periodic distance d in special cases is given as $d = m\lambda_0 / 2$. Figure. 4.4 shows that the width of the stopband becomes narrower as $\sqrt{1/m}$ with increasing m in special cases ($d = 0.5\lambda_0, 1.5\lambda_0, 3\lambda_0$). Thus, for the sake of having a broader stopband at resonance frequency, $d = \lambda_0/2$ ($m = 1$) is often chosen as periodic distance. Figure. 4.5 verifies $\overline{TL} = -20\log_{10}|\lambda_1|$ in cases of infinite resonators, and also compares three different cases ($d = 0.5\lambda_0, 0.68\lambda_0, \lambda_0$) with a single-branch HR. The theoretical $\overline{TL}$ of different cases are compared with the numerical simulation using three-dimensional FEM (dotted crosses). The predicted result fits well with the FEM results. In addition, the results illustrate that the broader the noise attenuation band, the lower the peak attenuation amplitude.

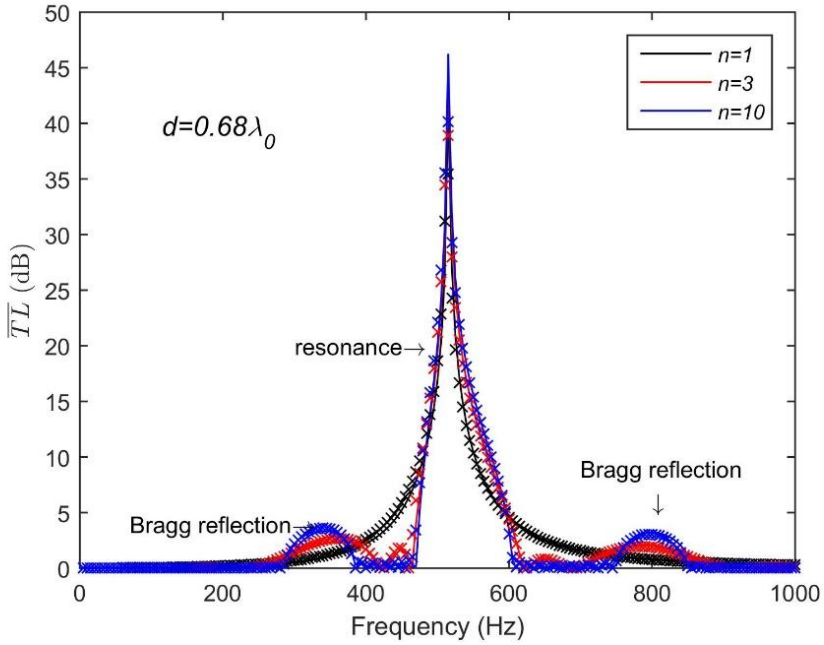

Figure 4.2 The average transmission loss $\overline{TL}$ of the duct resonator system with different numbers of HRs.

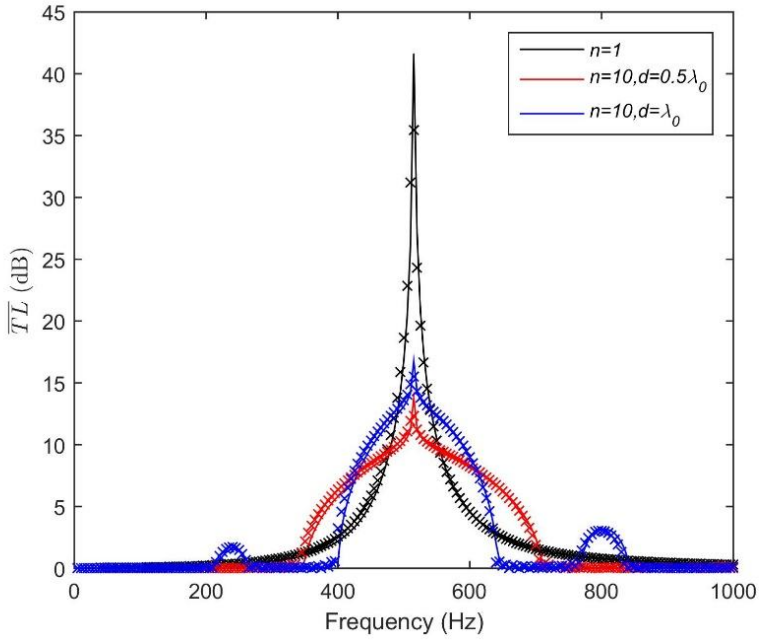

Figure 4.3 Comparison of the average transmission loss $\overline{TL}$ of different special cases and the single HR.

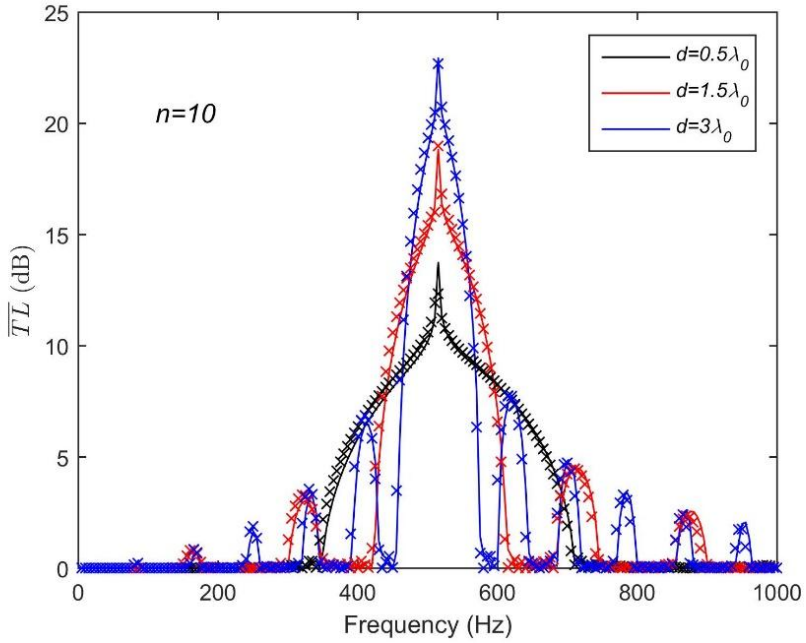

Figure 4.4 The average transmission loss $\overline{TL}$ of the duct resonator system with periodic distance.

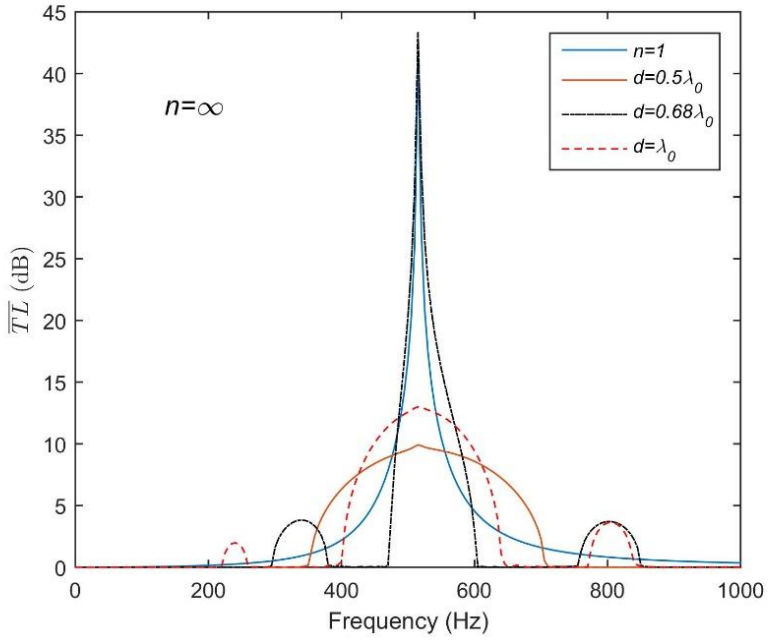

Figure 4.5 Comparison of the average transmission loss $\overline{TL}$ in cases of infinite resonators and the single-branch HR.

Based on the conservation of energy, the total energy W_{total} of all $\overline{TL}$ curves (the

average noise attenuation capacity) from 0 Hz to 1,000 Hz are almost the same, as is the area covered by $\overline{TL}$ curves. Table 4.1 and Table 4.2 show different cases with different periodic distances and numbers of resonators by both theoretical prediction and simulation. The maximum relative error of $\overline{TL}$ area and W_{total} between theoretical analysis and FEM are 3.6% (case: 64 HRs with distance λ) and 3.1% (case: single HR) respectively.

Table 4.1 $\overline{TL}$ area and W_{total} of ten HR duct resonators with different periodic distances

	Periodic d	0.5λ	λ	1.5λ	2λ	2.5λ	3λ	3.5λ
FEM	$\overline{TL}$ area ($\times 10^3$)	2.7092	2.7329	2.7364	2.747	2.7389	2.754	2.752
	W_{total} ($\times 10^{-4}$)	2.4631	2.4887	2.503	2.5123	2.4986	2.5206	2.5065
Theory	$\overline{TL}$ area ($\times 10^3$)	2.6249	2.6565	2.6672	2.6729	2.6767	2.6795	2.6807
	W_{total} ($\times 10^{-4}$)	2.4567	2.4618	2.4695	2.4853	2.5069	2.5098	2.5104

Table 4.2 $\overline{TL}$ area and W_{total} of a periodic ducted HR system with different numbers of HR

Resonator number	$d = 0.5\lambda$				$d = \lambda$			
	Theory		FEM		Theory		FEM	
	$\overline{TL}$ area ($\times 10^3$)	W_{total} ($\times 10^{-4}$)	$\overline{TL}$ area ($\times 10^3$)	W_{total} ($\times 10^{-4}$)	$\overline{TL}$ area ($\times 10^3$)	W_{total} ($\times 10^{-4}$)	$\overline{TL}$ area ($\times 10^3$)	W_{total} ($\times 10^{-4}$)
1	2.6766	2.4333	2.7532	2.5108	2.6766	2.4333	2.7532	2.5108
2	2.6562	2.5203	2.7378	2.5097	2.6654	2.5055	2.7445	2.5078
3	2.6422	2.5198	2.7272	2.5041	2.6596	2.4889	2.7396	2.5041
4	2.6337	2.5	2.7205	2.4987	2.6576	2.4745	2.7347	2.4958
5	2.6288	2.4845	2.7161	2.4954	2.6576	2.4743	2.7361	2.5022
6	2.6263	2.4742	2.7133	2.5002	2.6575	2.4695	2.7353	2.5001
7	2.6254	2.4678	2.7117	2.4932	2.6569	2.4652	2.7373	2.5256
8	2.6253	2.4362	2.71	2.4812	2.6565	2.4618	2.7378	2.5385
9	2.6252	2.4602	2.711	2.4798	2.6565	2.4617	2.7351	2.4995
10	2.6249	2.4567	2.7092	2.4631	2.6565	2.4618	2.7329	2.4887
12	2.6237	2.4496	2.7086	2.4569	2.6563	2.4592	2.7249	2.4754
16	2.6222	2.4406	2.7086	2.4569	2.6563	2.4595	2.7376	2.5002
24	2.6211	2.4313	2.703	2.4471	2.656	2.4564	2.7315	2.4841
32	2.6209	2.4272	2.7043	2.4521	2.6555	2.4552	2.7424	2.5012
48	2.6198	2.4237	2.7042	2.4536	2.6555	2.457	2.7469	2.5056
64	2.6201	2.4195	2.7077	2.4468	2.6554	2.4571	2.7536	2.5263

Table 4.3 Relative error between the minimum value and maximum value

	Theory		FEM	
	Min	Max	Min	Max
Case	48 HRs, 0.5λ	10 HRs, 3.5λ	24 HRs, 0.5λ	10 HRs, 3λ
$\overline{TL}$ area ($\times 10^3$)	T1=2.6198	T2=2.6907	T3=2.703	T4=2.754
Case	64 HRs, 0.5λ	2 HRs, 0.5λ	64 HRs, 0.5λ	8 HRs, λ
W_{total} ($\times 10^{-4}$)	T5=2.4195	T6=2.5203	T7=2.4468	T8=2.5385
Relative error (%)	T1/ T2: 2.6%; T3/ T4: 1.9%; T1/ T4: 4.9%;			
	T5/ T6: 4%; T7/ T8: 3.6%; T5/T8: 4.7%			

The relative errors between the minimum value and the maximum value are exhibited in Table 4.3. These three tables indicate that for the same system, no matter how many HRs are used or what the periodic distance is, the $\overline{TL}$ area and W_{total} are always the same. This means that HR's noise attenuation capacity remains the same for the same geometries of duct and resonator. As discussed above, the noise attenuation capacity of a HR is determined by its geometries of neck and the cross-sectional area of the duct. Therefore, for a certain periodic ducted HR system, the average noise attenuation capacity of a HR remains unchanged.

There is no trick to noise control. The broader the noise attenuation band, the lower the peak attenuation amplitude. Although different $\overline{TL}$ curves with different bandwidths and peak amplitudes could be obtained with different periodic distances,

$\overline{TL}$ area and W_{total} are always the same and $\overline{TL}$ curves always fall into the boundaries of a noise control zone. The noise control zone as shown in Figure. 4.6 is first proposed for noise control optimization design. It provides a clear indication of the limitation of noise control. No matter what optimizing distance is adopted in noise control, the values of the attenuation bandwidth and peak amplitude must be within the proposed noise control zone. The noise control zone can be used to analyze the feasibility of desired broad attenuation bandwidth and peak amplitude in noise control optimization. Figure. 4.6 shows the noise control zone for periodic ducted HRs, which is bounded by the highest $\overline{TL}$ amplitude for single resonator, and has the largest frequency bandwidth with lowest $\overline{TL}$ amplitude for $d = \lambda_0/2$.

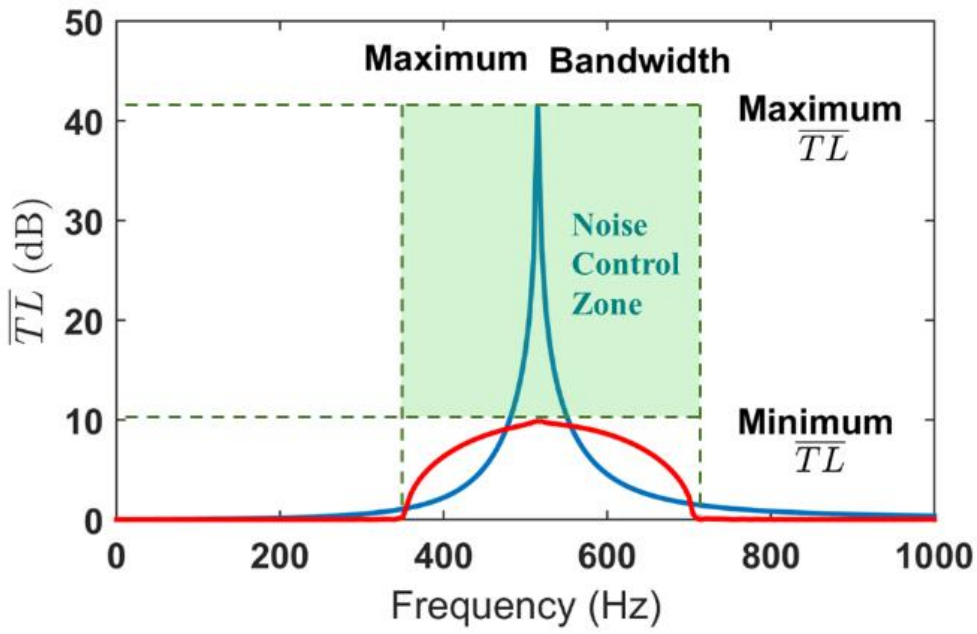

Figure 4.6 Noise control zone for ducted HRs

4.4 Summary

This Chapter presents a theoretical study of the dispersion characteristics of sound wave propagation in a periodic ducted HRs system. The predicted result fits well with the FEM results. Owing to the coupling of Bragg reflection and HR's resonances, a periodic system can provide much broader noise attenuation band at the designed resonance frequencies of the HR. The bandwidths and positions of noise attenuation bands have been investigated. This investigation indicates that for the same system, no matter how many HRs are connected or what the periodic distance is, the $\overline{TL}$ area and W_{total} are always the same. In other words, changing the resonator number or the value of the periodic distance has no effect on HR's noise attenuation capacity.

The broader the noise attenuation band the lower the peak attenuation amplitude. A noise control zone compromising the attenuation bandwidth or peak amplitude is first proposed to illustrate the limitation of noise control for ducted HR system and can be used to analyze the feasibility of desired broad attenuation bandwidth and peak amplitude in noise control optimization. $\overline{TL}$ curves always fall into the boundaries of the noise control zone as long as the geometries of the duct resonator are the same. The noise attenuation capacity of a HR has been verified from the aspect of sound power. Optimal transmission loss can be obtained by taking full advantage of periodicity and noise control zone in the design, achieving the required noise attenuation band and peak attenuation amplitude.

Chapter 5

Noise attenuation performance improvement of a ductwork system

5.1 Adding Helmholtz resonator on the periodic system

The transmission loss achieved by a periodic ducted HR system is depended on the structure and the number of HRs. However, the number of HRs is restricted by the available space in longitudinal direction of the duct. Moreover, such system will occupy a large space and may have some spare space in the transverse direction of the duct. By adding HRs on the available space in the transverse direction, a modified ducted HR system is therefore proposed and investigated. Both the noise attenuation band and peak amplitude are increased by adding HRs on arbitrary side of the cross-section of the duct. The proposed modified ducted HR system can improve the noise attenuation performance and fully utilize the available space, and it is practical to be used in an actual ventilation ductwork system.

5.1.1 Side-branch Helmholtz resonators

For the sake of completeness, a brief description of the transmission loss of a

side-branch Helmholtz resonator is necessary here. A single side-branch HR is shown in Figure. 5.1. On the basis of low-frequency range considered in this paper, only planar wave is assumed to propagate in the duct. By ignoring the time-harmonic disturbance and the reflected waves from downstream of the duct, the sound pressure and particle velocity can be expressed as:

$$p_1(x) = I_1 e^{-jkx} + R_1 e^{jkx}, \quad p_2(x) = I_2 e^{-jkx} \tag{5.1}$$

$$u_1(x) = \frac{I_1}{S_d Z_d} e^{-jkx} - \frac{R_1}{S_d Z_d} e^{jkx}, \quad u_2(x) = \frac{I_2}{S_d Z_d} e^{-jkx} \tag{5.2}$$

where k is the wave number, S_d is the cross-sectional area of the duct, Z_d is the acoustic impedance of the duct, and I_i (i=1,2) and R_1 represent respective complex wave amplitudes. Combining the continuity of sound pressure and volume velocity at the duct-neck interface at $x = 0$ yields:

$$\begin{bmatrix} p_1 \\ \rho_0 c_0 u_1 \end{bmatrix} = \begin{pmatrix} 1 & 0 \\ \frac{\rho_0 c_0}{S_d} \frac{1}{Z_r} & 1 \end{pmatrix} \begin{bmatrix} p_2 \\ \rho_0 c_0 u_2 \end{bmatrix} \tag{5.3}$$

Then the transmission loss of a single side-branch HR can be determined by the four-pole parameters method according to Eq. (2.17).

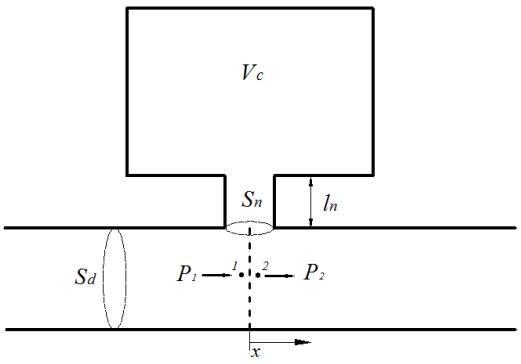

Figure 5.1 A single side-branch Helmholtz resonator.

It is well known that a single HR has a high transmission loss peak with narrow band. Several identical HRs installed on the same cross-section of the duct is a possible way to broaden the noise attenuation band. The side-branch HRs with N (N=4 here for example) identical HRs mounted on the same cross-section of the duct is illustrated in Figure. 5.2.

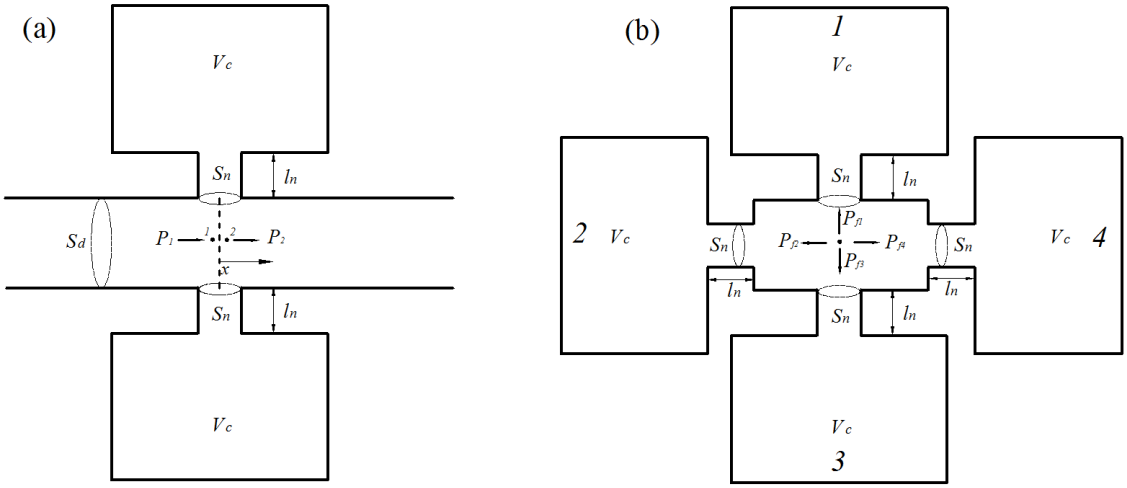

Figure 5.2 A side-branch Helmholtz resonators (a) side view (b) front view.

Similarly, by ignoring the time-harmonic disturbance and the reflected waves from downstream of the duct, the sound pressure and particle velocity of point 1 and point 2, as shown in Figure. 5.2 (a), can be expressed by Eq. (5.1) and Eq. (5.2) respectively. As depicted in Figure. 5.2 (a), the continuity condition of sound pressure at the duct-neck interface gives: $p_1 = p_2 = p_{fi}$ (i=1,2,3,4 represents each individual HR). The continuity condition of volume velocity at the same interface gives: $S_d u_1 = S_d u_2 + \sum_i^N p_{fi} / Z_r$. The relation of point 1 to point 2 could be obtained by

combining the continuity condition above. Then, according to the four-pole parameter method, the transmission loss of the side-branch HRs can be expressed as:

$$TL = 20\log_{10}\left(\frac{1}{2}\left|2 + N\frac{\rho_0 c_0}{S_d}\frac{1}{Z_r}\right|\right) \tag{5.4}$$

According to Eq. (5.4), it can be seen that the resonance frequency of side-branch HRs system still depends on the single HR. Several identical HRs mounted on the same cross-section of the duct could be considered as an equivalent "one HR" with acoustic impedance of Z_r / N. It indicates that the equivalent "one HR" remains the same resonance frequency as the single HR. The added HRs improve both the peak amplitudes and the attenuation band. It inspires us to improve the acoustic performance of the periodic ducted HRs system by adding HRs on the transverse direction of the duct.

5.1.2 Transmission loss of the modified ducted HR system

The transmission loss of a periodic ducted HR system is analyzed in Chapter 4. Generally, there are two formation mechanisms for the noise attenuation band: the HR's resonance mechanism and the Bragg reflection. Once the periodic distance is chosen to be $d = \lambda_0/2$, the designed HR's resonance frequency coincides with the first Bragg reflection. In this situation, a broader noise attenuation band at resonance frequency could be achieved.

A duct with periodic distributed identical HR has a unique attenuation characteristic due to the coupling of Bragg reflection and HR's resonance. However, for every single HR in the periodic ducted HR system, the noise attenuation capacity remains unchanged in spite of HR's number or the periodic distance. The broader the noise attenuation band, the lower the peak amplitude. It indicates that the transmission loss achievable by periodic ducted HR system is fairly depended on the HR's number, which is restricted to the available space in longitudinal direction of the duct. Besides, for a periodic system, there may also have some spare space in transverse direction of the duct. It is therefore that a modified ducted HR system is proposed to improve the noise attenuation performance and to fully utilize the available space.

As illustrated in Figure. 5.3, HRs are added on the cross-section of the periodic ducted HR system to form the modified ducted HR system. The number of HRs mounted on the same cross-section depends on the available space. Each cell of the modified ducted HR system could comprise different number of HRs. As discussed above, several identical HRs mounted on the same cross-section of the duct could be considered as an equivalent "one HR" with acoustic impedance of Z_r / N. It indicates that the resonance frequency of the equivalent "one HR" remains the same as the single HR.

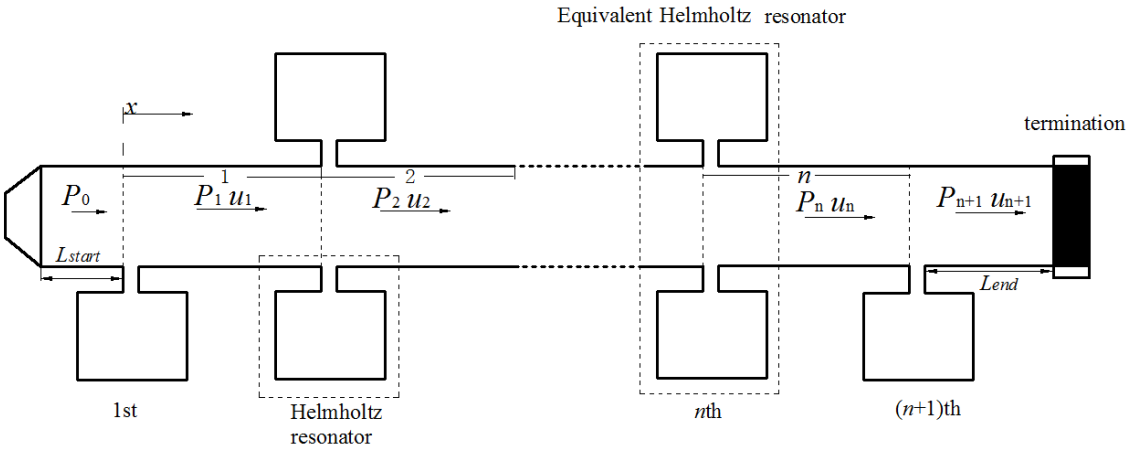

Figure 5.3 Schematic diagram of a modified ducted HR system.

It is therefore that the system can no longer be represented by the single transfer matrix $\mathbf{T}$ derived from Eq. (4.2). Instead, the transfer matrix between each two nearby cell should be specified as $\mathbf{T}_n$. Similar to the periodic ducted HR system, the sound characteristics in *nth* segment could be expressed by Eq. (5.1) and Eq. (5.2). By intruding the continuity conditions, the transfer matrix between *nth* and *n*+1*th* segment could be expressed as:

$$\begin{bmatrix} I_{n+1} \\ R_{n+1} \end{bmatrix} = \begin{bmatrix} (1-N\frac{Z_d}{2Z_r})\exp(-jkd) & -N\frac{Z_d}{2Z_r}\exp(jkd) \\ N\frac{Z_d}{2Z_r}\exp(-jkd) & (1+N\frac{Z_d}{2Z_r})\exp(jkd) \end{bmatrix} \begin{bmatrix} I_n \\ R_n \end{bmatrix} = \mathbf{T}_n \begin{bmatrix} I_n \\ R_n \end{bmatrix} \tag{5.5}$$

The complex wave amplitudes can be rewritten into a state vector as $\mathbf{a}_{n+1} = [I_{n+1} \quad R_{n+1}]^T$, where superscript *T* means transposition. Then, Eq. (5.5) could be simplified as:

$$\mathbf{a}_{n+1} = \mathbf{T}_n \mathbf{a}_n \tag{5.6}$$

The transfer matrix $\mathbf{T}_n$ could also be expressed in form of reflection and

transmission coefficients, t_n and r_n as[86]:

$$\begin{bmatrix} I_{n+1} \\ R_{n+1} \end{bmatrix} = \begin{bmatrix} e^{-jkL_n} & 0 \\ 0 & e^{jkL_n} \end{bmatrix} \begin{bmatrix} 1/t_n^{*} & -(r_n/t_n)^{*} \\ -(r_n/t_n) & 1/t_n \end{bmatrix} \begin{bmatrix} I_{n+1} \\ R_{n+1} \end{bmatrix} = \mathbf{T}_n \begin{bmatrix} I_n \\ R_n \end{bmatrix} \tag{5.7}$$

where the superscript * means conjugation. It follows immediately from Eq. (5.7) that:

$$\mathbf{a}_{n+1}\mathbf{a}_{n+1}^{T\ *} = \mathbf{T}_n(\mathbf{a}_n\mathbf{a}_n^{T*})\mathbf{T}_n^{T*} \tag{5.8}$$

Eq. (5.8) is a matrix equation and it can be re-expressed in vector form as:

$$\mathbf{e}_{n+1} = \mathbf{A}_n\mathbf{e}_n \tag{5.9}$$

where $\mathbf{e}_{n+1}$ and $\mathbf{e}_n$ can be represented as: $\begin{bmatrix} I_n I_n^{*} & I_n R_n^{*} & R_n I_n^{*} & R_n R_n^{*} \end{bmatrix}^T$ and $\begin{bmatrix} I_{n+1} I_{n+1}^{*} & I_{n+1} R_{n+1}^{*} & R_{n+1} I_{n+1}^{*} & R_{n+1} R_{n+1}^{*} \end{bmatrix}^T$ respectively.

According to the Eq. (5.9) and Eq. (5.10), the matrix $\mathbf{A}_n$ takes the form of $\mathbf{T}_n$ as[87]:

$$\mathbf{A}_n = \begin{bmatrix} 1/|t_n|^2 & -r_n/|t_n|^2 & -r_n^{*}/|t_n|^2 & |r_n|^2/|t_n|^2 \\ -r_n^{*}\delta_n/t_n^{*2} & \delta_n/t_n^{*2} & r_n^{*2}\delta_n/t_n^{*2} & -r_n^{*}\delta_n/t_n^{*2} \\ -r_n/\delta_n t_n^2 & r_n^2/\delta_n t_n^2 & 1/\delta_n t_n^2 & -r_n/\delta_n t_n^2 \\ |r_n|^2/|t_n|^2 & -r_n/|t_n|^2 & -r_n^{*}/|t_n|^2 & 1/|t_n|^2 \end{bmatrix} \tag{5.11}$$

where $\delta_n = \exp(-2jkd)$ (d should be replaced by L_{start} and L_{end} when sound propagates in the start and end segment of the whole system).

It can be seen from Eq. (5.11) that the value of $\mathbf{A}_n(4,4)$ is $1/|t_n|^2$. It indicates that the transmission loss between these two segments could be described as: $TL = 10\log_{10}(\mathbf{A}_n(4,4))$. When the duct ends with an anechoic termination, the whole HR system can be described as:

$$\mathbf{a}_{n+1} = \mathbf{T}_n\mathbf{a}_n = \mathbf{T}_n\mathbf{T}_{n-1}\mathbf{a}_{n-1} = \cdots = (\prod_{i=0}^{n}\mathbf{T}_i)\mathbf{a}_0 \tag{5.12}$$

With the introduction of Eq. (5.8) and Eq. (5.9), Eq. (5.12) could be expressed as:

$$\mathbf{e}_{n+1} = \left(\prod_{i=0}^{n} \mathbf{A}_n \right) \mathbf{e}_0 = \Lambda \mathbf{e}_0 \tag{5.13}$$

where Λ is the matrix of the whole ducted resonator system.

Similar to Eq. (5.14), $\Lambda(4,4)$ equals to the modulus squared transmission coefficient of the whole system. It is therefore that the average transmission loss of per HR in the whole system could be expressed as:

$$\overline{TL} = \frac{10}{N_{total}} \log_{10} \left(\Lambda(4,4) \right) \tag{5.14}$$

where N_{total} is the sum of HRs mounted on the duct.

5.1.3 Results and discussion

The single side-branch HR and the side-branch HRs are illustrated in Figure. 5.1 and Figure. 5.2 respectively. The geometries of the HR used in this paper are: cavity volume $V_c = 19.4\pi$ cm^3, neck area $S_n = 0.25\pi$ cm^2 and neck length $l_n = 2.5$ cm. The cross-section area of the main duct is $S_d = 25$ cm^2. The comparison of the transmission loss with respect to the number of identical HRs installed on the same cross-section of the duct is shown in Figure. 5.4. The transmission loss of a side-branch HR has a peak amplitude with narrow attenuation band, as is well known and depicted in Figure. 5.4 (N=1). By adding identical HRs on the same cross-section of the duct, it can be seen that both the magnitude of transmission loss and the noise

attenuation bandwidth are increased obviously. Furthermore, the added HRs has no effect on resonance frequency. The equivalent “one HR” has the same resonance frequency as the single HR. It means that the added HR changes the acoustic impedance of the “equivalent HR” without the changing of resonance frequency.

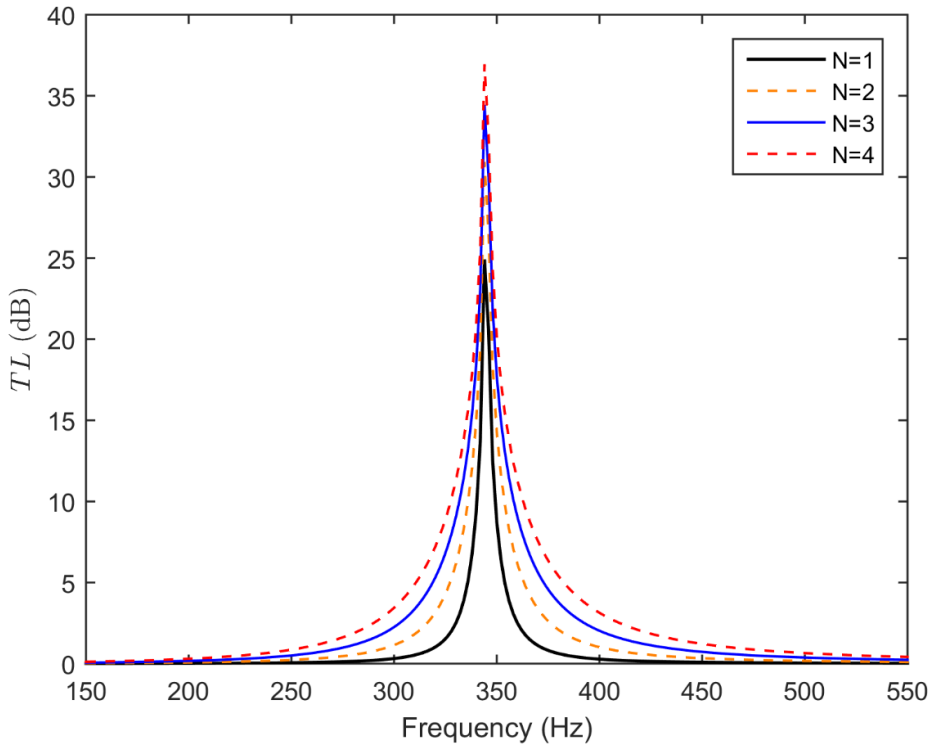

Figure 5.4 Comparison of the transmission loss with respect to the number of identical HRs mounted on a same cross-section.

The comparison of the analytical predictions and the FEM simulation with respect to different numbers of HR mounted on the same cross-section is exhibited in Figure. 5.5. It is shown that the predicted results fit well with the FEM simulation results. The solid lines represent the theoretical predictions, and dotted crosses represent the FEM

simulation results.

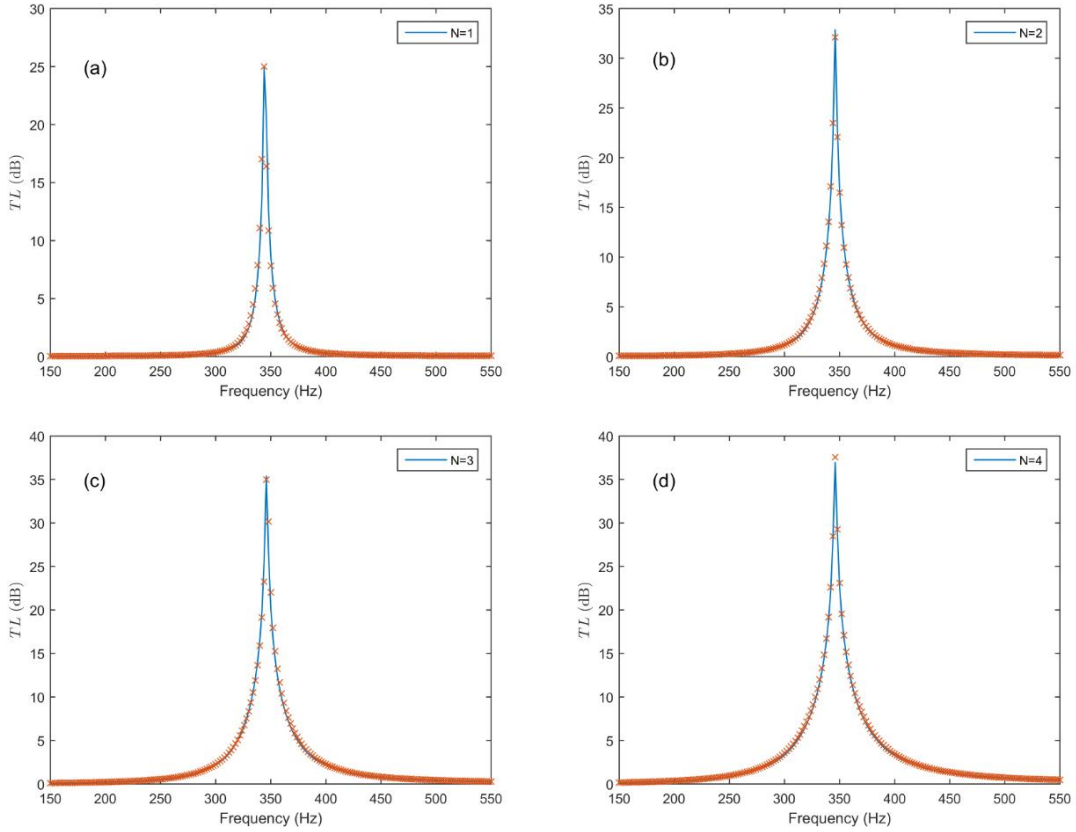

Figure 5.5 Comparison of the analytical predictions and the FEM simulation with respect to different numbers of HR mounted on the same cross-section.

For a periodic ducted HR system, a broader noise attenuation band could be achieved due to the coupling of the Bragg reflection and HR's resonance. However, such kinds of noise attenuation system will occupy a large space and it is impractical to be used in an actual ventilation ductwork system. The modified ducted HR system, as illustrated in Figure. 5.3, is proposed to improve the noise attenuation performance and to fully utilize the available space. The geometries of the HR and the main duct

are the same as the periodic ducted HR system as given above, as are as the beginning and end conditions. The duct segment length of the modified HR system is set to be $d = \lambda_0/2$ as well. On the basis of low-frequency range considered in this paper, only planar wave is assumed to propagated in the duct. It is therefore that the added HRs can be mounted on arbitrary side of the cross-section of the duct. Figure. 5.6 shows the configuration of three modified ducted HR system cases: 2143 model ,2131 model and 1121 model respectively.

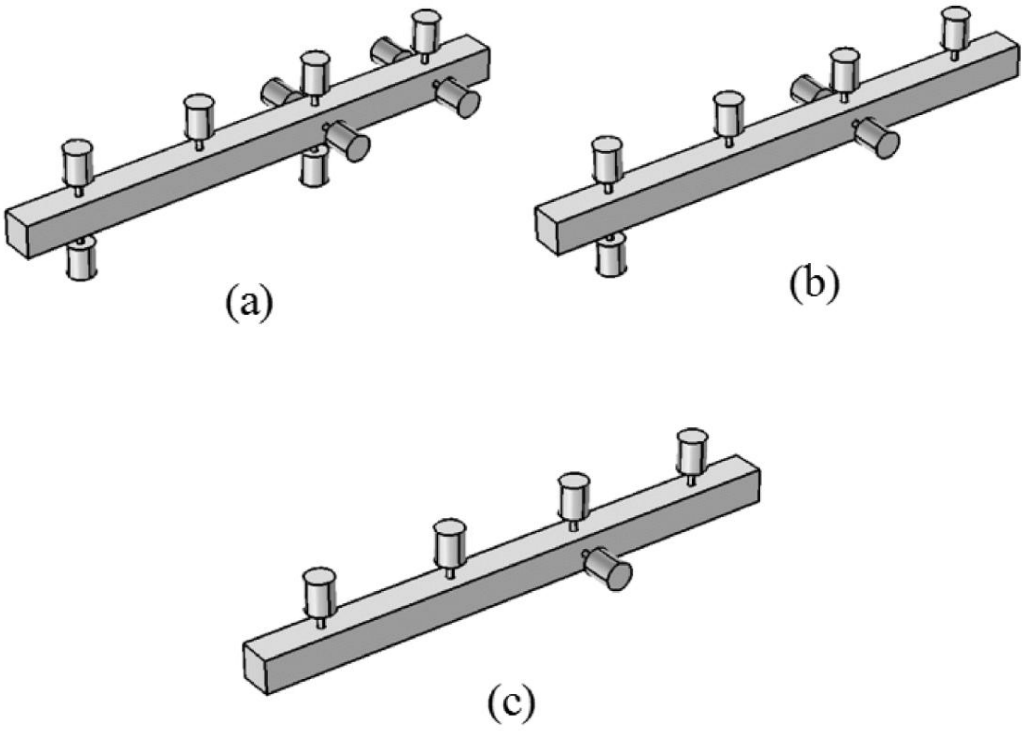

Figure 5.6 Configuration of three modified ducted HR system cases: (a) 2143 model, (b) 2131 model, (c) 1121 model (the integer means the number of HR mounted on the same cross-section in consecutive duct segment respectively).

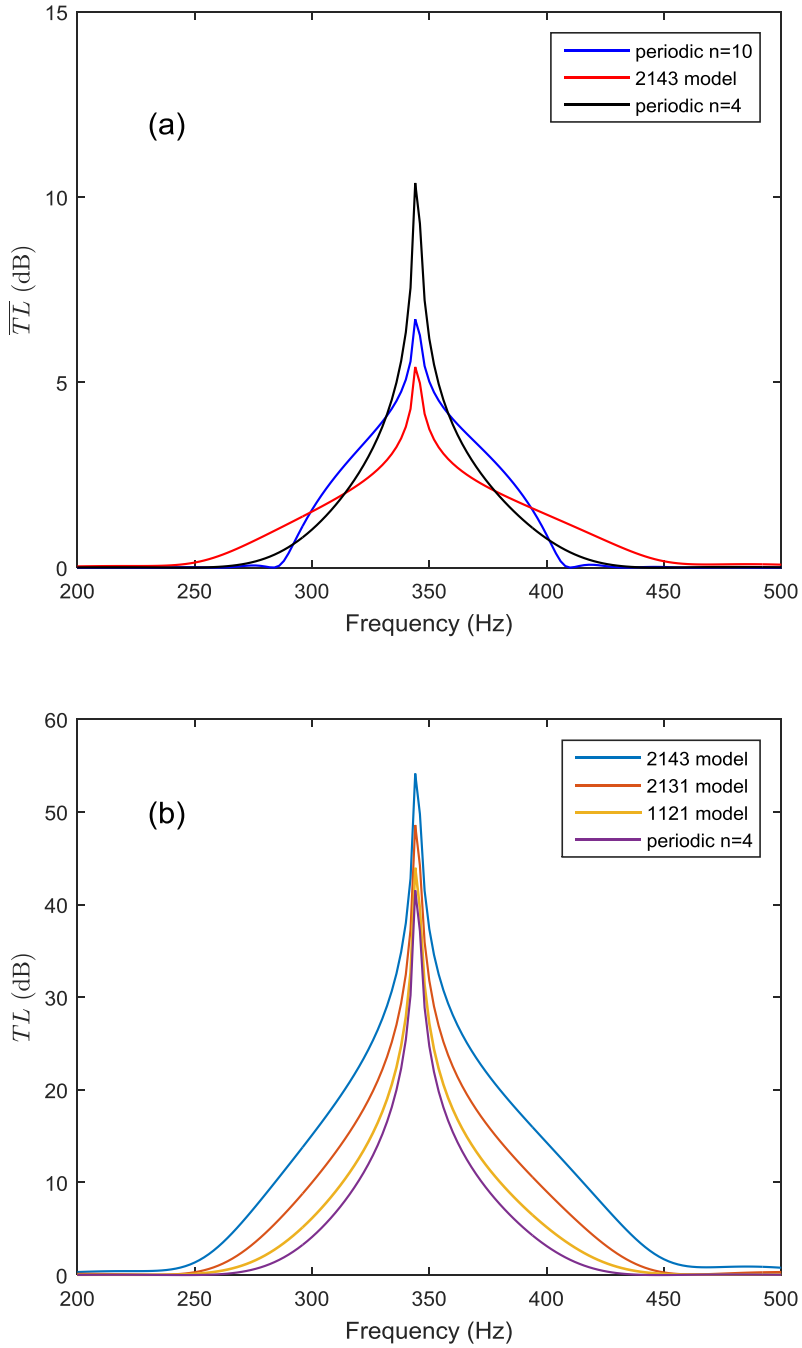

Figure 5.7 Comparison of transmission loss with respect to different ducted HR systems: (a) the average transmission loss of per HR in different systems, (b) the total transmission loss of different systems.

Figure. 5.7(a) compares the $\overline{TL}$ of 2143 model to two periodic ducted HR system cases (*n=4, 10*). The total HR number N_{total} of 2143 model equals to the periodic ducted HR system case *n=10*, while the duct's length of 2143 model is much less than the periodic one. The duct's length of 2143 model is the same as the periodic case *n=4*. However, it can be seen that a broader noise attenuation band could be achieved by this modified ducted HR system. Furthermore, the 2143 model has broader noise attenuation band and higher peak amplitude than the periodic ducted HR system (case: *n=4*), as shown in Figure. 5.7(b). The transmission loss of the four different HR systems with same duct segment number is also compared in Figure. 5.7(b). The comparison shows that both the peak amplitude and noise attenuation band are increased by adding HR on the duct, especially the noise attenuation band. The added HR mounted on the cross-section of the duct mainly broadens the noise attenuation band of the total transmission loss. Moreover, the $\overline{TL}$ bandwidth has an apparent increase due to the added HRs, as shown in Figure. 5.7(a). A good agreement between the theoretical predicted $\overline{TL}$ and the FEM simulation results can also be seen in Figure. 5. 8. The proposed modified ducted system can improve the noise attenuation performance and fully utilize the available space by adding HRs on arbitrary side of the cross-section of the duct.

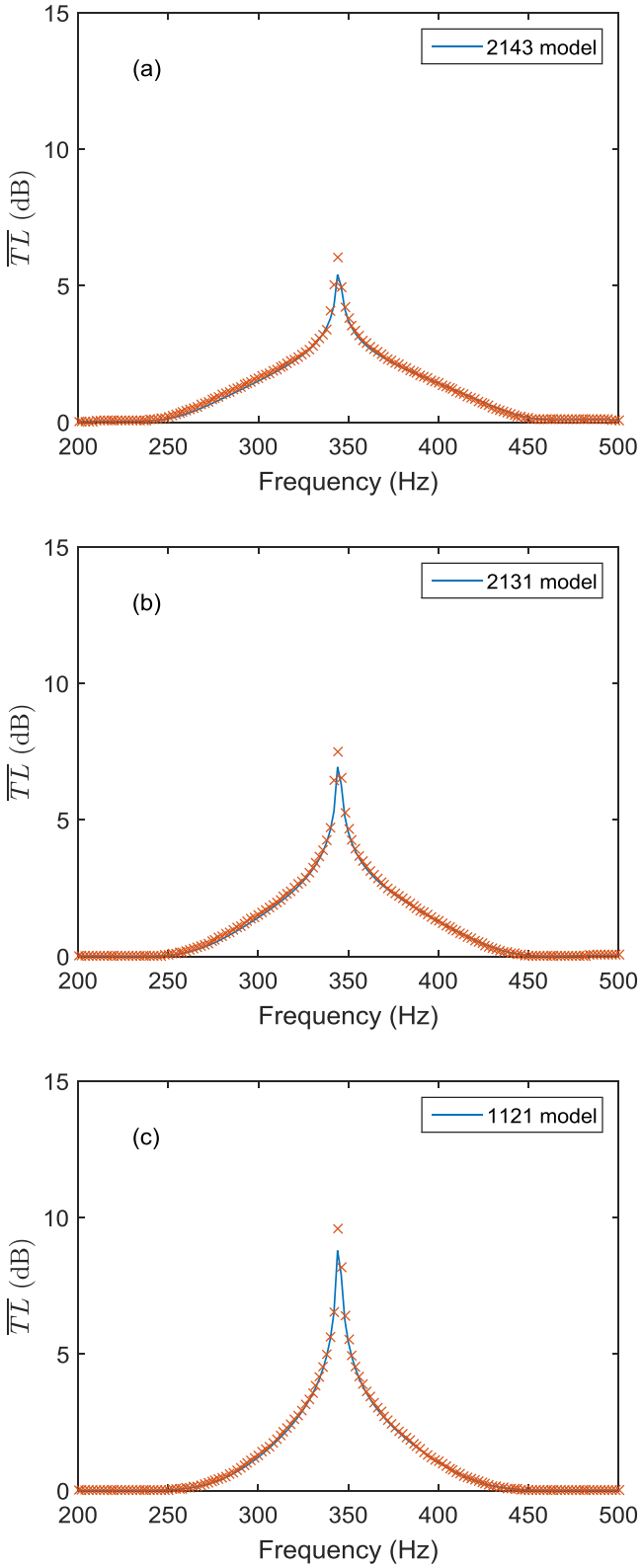

Figure 5.8 The average transmission loss of different modified HR systems (solid lines represents the theoretical predictions, and dotted crosses represent the FEM simulation results).

5.2 Hybrid noise control

In practical ventilation ductwork system, hybrid noise often occurs due to interaction effects of different localized turbulence and discontinuities. In order to deal with hybrid noise in ventilation ductwork system, a periodic dual HR array is introduced. The dual HR which consists of two HRs connected in series leads to two resonance frequencies. The mechanism of Bragg reflection and dual HR's resonances motivate us to achieve several broadband noise attenuation bands in low-frequency range.

5.2.1 Dual Helmholtz resonator

A dual HR could be analogous to a two degrees of freedom mechanical system, as illustrated in Figure. 3.1. The acoustic impedance of a dual HR is also given in Chapter 3. It is therefore that the dual HR's angular resonance frequencies are the roots of the following equation:

$$M_1 M_2 \omega^4 - \rho_0 c_0^2 [M_1 S_2^2 (\frac{1}{V_1} + \frac{1}{V_2}) + M_2 S_1^2 \frac{1}{V_1}] \omega^2 + \frac{\rho_0^{\,2} c_0^4 S_1^{\,2} S_2^{\,2}}{V_1 V_2} = 0 \qquad (5.15)$$

Then, the resonance frequencies of the dual HR can be derived from Eq. (5.15) and be expressed as:

$$f_{1,2} = \frac{1}{2\pi} \sqrt{\frac{\rho_0 c_0^2}{2} \left(\frac{S_2^2}{V_1 M_2} + \frac{S_2^2}{V_2 M_2} + \frac{S_1^2}{V_1 M_1} \right) \mp \sqrt{\frac{\rho_0^{\,2} c_0^4}{4} \left(\frac{S_2^2}{V_1 M_2} + \frac{S_2^2}{V_2 M_2} + \frac{S_1^2}{V_1 M_1} \right)^2 - \frac{\rho_0^{\,2} c_0^4 S_1^{\,2} S_2^{\,2}}{M_1 M_2 V_1 V_2}}} \qquad (5.16)$$

It can be observed from Eq. (5.16) that the resonance frequencies of the dual HR are only determined by its geometries. Therefore, it is straightforward to design a dual HR with desired resonance frequencies. Once the acoustic impedance is obtained, the transmission loss of the side-branch dual HR mounted on the duct with cross-sectional area S_d could be obtained according to Eq. (2.17).

5.2.2 Coupling of Bragg reflection and dual HR's resonance

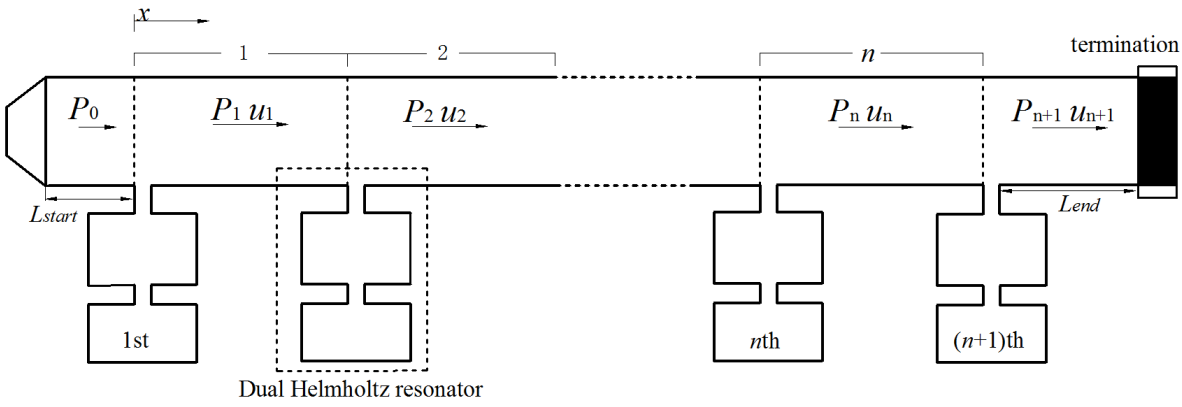

Figure 5.9 Schematic diagram of a periodic dual HR system.

The periodic dual HR system, consisting of a uniform duct with dual HRs attached periodically, is demonstrated in Figure. 5.9. A duct segment with a side-branch dual HR is considered as a typical periodic unit. The diameter of the dual HR's neck is inappreciable compared with the length of the duct segment in a periodic unit. Therefore, the length of the duct segment is regarded as the periodic distance. By

introducing the continuity conditions of the sound pressure and volume velocity at the duct-neck interface that at $x = nd$, the transfer matrix could be obtained as Eq. (4.2). Similar to the periodic structure aforementioned in Chapter 4, $\overline{TL} = -20\log_{10}|\lambda_1|$ could be derived to obtain the average transmission loss of a duct with an anechoic termination loaded with dual HRs periodically.

The transmission loss of the periodic dual HR system is only related to the solution of λ, as discussed above. Owing to the relation of q and λ, the transmission loss of the acoustic system refers to the solution of q. The solution of q, as a function of the wave frequencies, periodic distance and geometries of a duct resonator system, is allowed to be a complex. The real part and imaginary part of q are critical to distinguish the stopbands from passbands. The real part of q is referred to as passbands that have only a phase delay during wave propagation, and the imaginary part as attenuation constant named stopbands (decay of a wave happens from one unit to the following). It can be known that wave attenuation occurs for frequencies that provides an imaginary part to q. There are two mechanisms of the stopbands: dual HR's resonances and Bragg reflection. The stopbands caused by dual HR's resonances are situated near dual HR's resonance frequencies f_{01} and f_{02}, which is also the mechanism of a single dual HR case. The other kind of stopbands is brought about physically by Bragg reflection and will exist near $f_m = mc_0 / 2d$ (m is an integer). The width of the stopband decrease as $1/m^2$ and the maximum value of the

imaginary part becomes smaller as $1/m$.

For a general HR with single resonance frequency, the periodic distance is chosen to be half-wavelength of HR's resonance frequency for the sake of the coupling of first Bragg reflection and HR's resonance. The dual HR has two resonance frequencies f_{01} and f_{02} (assuming $f_{01} < f_{02}$). In order to obtain broader noise attenuation bands at these two resonance frequencies, both the resonance frequencies are designed to coincide with Bragg reflection. Note that the Bragg reflection is exiting at $f_m = mc_0/2d$ (m is an integer). It is therefore that the resonance frequencies of the dual HR should also satisfy the relation of $f_{02} = mf_{01}$ for broader noise attenuation bands at the designed resonance frequencies. The resonance frequencies of a dual HR could be tuned straightforward due to they are only determined by its geometries. Once a dual HR's resonance frequencies are designed to be $f_{02} = 2f_{01}$, the periodic distance could be set as $d = \lambda_{01}/2 = \lambda_{02}$ (λ_{01} and λ_{02} are wavelength of f_{01} and f_{02} respectively) to make the first and second Bragg reflection coincide with two resonance frequencies of the dual HR respectively for the sake of broader noise attenuation bands.

5.2.3 Results and discussion

The resonance frequencies of a dual HR are only determined by its geometries. The

geometries of the dual HR used in this paper are: neck areas $S_1 = 0.25\pi$ cm^2 and $S_2 = 0.25\pi$ cm^2, neck lengths $l_{n1} = 2.5$ cm and $l_{n2} = 2.1$ cm, cavity volumes $V_1 = 115.2\pi$ cm^3 and $V_2 = 62.4\pi$ cm^3. The cross-sectional area of the main duct is $S_d = 25$ cm^2. Thus the resonance frequencies of the dual HR are 301 Hz and 602 Hz, which are calculated directly by Eq. (5.16).

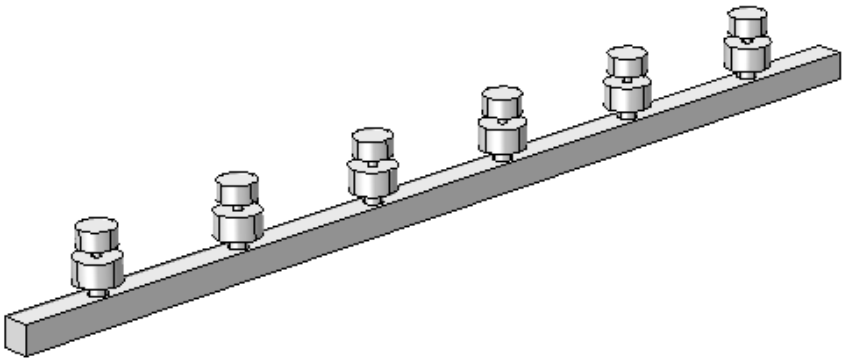

Figure 5.10 Configuration of the periodic dual HR system consisting of six dual HRs.

The geometries of the dual HR and the main duct used here are the same as given above. The periodic dual HR system with an anechoic termination to avoid reflected waves from downstream is exhibited in Figure. 5.9. An oscillation sound pressure at a magnitude of $P_0 = 1$ is applied at the beginning of the duct as the initial boundary conditions. Figure. 5.10 shows the configuration of the periodic dual HR system consisting of six identical dual HRs mounted on the duct periodically. The average transmission loss ($\overline{TL}$) of a periodic dual HR array system is expressed as $\overline{TL} = -20\log_{10}|\lambda_1|$, which is only related to the solution of q. For the certain dual

HR and main duct used in this paper, it indicates that the shape of $\overline{TL}$ is depended on the periodic distance. When the periodic distance is chosen to be $d = 0.58\lambda_{01}/2$, it can be observed from Figure. 5.11 that the dual HR's resonances and Bragg reflection have separated effects on the noise attenuation bands. The stopbands caused by resonance are situated near dual HR's resonance frequencies, and are the mechanism of a single dual HR case.

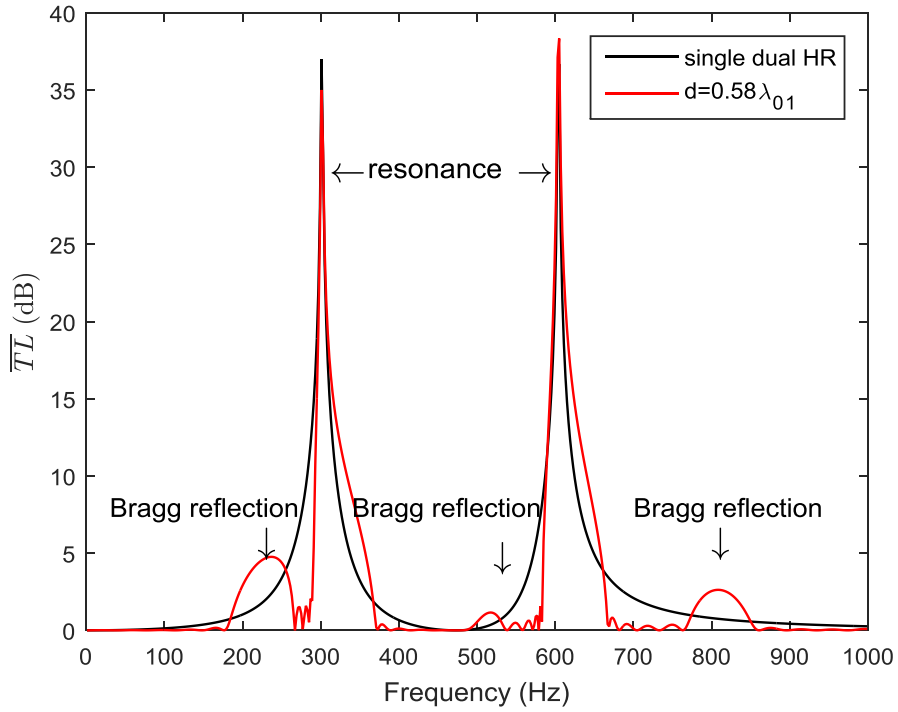

Figure 5.11 Noise attenuation bands of the periodic dual HR system due to Bragg reflection and dual HR's resonances separately.

In order to obtain broader noise attenuation bands at designed resonance frequencies of the dual HR, the Bragg reflection is intended to coincide with resonance

frequencies. The resonance frequencies of the dual HR are 301 Hz and 602 Hz, which is designed to satisfy the relation of $\lambda_{01} = 2\lambda_{02}$. Once the periodic distance is chosen to be $d = m\lambda_{01}/2$ (m is an integer), broader noise attenuation bands could be achieved at both resonance frequencies due to the coupling effect of Bragg reflection and dual HR's resonances, as illustrated in Figure. 5.12. It can be seen from Figure. 5.12 that the width of noise attenuation bands at resonance frequencies decrease with the increasing of m. It is because of the stopbands brought by Bragg reflection decrease as $1/m^2$ in width. For the sake of broader noise attenuation bands at designed resonance frequencies of the dual HR, the periodic distance is chosen to be $d = \lambda_{01}/2 = \lambda_{02}$. Therefore, the first and second Bragg reflection can coincide with two resonance frequencies of the dual HR respectively. Figure. 5.13 compares noise attenuation bands of different periodic distance cases ($d = 0.5\lambda_{01}$ and $d = 0.58\lambda_{01}$) with or without considering coupling effects. The coupling of Bragg reflection and dual HR's resonances results in much broader noise attenuation bands at resonance frequencies of the dual HR. The FEM simulation used here is similar to the aforementioned description. The comparisons of the theoretical predicted results and the FEM simulation results with respect to different periodic distances are illustrated in Figure. 5.14, and the theoretical predictions fit well with the FEM simulation results.

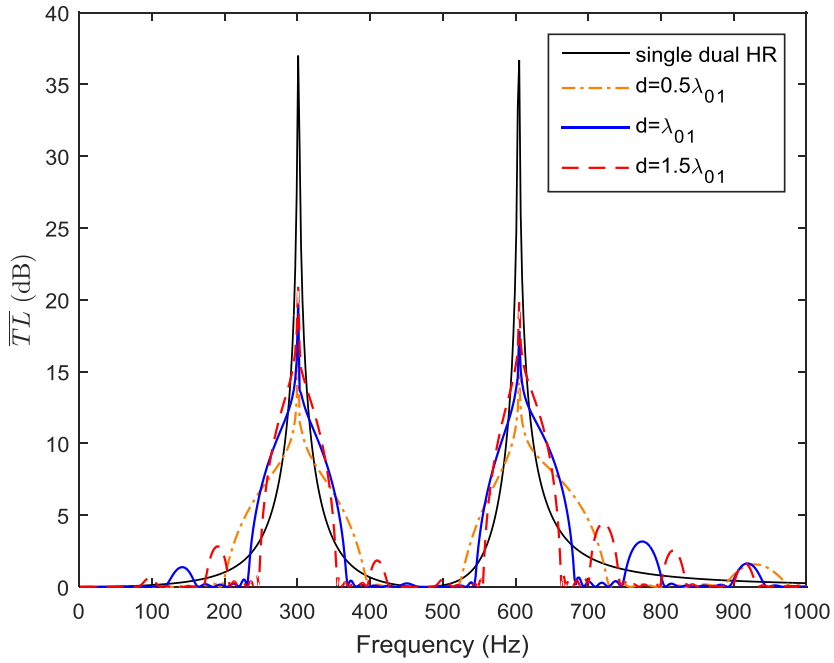

Figure 5.12 Noise attenuation bands of the periodic dual HR system due to the coupling of Bragg reflection and dual HR's resonances.

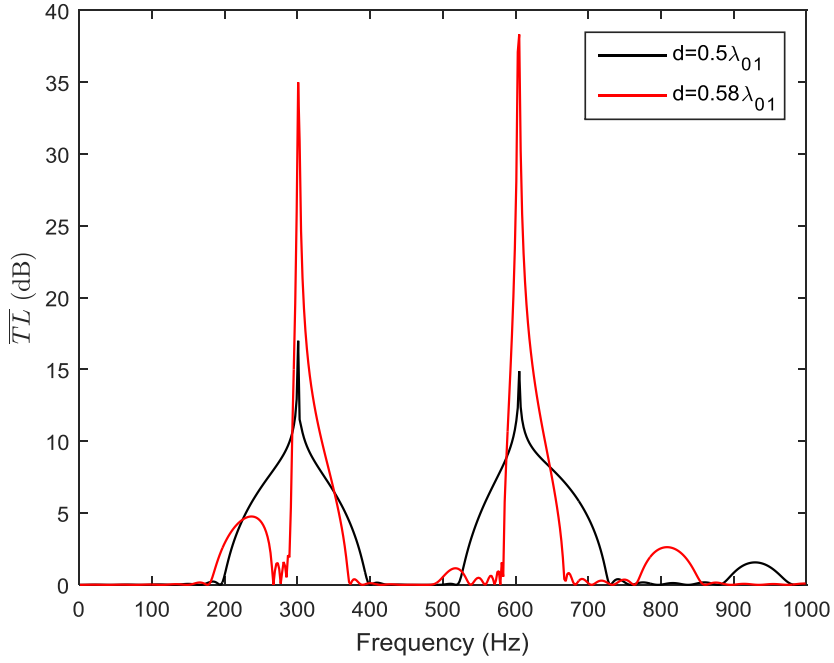

Figure 5.13 Noise attenuation bands of the periodic dual array system with and without coupling effects.

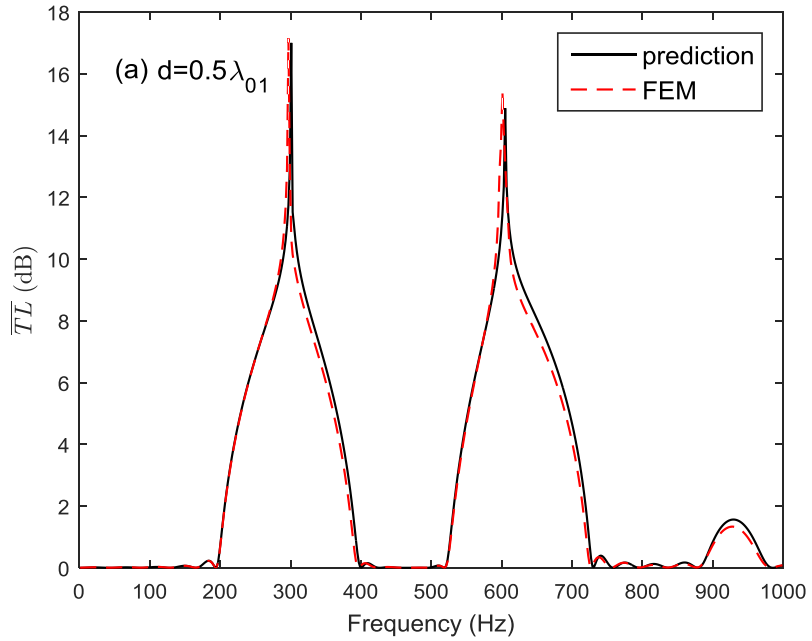
(a) d=0.5λ_{01}
prediction
FEM
$\overline{TL}$ (dB)
Frequency (Hz)
0
2
4
6
8
10
12
14
16
18
0
100
200
300
400
500
600
700
800
900
1000

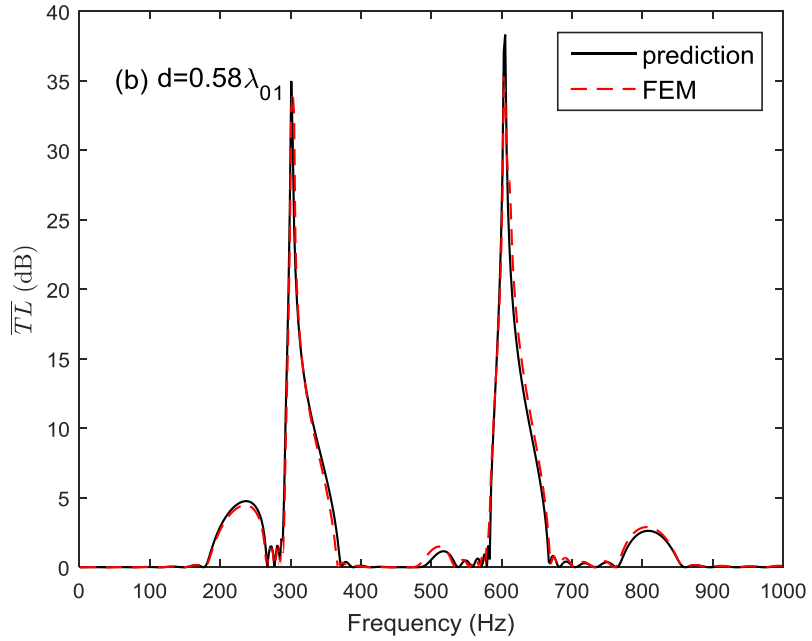
(b) d=0.58λ_{01}
prediction
FEM
$\overline{TL}$ (dB)
Frequency (Hz)
0
5
10
15
20
25
30
35
40
0
100
200
300
400
500
600
700
800
900
1000

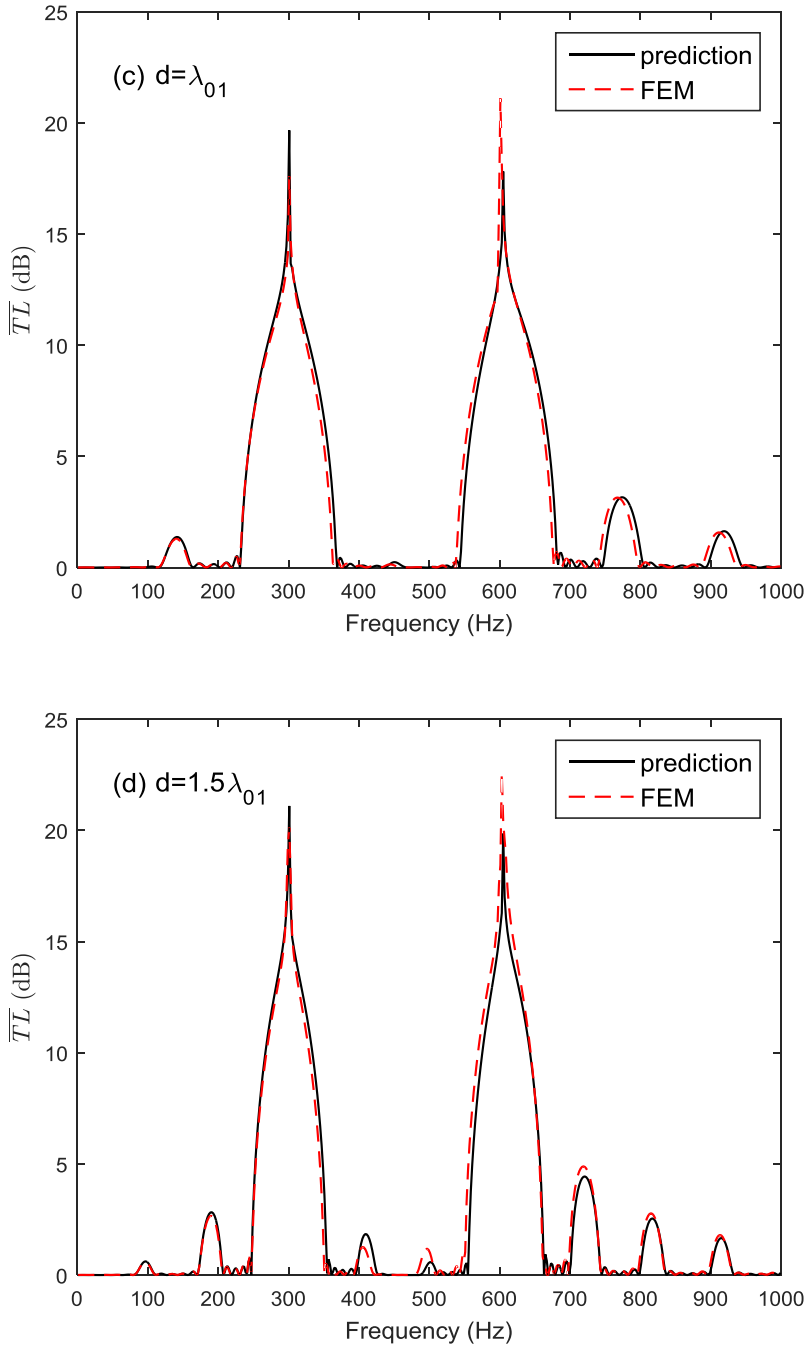

Figure 5.14 The average transmission loss of the periodic dual HR system in respect of different periodic distances (solid lines represent the theoretical predictions, and dashed lines represent the FEM simulation results).

5.3 Summary

The periodic ducted HR system could provide broader noise attenuation band due to the coupling of the Bragg reflection and the HR's resonance. For the sake of a broader noise attenuation band at the resonance frequency, $d = \lambda_0/2$ is often chosen as a periodic distance. However, the noise attenuation performance of the system fairly depends on the number of HRs, which is restricted by the available space in longitudinal direction of the duct. However, there may have some spare space in the transverse direction of the duct. By adding HRs on the available space in the transverse direction, a modified ducted HR system is proposed. Several identical HRs mounted on a same cross-section of a duct has broader noise attenuation band and higher peak amplitude without effects on the HR's resonance frequency. It means the modified ducted HR can also take full advantage of periodicity to obtain a broader noise attenuation band. Besides, added HRs can improve the noise attenuation performance of the whole system. The more HRs added, the better noise attenuation performance of the system. The proposed modified ducted HR system fully utilizes the available space to improve noise attenuation performance. It is practical to use the modified system in an actual ventilation ductwork system, and it has a potential application in noise control with longitudinal space limitation.

In practical ventilation ductwork system, hybrid noise often occurs due to interaction effects of different localized turbulence and discontinuities. In order to deal with

hybrid noise in ventilation ductwork system, a periodic dual HR array is introduced. The theoretical and numerical studies of a periodic dual HR system is presented. The dual HR which consists of two HRs connected in series (neck-cavity-neck-cavity) leads to two resonance frequencies. The geometries of the dual HR are significant small compared with the wavelengths. Hence, the lumped parameter theory is employed to approximate the dual HR as an equivalent two degrees of freedom mechanical system. The resonance frequencies and transmission loss of a dual HR have been derived. Aiming at broader noise attenuation bands for hybrid noise control at low frequencies, a duct with an array of dual HRs distributed periodically is investigated. In the interest of low frequencies, the frequency range considered in this paper is well below the duct's cutoff frequency. It is therefore that only planar wave is allowed to propagate in the duct. Owing to the coupling of Bragg reflection and dual HR's resonances, a periodic dual array can provide much broader noise attenuation bands at the designed resonance frequencies of the dual HR. In order to make the first and second Bragg reflection coincide with two resonance frequencies of the dual HR respectively, the periodic distance is set to be $d = \lambda_{01}/2 = \lambda_{02}$. Therefore, two broader noise attenuation bands at the dual HR's resonances can be achieved.

Chapter 6

Conclusion and Suggestions for Future Work

6.1 Conclusion

Noise control in ventilation ductwork system is of importance in improving the indoor environmental quality. The unavoidable components of the ductwork system, for instance, dampers, bends, transition pieces, corners or even attenuators punctate the original uniform ductwork. These discontinuities in a ventilation ductwork system results in the generations of localized turbulence. The turbulences are responsible for generation of the undesired noise as the ductwork system begins to work. This thesis therefore aims at investigating low-frequency broadband noise control in ventilation ductwork systems based on Helmholtz resonator arrays. The theoretical analysis of the ventilation ductwork systems has been validated by Finite Element Method using the commercial software (COMSOL Multiphysics).

First of all, a Helmholtz resonator with different types of neck has been investigated. An extended neck or a spiral neck takes the place of the traditional straight neck of the HR. The acoustic performance of the HR with these two types of necks is

analyzed theoretically and numerically. The length correction factor is introduced through a modified one-dimensional approach to account for the non-planar effects that result from the neck being extended into the cavity. The spiral neck is transformed to an equivalent straight neck, and the acoustic performance is then derived by a one-dimensional approach. The theoretical prediction results fit well with the Finite Element Method simulation results. Without changing the cavity volume of the HR, the resonance frequency shows a significant drop when the extended neck length or the spiral neck length is increased. An identical change in the extension neck length or the spiral neck length will produce the same decrease in resonance frequency. For a certain designed resonance frequency of HR, the utilization of the extended neck or the spiral neck can reduce the cavity volume. Then, the noise attenuation capacity of a HR is proposed and the theoretical formula of it has been derived theoretically. The noise attenuation capacity is defined as the integral of transmission loss in the frequency domain. The transmission loss index is mainly used to evaluate the acoustic transmission performance in the frequency domain. However, it cannot provide a quantitative characteristic of the noise attenuation band. The proposed noise attenuation capacity index can be considered as one of the key parameters to evaluate the HR's noise attenuation performance quantitatively and distinctly. The effects of the neck length, cross-sectional area of the neck, cavity volume and cross-sectional area of the duct on the noise attenuation capacity are analyzed theoretically and numerically. The results show that the noise

attenuation capacity is only related to the geometries of the neck and the cross-sectional area of the duct. The cavity volume has no effects on it. Similar to the significance of the HR's resonance frequency, the proposed theoretical formula of the noise attenuation capacity provides a distinct parameter to evaluate the HR's noise attenuation band quantitatively and illuminates the limitations in HR's noise control applications. It is an important supplement to the theoretical studies and engineering applications of HRs.

Secondly, the acoustic performance of three kinds of HR arrays are investigated theoretically and numerically. The dual HR consisting of two HRs connected in series is considered as a serial HR array. Two HRs mounted on the same cross-section of the duct constitute a parallel HR array. The lined HR array is composed of two HRs installed on the longitudinal direction of the duct. Different installation methods have significant effects on transmission loss performance. The dual HR could provide two resonance frequencies, which the first and second resonance frequency are lower and higher than the resonance frequency of any component HRs respectively. By altering the connected sequence of two HRs in the dual HR, the reduced first resonance frequency compromises an increasing second resonance frequency could be observed. The parallel HR array has two resonance frequencies with nearly the same peak amplitudes corresponding to each HR's resonance frequency and peak amplitude. It could be approximated as the superposition of two individual HRs' transmission loss

curve. The lined HR array provides a much broader noise attenuation band between the resonance frequencies of these two HRs. The two resonance frequencies corresponding to each HR's resonance frequency could also be observed. In consideration of noise attenuation capacity, it should be noted the noise attenuation capacity of the dual HR equals to the noise attenuation capacity of each single HR mounted on the ducted. The added HR in series could be considered as the added volume of the cavity, which indicates it has no effects on the noise attenuation capacity. The noise attenuation capacity of the parallel HR array and the lined HR array is the same, which is twice of the dual HR or each component HR. The quantitative parameter has potential applications to be used in the noise control optimization and HR design to evaluate the acoustic performance.

Thirdly, a theoretical study of the dispersion characteristics of sound wave propagation in a periodic ducted HRs system has been presented. Owing to the coupling of Bragg reflection and HR's resonances, a periodic system can provide much broader noise attenuation band at the designed resonance frequencies of the HR. However, the broader the noise attenuation band the lower the peak attenuation amplitude. The noise attenuation capacity of a HR has been verified from the aspect of sound power. Although different average transmission loss curves with different bandwidths and peak amplitudes could be obtained with different periodic distances, the area under the average transmission loss curve and the sound power storage W_{total}

are always the same and average transmission loss curves always fall into the boundaries of a noise control zone. A noise control zone compromising the attenuation bandwidth or peak amplitude is first proposed to illustrate the limitation of noise control for ducted HR system and can be used to analyze the feasibility of desired broad attenuation bandwidth and peak amplitude in noise control optimization.

Last but not least, a modified ducted HR system based on the periodic ducted HR system is proposed and investigated. The transmission loss achieved by a periodic ducted HR system is depended on the structure and the number of HRs. However, the number of HRs is restricted by the available space in longitudinal direction of the duct. Moreover, such system will occupy a large space and may have some spare space in the transverse direction of the duct. By adding HRs on the available space in the transverse direction, a modified ducted HR system is therefore proposed. Several identical HRs mounted on a same cross-section of a duct has broader noise attenuation band and higher peak amplitude without effects on the HR's resonance frequency. It means the modified ducted HR can also take full advantage of periodicity to obtain a broader noise attenuation band. Besides, added HRs can improve the noise attenuation performance of the whole system. The more HRs added, the better noise attenuation performance of the system. It is flexible to install added HRs on the unoccupied space of the transverse direction of the duct. The

proposed modified ducted HR system fully utilizes the available space to improve noise attenuation performance. Aiming at broader noise attenuation bands for hybrid noise control at low frequencies, a duct with an array of dual HRs distributed periodically is investigated. Owing to the coupling of Bragg reflection and dual HR's resonances, a periodic dual array can provide much broader noise attenuation bands at the designed resonance frequencies of the dual HR.

6.2 Suggestions for Future Work

On the basis of the present studies, several suggestions for future work are recommended as follows:

1. The transmission loss performance of a Helmholtz resonator with a spiral neck or an extended neck is analyzed without the effect of the flows. However, the flow effects have significant impact on the transmission loss performance. A theoretical model considering the flow effects should be developed in the future work.

2. The theoretical formula of the Helmholtz resonator's noise attenuation capacity can be investigated and compared with that under different flow conditions, i.e. laminar flow, turbulent flow and different Mach numbers. Moreover, the

concept of the noise attenuation capacity can be extended to other silencer. It can also be adopted to other research areas related to HR, like notch filter and metamaterials, with further investigations.

3. Flow is inevitable in ventilation ductwork system and the Helmholtz resonator array mounted on the duct can produce additional noise. The effects of localized turbulence due to Helmholtz resonator arrays should be taken into account. The complicated acoustic and turbulent interaction of different Helmholtz resonator arrays, i.e. the periodic ducted HR array, the periodic dual HR array and the modified HR array, is the main content of future work.

4. The tunnel aerodynamics and acoustics becomes a significant issue with the rapid developing high-speed trains project combined a lot of tunnel structures, and the ideal capsule pipelines project. The micro-pressure waves generated by a high-speed train entering and moving in a tunnel become significant problem related to passengers' health and comfort. The Helmholtz resonator array might be an effective method to suppress the propagation of micro-pressure waves in tunnels. Future investigations included theoretical analysis, numerical and experimental works in this area would be meaningful.

References

[1] J. F. Kreider, *Handbook of heating, ventilation and air conditioning* (CRC Press, Boca Raton, 2000).

[2] F. Fahy, *Foundations of engineering acoustics* (Elsevier, Amsterdam,2001).

[3] X. Gao and B. Sundén, "PIV measurement of the flow field in rectangular ducts with 60 ° parallel, crossed and V-shaped ribs," *Exp. Therm Fluid. Sci.* **28(6)**, 639-653 (2004).

[4] C.G. Gordon, "Spoiler-generated flow noise. II: results," *J. Acoust. Soc. Am.* **45**, 214--233 (1969).

[5] C.M. Mak, J. Wu, C. Ye and J. Yang, "Flow noise from spoilers in ducts," *J. Acoust. Soc. Am.* **125(6)**, 3756-3765 (2009).

[6] C.M. Mak, "A prediction method for aerodynamic sound produced by multiple elements in air ducts," *J. Sound Vib.* **278**, 395-403 (2005).

[7] S. Wallin and A. Johansson, "A complete explicit algebraic Reynolds stress model for incompressible and compressible flows," *J. Fluid Mech.* **278**, 395-403 (2005).

[8] CIBSE Guide B4 Regeneration of noise by duct components and terminations, The Charted Institution of Building Services Engineers, London, (2007).

[9] CIBSE Guide C Reference data, The Charted Institution of Building Services Engineers, London, (2007).

[10] ASHRAE Handbook-HVAC Applications(SI), ISBE 9781936504084, ASHRAE,

Inc., Atlanta, GA, (2007).

[11] H. H. Colin, *The effects of low-frequency noise and vibration on people* (Multi-Science Publishing Co. Ltd, Brentwood, 2007).

[12] I. Alimohammadi, S. Sandrock and M.R. Gohari, "The effects of low frequency noise on mental performance and annoyance," *Environ. Monit. Assess.* **185**, 7043-7051 (2013).

[13] C.M. Mak and Y. P. Liu, "The effect of sound on office productivity," *Build. Serv. Eng. Res T.* **33(3)**, 339-345 (2012).

[14] S. Namba, S. Kuwano and T. Okamoto, "Sleep disturbance caused by meaningful sounds and effect of background noise," *J. Vib. Acoust.* **277**, 445-452 (2004).

[15] P. Lueg, *Process of silencing sound oscillations*, US Patent 2,043,416 (1936).

[16] G. Canevet, "Active sound absorption in an air conditioning duct," *J. Sound Vib.* **58(3)**, 333-345 (1978).

[17] S. M. Kuo and D. R. Morgan, *Active Noise Control System Algorithms and DSP Implementation* (Wiley, New York, 1996).

[18] C. H. Hansen and S. D. Snyder, *Active Control of Noise and Vibration* (E&FN Spon, London, 1997).

[19] J. Rohlfing and P. Gardonio, "Ventiliaton duct with concurrent acoustic feed-forward and decentralised structural feedback active control," *J. Sound Vib.* **333(3)**, 630-645 (2014).

[20] J. C. Burgess, "Active adaptive sound control in a duct: a computer simulation," *J.*

Acoust. Soc. Am. **70**, 715-726 (1981).

[21] M. Utsumi, “Reduction of Noise Transmission in a duct by termination impedance control of a sidebranch resonator,” *J. Vib. Acoust.* **123(3)**, 289-296 (2001).

[22] K. S. Peak and K. L. Rathi, “A finite element analysis of the convected acoustic wave motion in dissipative silencers,” *J. Sound Vib.* **184(3)**, 529-545 (1995).

[23] C. N. Wang, “Numerical decoupling analysis of a resonator with absorbent material,” *Appl. Acoust.* **58(2)**, 109-122 (1999).

[24] F. D. Denia, A. Selamet, F. J. Fuenmayor and R. Kirby, “Acoustic attenuation performance of perforated dissipative mufflers with empty inlet/outlet extensions,” *J. Sound Vib.* **302**, 1000-1017 (2007).

[25] A. F. Seybert, R. A. Seman, and M. D. Lattuca, "Boundary element prediction of sound propagation in ducts containing bulk absorbing materials," *J. Vib. Acoust.* **120(4)**, 976-981 (1998).

[26] R. Kirby, P. Williams and J. Hill, “A three dimensional investigation into the acoustic performance of dissipative splitter silencers,” *J. Acoust. Soc. Am.* **135(5)**, 2727-2737 (2014).

[27] B. Nennig, E. Perrey-Debain, and M. Ben Tahar, “A mode matching method for modeling dissipative silencers lined with poroelastic materials and containing mean flow,” *J. Acoust. Soc. Am.* **128**, 3308–3320 (2010).

[28] A. Selamet, F. D. Denia and A. J. Besa, “Acoustic behaviour of circular dual-chamber mufflers,” *J. Sound Vib.* **265**, 967-985 (2003).

[29] X. Yu and L. Cheng, “Duct noise attenuation using reactive silencer with various internal configurations,” *J. Sound Vib.* **335**, 229-244 (2015).

[30] X. Yu, F. S. Cui and L. Cheng, “ On the acoustic analysis and optimization of ducted ventilation systems using a sub-structuring approach,” *J. Acoust. Soc. Am.* **139(1)**, 279-289 (2016).

[31] U. Ingard, “ On the theory and design of acoustic resonators,” *J. Acoust. Soc. Am.* **25**, 1037-1061 (1953).

[32] R. T. Beyer, *Sounds of Our Times: Two Hundred Years of Acoustics* (Spiniger, Verlag, 1999).

[33] L. Li, Y. Liu, F. Zhang and Z. Sun, “ Several explanations on the theoretical formula of Helmholtz resonator,” *Adv. Eng Softw.* **114**, 361-371 (2017).

[34] S. H. Park, “Acoustic properties of micro-perforated panel absorbers backed by Helmholtz resonators for the improvement of low-frequency sound absorption,” *J. Sound Vib.* **332**, 4895-4911 (2013).

[35] S. H. Seo and Y. H. Kim, “Silencer design by using array resonators for low-frequency band noise reduction,” *J. Acoust. Soc. Am.* **118(4)**, 2332-2338 (2005).

[36] D. Zhao, “Transmission loss analysis of a parallel-coupled Helmholtz resonator network,” *AIAA J.* **50(6)**, 1339-1346 (2012).

[37] M. Terao, H. Sekine and M. Suzuki, “Implementation of a tuning system for Helmholtz resonator arrays in HVAC ducts,” *Noise. Control. Eng. J.* **59(5)**,

1339-1346 (2012).

[38] J. M. Coulon, N. Atalla and A. Desrochers, “Optimization of concentric array resonators for wide band noise reduction,” *Appl. Acoust.* **113**, 109-115 (2016).

[39] A. Trochidis, “Sound transmission in a duct with an array of lined resonators,” *J. Vib. Acoust.* **113**, 245-249 (1991).

[40] S. R. Kim, Y. H. Kim and J. H. Jang, “A theoretical model to predict the low-frequency sound absorption of a Helmholtz resonator array,” *J. Acoust. Soc. Am.* **119(4)**, 1933–1936 (2006).

[41] C. E. Bradley, “Time harmonic acoustic Bloch wave propagation in periodic waveguides. Part I. Theory,” *J. Acoust. Soc. Am.* **96(3)**, 1844-1853 (1994).

[42] C. E. Bradley, “Time harmonic acoustic Bloch wave propagation in periodic waveguides. Part II. Experiment,” *J. Acoust. Soc. Am.* **96(3)**, 1854-1862 (1994)

[43] N. Sugimoto and T. Horioka, “Dispersion characteristics of sound waves in a tunnel with an array of Helmholtz resonators,” *J. Acoust. Soc. Am.* **97(3)**, 1446-1459 (1995).

[44] N. Sugimoto, “Propagation of nonlinear acoustic waves in a tunnel with an array of Helmholtz resonators,” *J. Fluid Mech.* **244**, 55-78 (1992).

[45] D. J. Mead, “A general theory of harmonic wave propagation in linear periodic system with multiple coupling,” *J. Sound Vib.* **27(2)**, 235-260 (1973).

[46] Z. Y. Tao, W. Y. He and X. L. Wang, “Resonance-induced band gaps in a periodic waveguide,” *J. Sound Vib.* **313**, 830-840 (2008).

[47] X. Wang and C. M. Mak, “Wave propagation in a duct with a periodic Helmholtz resonators array,” *J. Acoust. Soc. Am.* **131(2)**, 1172-1182 (2012).

[48] Y. F. Li, H. J. Shen, L. K. Zhang, Y.S. Su and D.L. Yu, “Control of low-frequency noise for piping system via the design of coupled band gap of acoustic metamaterials,” *Phys. Lett A.* **380**, 2322-2328 (2016).

[49] Y. T. Duan, W. Koch, C. M. Linton and M. Mciver, “Complex resonances and trapped modes in ducted domains,” *J. Fluid Mech.* **571**, 119-147 (2007).

[50] X. Shi and C. M. Mak, “Sound attenuation of a periodic array of micro-perforated tube mufflers,” *Appl. Acoust.* **115**, 15-22 (2017).

[51] M. Harris, *Handbook of noise control* (McGraaw-Hill, New York, 1979).

[52] M. L. Munjal, *Acoustic of Ducts and Mufflers. 2nd ed* (Wiley, New York, 1987).

[53] A. Vardy and J. Brown, “Influence of ballast on wave steepening in tunnels,” J. *Sound Vib.* **238(4)**, 595-615 (2000).

[54] A. D. Quinn, M. Hayward, C. J. Baker, F. Schmid, J. A. Priest and W. Powrie, “A full-scale experimental and modelling study of ballast flight under high-speed trains,” *P. I. Mech Eng. F-J. Rai.* **224(2)**, 61-74 (2010).

[55] J. A Tebbutt, M. Vahdati, D. Carolan and J. P. Dear, “Numerical investigation on an array of Helmholtz resonators for the reduction of micro-pressure waves in modern and future high-speed rail tunnel systems,” *J. Sound Vib.* **400**, 606-625 (2007).

[56] A. Selamet and N. S. Dickey, “Theoretical, computational and experimental

investigation of Helmholtz resonators with fixed volume: lumped versus distributed analysis," *J. Sound Vib.* **187(2)**, 358-367 (1995).

[57] A. Selamet and Z. L. Ji, "Circular asymmetric Helmholtz resonators," *J. Sound Vib.* **107(5)**, 2360-2369 (2000).

[58]L. L. Thompson, "A review of finite-element methods for time-harmonic acoustic," *J. Acoust. Soc. Am.* **119(3)**, 1315-1330 (2006).

[59] P. A. Monkewitz and N. M. Nguyen-Vo, "The response of Helmholtz resonators to external excitation. Part 1. Single resonators," *J. Fluid Mech.* **151**, 477-497 (1985).

[60] R. C. Chanaud, "Effects of geometry on the resonance frequrncy of Helmholtz resonator," *J. Sound Vib.* **178(3)**, 337-348 (1994).

[61] P. K. Tang and W. A. Sirignano, "Theory of a generlized Helmholtz resoator," *J. Acoust. Soc. Am.* **26(2)**, 247-262 (1973).

[62] A. Selamet and I. J. Lee, "Helmholtz resonator with extended neck," *J. Acoust. Soc. Am.* **113(4)**, 1975-1985 (2003).

[63] X. Shi and C. M. Mak, "Helmholtz resonator with a spiral neck," *Appl. Acoust.* **99**, 68-71 (2015).

[64] S. K. Tang, "On Helmholtz resonators with tapered necks," *J. Sound Vib.* **279(3-5)**, 1085-1096 (2005).

[65] S. Griffin, S. A. Lane and S. Huybrechts, "Coupled Helmholtz resonators for acosutic attenatuion," *J. Vib. Acoust.* **123**, 11-17 (2001).

[66] M. B. Xu, A. Selamet and H. Kim, “Dual Helmholtz resonator,” *Appl. Acoust.* **71**, 822-829 (2010).

[67] A. Selamet, M. B. Xu, I. J. Lee and N. T. Huff, “Helmholtz resonator lined with absorbing material,” *J. Acoust. Soc. Am.* **117(2)**, 725-733 (2005).

[68] A. D. Sahasrabudhe, M. L. Munjal and S. Anantha Ramu, “Analysis of inertance due to the higher order mode effects in a sudden area discontinuity,” *J. Sound Vib.* **185(3)**, 515-529 (1995).

[69] J. Kergomard, “Simple discontinuty in acoustic waveguides at low frequency: cirtical analysis and formula,” *J. Sound Vib.* **114(3)**, 465-479 (1987).

[70] Z. X. Kang and Z. L. Ji, “Acoustic length correction of duct extension into a cylindrical chamber,” *J. Sound Vib.* **310(4-5)**, 782-791 (2008).

[71] S. Felix and V. Pagneux, “Sound propagation in rigid bends: A multimodal approach,” *J. Acoust. Soc. Am.* **110(3)**, 1329-1337 (2001).

[72] C. J. Nederveen, “Influence of a toroidal bend on the wind structure tuning,” *J. Acoust. Soc. Am.* **104**, 1616-1626 (1998).

[73] Z. L. Ji and J. Z. Sha, “Four-pole parameters of a duct with low Mach number flow,” *J. Acoust. Soc. Am.* **98(5)**, 2848-2850 (1995).

[74] K. S. Peat, “A transfer matrix for an absorption silencer element,” *J. Sound Vib.* **146(2)**, 353-360 (1991).

[75] COMSOL. Acoustics Module User’s Guide. version 5.1 (2015).

[76] COMSOL. COMSOL Multiphysics Reference Guide, version 5.1 (2015).

[77] A. Isozaki, H. Takahashi, H. Tamura, T. Takahata, K. Matsumoto and I. Shimoyama, "Parallel Helmholtz resonators for a planar acoustic notch filter," *Appl. Phys Lett.* **105**, 241907 (2014).

[78] J. Mei, G. Ma, M. Yang, Z. Yang, W. Wei, and P. Sheng, "Dark acoustic metamaterials as super absorbers for low-frequency sound," Nat. Commun. **3**, 756 (2012).

[79] G. Ma and P. Sheng, "Acoustic metamaterials: From local resonances to broad horizons," *Sci Adv.* **2**, e1501595 (2016).

[80] J. Li, W. Wang, Y. Xie, B. Popa, S. A. Cummer, "A sound absorbing metasurface with coupled resonators," *Appl. Phys Lett.* **109**, 091908 (2016).

[81] Y. Li and B. M. Assouar, "Acoustic metasurface-based perfect absorber with deep subwavelength thickness," *Appl. Phys Lett.* **108**, 063502 (2016).

[82] J. E. Kinsler, A. R. Frey, A. B. Coppens and J. V. Sanders, *Fundamentals of Acoustics* (Wiley, New York, 1982).

[83] D. Wu and N. Zhang, " The improvement on noise attenuation performance of a duct-resonator system," *J. Asian. Archit. Build.* **16**;669-674 (2017).

[84] J. W. S. Rayleigh, *The Theory of Sound, Volume II* (Dover, New York, 1945).

[85] Y. Yun and C. M. Mak, "A study of coulped flexural-longitudinal wave motion in a periodic dual-beam structure with transverse connection," *J. Acoust. Soc. Am.* **117(2)**, 725-733 (2005).

[86] R. S. Langley, "Wave transmission through one-dimensional near periodic

structures: optimum and random disorder," *J. Sound Vib.* **188(5)**, 717-743 (1995).

[87] B. R. Mace, "Reciprocity, conservation of energy and some properties of reflection and transmission coefficients," *J. Sound Vib.* **155**, 375-381 (1992).